UNIVERSIDAD NACIONAL AUTÓNOMA DE MÉXICO
POSGRADO EN CIENCIAS FÍSICAS

LINEAR MOMENTUM TRANSFER FROM SWIFT ELECTRONS TO SMALL METALLIC NANOPARTICLES: DIPOLE APPROXIMATION

TESIS
QUE PARA OPTAR POR EL GRADO DE:
MAESTRO EN CIENCIAS (FÍSICA)

PRESENTA:
CARLOS ALBERTO MACIEL ESCUDERO

TUTOR:
DR. ALEJANDRO REYES CORONADO
FACULTAD DE CIENCIAS, UNAM

MIEMBROS DEL COMITÉ TUTOR:
DRA. KAREN VOLKE SEPÚLVEDA
INSTITUTO DE FÍSICA, UNAM
DR. AUGUSTO GARCÍA VALENZUELA
CCADET, UNAM

CIUDAD DE MÉXICO, OCTUBRE DE 2017

Linear Momentum Transfer from Swift Electrons to Small Metallic Nanoparticles: Dipole Approximation

Carlos Maciel Escudero

October, 2017

Master's Thesis in Theoretical Physics
Carlos Alberto Maciel Escudero
Posgrado en Ciencias (Física)

Universidad Nacional Autónoma de México
Advisor: Alejandro Reyes Coronado

Universidad Nacional
Autónoma de México
"Por mi raza hablará el espíritu"

To Natalia and both Zoraydas.
Because if the first one is correct,
we do not have to worry, we are
predetermined to be together

AGRADECIMIENTOS

En esta ocasión quiero agradecerle a todas aquellas personas que me permitieron lograr lo que soy hoy en día. En primer lugar quiero agradecerle a mis tres pilares, que además de haberles dedicado la tesis, les estoy infinitamente agradecido por lo que han aportado a mi vida. Gracias mamá, por ser siempre mi guía y mostrarme con fortaleza el camino que debo seguir. Gracias gorda, porque tú siempre me demuestras que la vida simplemente no tiene límites, admiro tu perseverancia donde es imposible tenerla. Mi güera, qué decir, gracias por ser quien eres, por escuchar, por derrumbar paredes y escalar prejuicios, por enseñarme a ser libre, pero sobre todo por estar a mi lado. Hoy tengo claro que nuestras discusiones de física me han hecho comprender y profundizar en esas pequeñas grietas de la física llamadas localidad, contextualidad y factualidad. Prometo de ahora en adelante poner a juicio los fundamentos en los que se basa una teoría.

Gracias a todos los profesores que me han formado, en especial: al Dr. Claudio Pita, por transmitirme su pasión en las matemáticas, gracias a usted mi interés en el rigor va más allá de un mero formalismo. A Alex Ordoñez, por nunca dejar de creer en mí, por apoyarme durante mis días como estudiante de ingeniería, pero sobre todo por ser un incomparable amigo. Al Dr. Antonmaría Minzoni, gracias por todo lo que me enseñó, prometo jamás olvidarlo. Al Dr. Chumin Wang, por su apoyo en mi formación como físico y por enseñarme que el trabajo, la dedicación y el esfuerzo son tres ingredientes fundamentales para el éxito.

Gracias a Alejandro Reyes Coronado, el tutor de este trabajo, por tu paciencia y tus pláticas. Por tu apoyo, consejos, guía y entusiasmo. Al Dr. Rubén Barrera, por su constante ayuda tanto en mi investigación como en mis decisiones académicas. A mi Comité Tutor, la Dra. Karen Volke y el Dr. Augusto García Valenzuela, que siempre estuvieron al pie del cañón supervisando mi desempeño y guiándome en el transcurso de mi maestría. A los miembros del jurado, la Dra. Ana Lilia González, el Dr. Eduardo Nahmad, el Dr. Carlos Ramírez y el Dr. Raúl Esquivel, por el tiempo que dedicaron al revisar esta tesis y por sus valiosos comentarios que hicieron de éste, un mejor trabajo de investigación.

A mis profesores del Posgrado en Ciencias Físicas: al Dr. Victor Romero Rochín, al Dr. Rafael Pérez Pascual, al Dr. Daniel Sudarsky, al Dr. Luis Mochán y en especial al Dr. Pier Mello, cuyo entusiasmo en la docencia y en la Mecánica Cuántica han impactado en mis futuras decisiones.

A la Universidad Nacional Autónoma de México (UNAM), al Posgrado en Ciencias Físicas (PCF) de la UNAM, a la Facultad de Ciencias (FC) de la UNAM y al Instituto de Físca (IF) de la UNAM que permitieron el desarrollo y la conclusión de este trabajo. Gracias a CONACyT por la beca que me brindó durante los dos años de mi maestría, al Doctor Alejandro Reyes

A mis abuelos y a mi Pepe Grillo, Jaime, gracias por tus sabios consejos e irrefutables regaños. Por ser oídos, por ser amigo, enemigo, cómplice y hasta papá. Tú me has mostrado el lado bonito de la vida, y gracias a ti hoy logro distinguir matices donde el blanco y el negro nublaban mi visión.

También quiero agradecerle a todos mis compañeros de la UP y de la UNAM. En especial a Ángel y a Adrián, porque ustedes dos son el mejor equipo de trabajo que me pudo haber tocado. Gracias Ángel, por acompañarme, por tu sinceridad, por tu amistad, por tu preocupación, por estos cinco años de discusiones científicas y retos permanentes. Y gracias a ti Adrián, por estar en las buenas y en las malas, por tus bromas y buenos consejos. Me han enseñado que darse por vencido no es una opción.

Por último, quisiera agradecerle a todas las personas que yacen debajo del edificio de Petén y Zapata por enseñarme la fragilidad de la vida y la angustia inconsolable, por hacerme más fuerte. Jamás dejaré de llevar mi puño en alto y sus voces quedarán siempre en mi mente y en mi corazón.

Abstract

The electromagnetic interaction between fast electrons and small metallic nanoparticles can be both attractive or repulsive, depending on the electron's velocity and the impact parameter between the two particles. This assertion has been recently demonstrated both theoretically [23] and experimentally [5]. A way to study this interaction is by means of the total linear momentum transferred from the swift electron to the nanoparticle. In this work, we present the developments achieved regarding the total linear momentum transferred within the *dipole approximation*. This approximation stands for the contribution of the first multipole of the scattered field to the linear momentum transfer mechanism—in the interaction between the electron and the metallic nanoparticle.

The dissertation aims two main goals: the first is to study an analytical approach to the spectral contribution of the momentum transfer, that is, to point out a path for calculating a closed expression of the surface integral of the Maxwell stress tensor—involved in the momentum transfer calculations—, composed by both the electromagnetic field produced by the electron and the electromagnetic field scattered by the nanoparticle. The second goal is to study the contribution of the first multipole ($\ell = 1$) of the scattered field to the total linear momentum transferred. For this second part, numerical calculations were performed in order to compare the dipole approximation and previous results (for $\ell = 15$ multipoles) for aluminium [25], [10] and for gold [23] nanoparticles.

Resumen

La interacción electromagnética entre electrones rápidos y pequeñas nanopartículas metálicas puede ser atractiva o repulsiva, dependiendo de la rapidez con la que viajan los electrones y del parámetro de impacto presente entre ambas partículas. Esta afirmación ha sido corroborada tanto teórica [23] como experimentalmente [5] para nanopartículas metálicas, y una forma de analizar dicha interacción es mediante la transferencia de momento lineal total cedido por el electrón rápido a la nanopartícula. En este trabajo se presentan los desarrollos teóricos que muestran la contribución por parte del primer multipolo del campo esparcido por la NP, a la transferencia de momento lineal. A ésta la denominamos como *aproximación dipolar*.

La tesis tiene dos objetivos principales: el primero de ellos consiste en estudiar un enfoque analítico a la contribución espectral del momento transferido, esto es, indicar un camino para calcular una expresión analítica de la integral de superficie del tensor de esfuerzos de Maxwell—presente en los cálculos de momento lineal transferido—, compuesto tanto por el campo electromagnético producido por el electrón como por el campo electromagnético esparcido por la nanopartícula. El segundo objetivo consiste en estudiar la contribución del primer multipolo ($\ell = 1$) del campo esparcido al mecanismo de la transferencia de momento lineal. Para esta segunda parte se realizaron cálculos numéricos con los cuales se comparó la aproximación dipolar con resultados previamente calculados (para $\ell = 15$ multipolos) para nanopartículas de aluminio [25], [10] y oro [23].

CONTENTS

LIST OF SYMBOLS

Symbol	Meaning	Definition
a	Nanoparticle's radius	
$\mathbf{A}(\mathbf{r};t)$	Vector potential in time domain and real space	Appendix A
$\mathbf{A}(\mathbf{r};\omega)$, $\mathbf{A}(\mathbf{k};\omega)$	Time and space Fourier Transform of vector potential	Appendix A
A_i	Oscillator strength in the Drude-Lorentz model	
$\alpha(\omega)$	Polarizability	Section 4.2
$\mathbf{B}(\mathbf{r};t)$	Magnetic field in time domain and real space	
$\mathbf{B}(\mathbf{r};\omega)$, $\mathbf{B}(\mathbf{k};\omega)$	Time and space Fourier Transform of magnetic field	Section 2.3
$\mathbf{B}^{ext}$	Magnetic field produced by the swift electron	Section 2.1
$\mathbf{B}^{scat}$	Magnetic field scattered by the nanoparticle	Section 2.2
$B(z,u)$	Beta function	Appendix A
β	Relativistic beta	Section 2.1
$\mathbb{B}_{ij}$	Auxiliary magnetic functions	Section 3.3
c	Speed of light	
γ	Lorentz factor	Section 2.1
Γ, Γ_i	Phenomenological damping constant	Section 4.1
$d\mathbf{a} = \hat{\mathbf{n}}\,da$	Normal surface element	Section 2.3
δ_{ij}	Kronecker's delta	
$\delta(\mathbf{r})$	Dirac delta function	
e	Electron's charge	
$\hat{\mathbf{e}}_i$	Unit vector	
$\mathbf{E}(\mathbf{r};t)$	Electric field in time domain and real space	
$\mathbf{E}(\mathbf{r};\omega)$, $\mathbf{E}(\mathbf{k};\omega)$	Time and space Fourier Transform of electric field	Section 2.3
$\mathbf{E}^{ext}$	Electric field produced by the swift electron	Section 2.1
$\mathbf{E}^{scat}$	Electric field scattered by the nanoparticle	Section 2.2
$\mathbb{E}_{ij}$	Auxiliary electric functions	Section 3.3
ϵ	Permittivity of the surrounding medium	
ϵ_0	Permittivity of free space in SI units	
$\epsilon_i(\omega)$	Nanoparticle's dielectric function	
$\epsilon_i'(\omega)$	Real part of the dielectric function ϵ_i	Section 4.1
$\epsilon_i''(\omega)$	Imaginary part of the dielectric function ϵ_i	Section 4.1
ϵ_{ijk}	Levi-Civita symbol	
$\eta^{\mu\nu}$	Minkowski metric tensor	Appendix B
$\mathbf{f}(\mathbf{r};t)$	Lorentz force density	Section 2.3
$\mathbf{F}(t)$	Lorentz force	Section 4.2

iv

$F^{\mu\nu}$	Faraday's tensor	Section 2.1
$\mathbf{g}(\mathbf{r};t)$	Electromagnetic linear momentum density	Section 2.3
$\mathbf{G}(t)$	Electromagnetic linear momentum	Section 2.3
$\Delta\mathbf{G}$	Total change of electromagnetic linear momentum	Section 2.3
G_0	Green function of Helmholtz equation	Appendix A
$\hbar$	Planck's constant ($h/2\pi$)	
$h_\ell^{(+)}$	Spherical Hankel functions of the first kind multiplied by the imaginary unit i	
$\mathbf{H}$	Auxiliary magnetic field ($\mathbf{B} = \mu\mathbf{H}$)	
$\overset{\leftrightarrow}{\mathbf{I}}$	Unit dyadic	
j_ℓ	Spherical Bessel functions	
$\mathbf{J}(\mathbf{r};t)$	Current distribution	
$\mathbf{J}_{tot}(\mathbf{r};t)$	Total current distribution	
k	Magnitude of wave vector	Section 2.2
k_0	Magnitude of wave vector in free space	Section 2.2
k^μ	Wave 4-vector	Section 2.1
K_ν	Modified Bessel function of the second kind	
$\mathbf{L}$	Orbital-angular momentum operator	Section 2.2
m_e	Electron's mass	
$\mathbf{M}, \mathbf{N}$	Vector harmonics	Section 2.2
$\Theta^{\mu\nu}$	Symmetrical electromagnetic energy-momentum tensor	Appendix B
$\Lambda^\mu_{\nu'}$	Lorentz transformation matrix	Section 2.1
μ	Permittivity of the surrounding medium	
n	Number of electrons per unit volume	
n^μ	Unit normal 4-vector	Appendix B
$\mathbf{p}(\omega)$	Dipole moment	Section 4.2
$\mathbf{p}(\mathbf{r};t)$	Total mechanical linear momentum density	Section 2.3
$\mathbf{P}(t)$	Total mechanical linear momentum	Section 2.3
$\Delta\mathbf{P}$	Total change of mechanical linear momentum	Section 2.3
$\boldsymbol{\mathcal{P}}(\omega)$	Spectral contribution to the total linear momentum transferred	Section 2.3
$\boldsymbol{\mathcal{P}}_{\mathbf{E}}^{ext}$	Electric spectral contribution of the external electromagnetic field	Section 3.2
$\boldsymbol{\mathcal{P}}_{\mathbf{B}}^{ext}$	Magnetic spectral contribution of the external electromagnetic field	Section 3.3
$\boldsymbol{\mathcal{P}}_{\mathbf{E}}^{scat}$	Electric spectral contribution of the scattered electromagnetic field	Section 3.2
$\boldsymbol{\mathcal{P}}_{\mathbf{B}}^{scat}$	Magnetic spectral contribution of the scattered electromagnetic field	Section 3.3
$\boldsymbol{\mathcal{P}}_{\mathbf{E}}^{(ext, scat)}$	Electric spectral contribution of the coupled term	Section 3.2
$\boldsymbol{\mathcal{P}}_{\mathbf{B}}^{(ext, scat)}$	Magnetic spectral contribution of the coupled term	Section 3.2
P_ℓ^m	Associated Legendre polynomials	
P^μ	Momentum 4-vector	Appendix B
Q_i	Charge of particle i	
$\mathbb{R}^{1,3}$	Minkowski spacetime	
r	Radius of the integration surface	

Re	Real part of a complex number	
$\rho(\mathbf{r};t)$	Charge distribution	
$\rho_{tot}(\mathbf{r};t)$	Total charge distribution	
$\mathbf{S}(\mathbf{r};t)$	Poynting vector	Section 2.3
S	Integration surface	Section 2.3
$S(\mathbf{r}_0)$	Integration sphere located at $\mathbf{r}_0$	Appendix B
σ	Spacelike surface	Appendix B
t_ℓ^E, t_ℓ^M	Scattering (Mie) coefficients	Section 2.2
$\overset{\leftrightarrow}{\mathbf{T}}(\mathbf{r};t)$	Maxwell stress tensor	Section 2.3
$\overset{\leftrightarrow}{\mathbf{T}}_{\mathbf{E}}(\mathbf{r};\omega)$	Time Fourier transform of the electric Maxwell stress tensor	Section 2.3
$\overset{\leftrightarrow}{\mathbf{T}}_{\mathbf{B}}(\mathbf{r};\omega)$	Time Fourier transform of the magnetic Maxwell stress tensor	Section 2.3
$\overset{\leftrightarrow}{\mathbf{T}}^{ext}$	External contribution to the Maxwell stress tensor	Section 3.2
$\overset{\leftrightarrow}{\mathbf{T}}^{scat}$	Scattered contribution to the Maxwell stress tensor	Section 3.2
$\overset{\leftrightarrow}{\mathbf{T}}^{(ext,scat)}$	Coupled contribution of the Maxwell stress tensor	Section 3.3
$\mathbb{T}_i^E$	Auxiliary electric functions	Section 3.3
$\mathbb{T}_i^B$	Auxiliary magnetic functions	Section 3.3
τ	Proper time	
$\mathbf{v}$	Electron's velocity	
V	Integration volume	Section 2.3
$\phi(\mathbf{r};t)$	Scalar potential in time domain and real space	Appendix A
$\phi(\mathbf{r};\omega)$, $\phi(\mathbf{k};\omega)$	Time and space Fourier Transform of scalar potential	Appendix A
$\boldsymbol{\Phi}^{ext}$	Flux of the external Maxwell stress tensor	Appendix B
ψ^L	Longitudinal scalar function	Section 2.2
ψ^E, ψ^M	Electric and magnetic scalar functions	Section 2.2
$\psi_{\ell,m}^{E,ext}$, $\psi_{\ell,m}^{M,ext}$	Expansion coefficients for the external electromagnetic field	Section 2.2
$\psi_{\ell,m}^{E,scat}$, $\psi_{\ell,m}^{M,scat}$	Expansion coefficients for the scattered electromagnetic field	Section 2.2
ψ_ℓ, ξ_ℓ	Riccati-Bessel functions	Appendix C
x_0	Electron's impact parameter	Chapter 1
x^μ	Position 4-vector	Section 2.1
Y_{lm}	Scalar spherical harmonics	
ω	Frequency	
ω_ℓ	Resonance frequency (frequencies) for the ℓ mode	Section 4.1
ω_ℓ'	Real part of the ℓ-mode eigenfrequency	Section 4.1
ω_ℓ''	Imaginary part of the ℓ-mode eigenfrequency	Section 4.1
ω_d	Eigenfrequency of the dipolar plasmon mode	Section 4.1
ω_i	Spring natural frequency in the Drude-Lorentz model	Section 4.1
ω_p	Bulk plasma frequency	Section 4.1
ω_s	Eigenfrequency of the surface plasmon mode	Section 4.1
$\Omega_{\mathbf{r}}$	Solid angle of point $\mathbf{r}$	
$\perp$	Perpendicular (transverse) to the electron's velocity	Section 2.1
$\parallel$	Parallel (longitudinal) to the electron's velocity	Section 2.1

INTRODUCTION

During the past few years an interest has been directed towards understanding optical phenomena related to the electromagnetic response of nanometer-sized metals, where collective charge densities—called plasmons—naturally emerges from the description of such response. Plasmonics, is a rather new physics research field which promises to understand the coupling between light and subwavelenght objects. In fact, plasmonics glamour and its accelerated growth rely in the nanoscale bridge brought as for example: in ultra-sensitive molecular detectors [1]; in novel biomedical applications such as bio-imaging [2] and cancer detection [3]; and in the same level of importance, the quality to enhance local electric fields which is useful in experimental methods like Surface-Enhanced Raman Spectroscopy (SERS) [4]. Indeed, plasmonics points out a path to find out the excitations a "small" object can sustain.

This thesis is devoted to study the interaction between swift electrons and small metallic nanoparticles (NPs). Particularly, we are interested in the total linear momentum transferred from a fast electron to a NP as a mechanism to quantify the "push" or the "pull" felt by the NP due to the presence of the electron. The motivation to address this problem arouse in 2008, where experimental results regarding Scanning and Transmission Electron Microscopy (STEM) of gold NPs reported movement in clusters of Au atoms when pumped by electron beams. This sub-Ångstrom microscopy was achieved using a modified VG Microscope HB501 STEM with an energy pumping beam of 120 keV (almost 60% the speed of light), while Au atoms were put onto a thin amorphous carbon substrate [5]. Figure 1.1 resembles the movements observed during the experiments. In Fig. 1.1(a) a sequence of images is shown where groups of 20-30 Au atoms that, happen to be close to a large Au island, coalesce. This pair of islands remained separated for almost 50 s under the beam, and then, during about 0.6 s, the smaller island moved toward the larger island, and merged with it. In Fig. 1.1(b) the coalescence between two 4-nm-diameter islands occur when a ×4 magnification in the illumination is performed.

Further experiments and theoretical calculations[1] were also reported in 2010 [7] related to the observation of electromagnetic forces in groups of nanoscale metallic particles, derived from the plasmonic response to the passage of a swift electron beam. In this experiments, the coalescence phenomena between Au NPs is suggested to be a function of electron's velocity and it's impact parameter (distance between the electron's trajectory and the studied sample).

---

[1]The first theoretical calculation regarding the interaction between fast electrons and metallic nanoparticles was reported in 1999 by Prof. Javier García de Abajo [6].
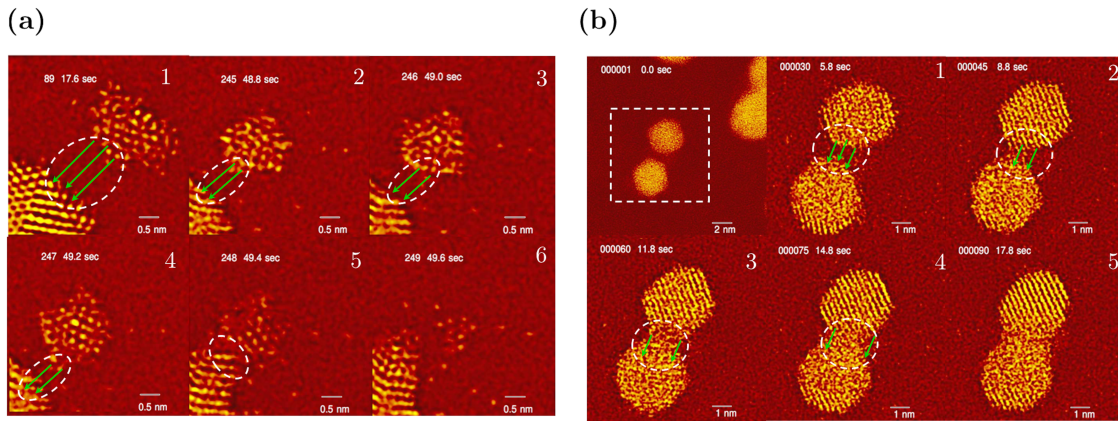
Figure 1.1. Two different experiments of Au NPs being pumped with an STEM electrons, showing the induced coalescence effects. (a) Shows a heterodimer composed of one $\sim 1\,\text{nm}$ diameter NP and a second NP of $\sim 5\,\text{nm}$ in diameter. (b) Shows a homodimer compose by similar Au NPs of $2\,\text{nm}$ in diameter each. The images were taken from [5].

Figure 1.2 exhibits the attractive and repulsive motion of a $1.5\,\text{nm}$ in diameter Au NP on amorphous carbon while being observed using two effective impact parameter in the pumped electron beam, $\sim 4.5\,\text{nm}$ and $\sim 1\,\text{nm}$. These images were obtained from [7], and were achieved using the same microscopy technique (STEM) as the one discussed previously for the movement of Au clusters reported in [5]. Figure 1.2(a) displays a sequence of images where a $1.5\,\text{nm}$ Au NP is attracted to the electron beam with an effective impact parameter of $\sim 4.5\,\text{nm}$. The movement of the $1.5\,\text{nm}$ Au NP is measured using a larger $\sim 5\,\text{nm}$ radius NP as reference. The conditions of the experiment were such that the scanning probe-pair geometry was chosen to minimize forces between the electron probe and the $\sim 5\,\text{nm}$ particle. On the other hand, Fig. 1.2(b) displays a sequence of images where now the $1.5\,\text{nm}$ Au NP is repelled from the electron beam when a zoom in the resolution of the image is performed. This zoom leads to a lower effective impact parameter of $\sim 1\,\text{nm}$, compared to $\sim 4.5\,\text{nm}$ used in Fig. 1.2(a).
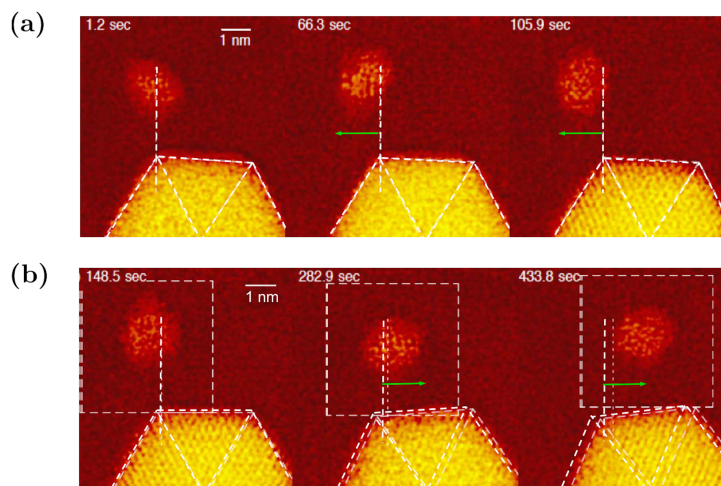

Figure 1.2. Time sequence of the position of a $1.5\,\text{nm}$ in diameter Au NP while interacting with an electron beam, using the vertical (white) dashed line as a reference. Figure (a) shows attraction to the electron beam for an effective impact parameter of $\sim 4.5\,\text{nm}$, and Figure (b) shows repulsion to the electron beam for an effective impact parameter of $\sim 1\,\text{nm}$. The images were taken from [7].

The theoretical model [Fig. 1.3(b)] used to describe the interaction between the electron beam and the nanoparticle cluster on one hand starts from considering the metallic island samples as a metallic non magnetic homogeneous sphere centered at origin, embedded in vacuum, with radius a and frequency dependent bulk dielectric function ϵ_i. On the other hand, the electron beam produced in STEM experiments is simulated as one electron, with charge e, traveling along the $\hat{z}$ direction with constant velocity $\mathbf{v}$ and impact parameter x_0. This model is in agreement with experimental results since the beam current in the STEM varied from 50-150 pA [8], which results in a mean pumped time for each electron of 1 ns, while the lifetime of bulk plasmons, for example in Au, are almost 1 fs as reported in [9]. Thus, when one pumped electron interacts with the sample, the plasmons and all other excitations vanishes when another electrons is approaching.

The scanning process within the microscopy technique is depicted in Fig. 1.3(a), where it is shown how the STEM form images by scanning the sample area (white lines) with a $x-y$ raster using, for example, scattered electron signals. The scanned area, encloses small target particles located within a larger neighborhood which may include other, non-moving large particles. At the beginning of each line in the scanned area, the electron beam is stopped for about 20% of the line time (waiting for a synchronization signal), producing an aloof beam current density with respect to the Au particle, schematically illustrated by the pencil-shaped probe in Fig. 1.3(a). Thus, the particles are influenced by the electron beam during $x-y$ scanning, but they also experience electric fields from a stopped beam, positioned at the beginning of each line, to the left of the scanned area. Therefore an effective impact parameter can be considered between the waiting line and the sample[2].
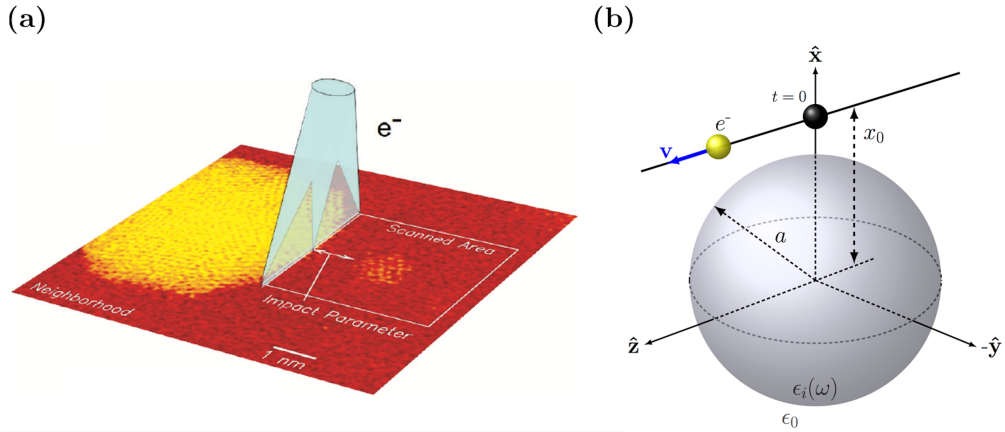

Figure 1.3. (a) represents a schematic diagram of the electron beam (cyan cone) pumped by the STEM over the scanned area (imaging a Au NP). (b) depicts a schematic diagram of the theoretical model for a metallic nanoparticle (grey sphere) with dielectric function $\epsilon_i(\omega)$, embedded in vacuum, interacting with an electron (yellow spot) traveling in the $\hat{z}$ direction with velocity $\mathbf{v}$ and impact parameter x_0.

---

[2]The largest contribution to the movement of the Au NPs is due to the electron beam standing by 20% of the time line, given that when the electron beam passes through the scanned area, the friction between the NP and the substrate prevents the sample to move.

Structure of the thesis

The thesis is divided into three main Chapters. Chapter 2 aims at providing the theoretical basis for calculating the linear momentum transfer as a function of frequency by means of the linear momentum conservation law in classical electrodynamics. The linear momentum transfer involves a spatial-surface and a frequency integral of Maxwell stress tensor composed by both, the electromagnetic field generated by the moving electron and the scattered field spread by the nanoparticle due to the presence of the electron, for this reason both fields are constructed in the frequency domain in the first two sections.

In Chapter 3 the theoretical part is then used to obtain a closed expression for the induced electric and magnetic fields, taking only into account the first multipole ($\ell = 1$) in the scattered field, named in this thesis as the *dipole approximation*. With this expression, an analytical approach to the Maxwell stress tensor surface integral is presented and pointed out that the total linear momentum transferred, from the electron to the nanoparticle, is determined only by two spectral contributions: the spectral contribution given solely by the electromagnetic field scattered by the nanoparticle and the spectral contribution given by the coupling between the electromagnetic field produced by the electron and the induced one.

Chapter 4 represents the essential outcome of the contribution of this dissertation. In this, numerical results concerning the total momentum transfer within the dipole approximation are discussed and furthermore, numerical comparisons between the latter and an approximation presented in [10], where the nanoparticle is modeled as a pure point-like dipole, are analyzed.

After the conclusions and outlooks, the last part of the thesis is dedicated to supplementary material, such as Appendices and cross-reference index. In Appendix A further calculations related to the extended Mie solution are presented in order to elucidate some key steps in the construction of the scattered electromagnetic field. Appendix B is devoted to prove, in a general covariant way, that the flux of the external (the one the electron produces) Maxwell stress tensor over a surface not intersecting the trajectory of the electron and integrated along the whole trajectory of the latter is equal to zero. Finally, in Appendix C, details of the Python program code are discussed and, in fact, the numerical code for the dipole approximation is exhibited.

A list of symbols is given at the beginning of this document to state the convention used along the research work.

THEORETICAL FRAMEWORK: SWIFT ELECTRON INTERACTING WITH A SPHERICAL NANOPARTICLE

The problem studied in this thesis corresponds to the theoretical analysis and numerical calculations of the total linear momentum transfer from a fast electron, like those typically used in STEM [5], to a single nanoparticle. In the theoretical approach to the problem, in the framework of classical electrodynamics, the following assumptions were taken: the nanoparticle was considered as a non magnetic homogeneous spherical particle centered at the origin, characterized by a bulk dielectric function, while the electron was assumed to travel, in an aloof trajectory, with constant velocity in a straight line. The electromagnetic field produced by the electron is obtained in the nanoparticle's frame of reference, for both time and frequency domain. And using an extended Mie solution, the scattered electromagnetic field spread by the spherical nanoparticle is obtained, in the frequency domain, through the scalar function method [6].

2.1 Electromagnetic field produced by the electron

In the problem addressed (a fast electron interacting with a spherical nanoparticle as shown in Fig. 1.3(b)) the electron transfers linear momentum to the NP via the electromagnetic field produced by the charged particle. At the same time, the electron induces charges and currents within the NP and as the result of this induction a second electromagnetic field appears along the region of interest: the space surrounding the NP. For these reasons, the electromagnetic field produced by the electron is taken as the external field source, while the electromagnetic field produced by the induced charges and currents is considered as the scattered—or induced—one by the NP, due to the presence of the electron.

The theoretical model considered is a spherical metallic nanoparticle with radius a, which is centered at origin and a particle traveling in straight-line along the $\hat{\mathbf{e}}_z$ direction with charge e, constant velocity $\mathbf{v} = v\hat{\mathbf{e}}_z$ and impact parameter x_0 with respect to the origin, Fig. 2.1. Thus, the electromagnetic field produced by the electron is equivalent to the field that a charge particle produces in it's own frame of reference and then "looked" in the NP's frame of reference.

Electromagnetic field in the time domain of the nanoparticle

Let us denote the NP's frame of reference by S and the electron's frame of reference by S', as it is shown in Fig. 2.1. According to the principle of relativity, the electromagnetic quantities
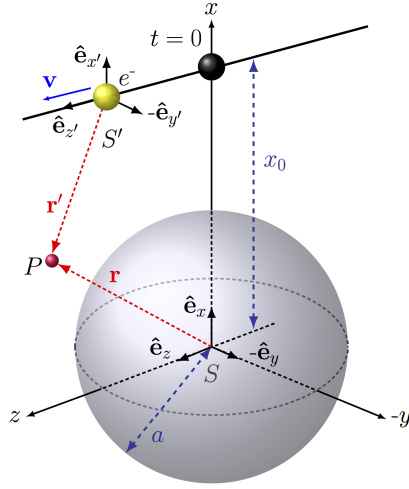
Figure 2.1. Schematic diagram of the two frames of references involved in the interaction electron-nanoparticle. S' stands for the frame of reference of the electron with constant velocity $\mathbf{v}$ and impact parameter x_0, while S stands for the frame of reference of the nanoparticle. Any space point P can be described in both frames of references: by $\mathbf{r}$ if it is looked from S or by $\mathbf{r}'$ if it is looked from S'.

(scalars, vectors and tensors) between both frames of reference S and S' are related via Lorentz transformations, given that the electron is traveling with constant velocity $\mathbf{v} = v\hat{\mathbf{e}}_z$ with respect to an observer in S. Then, the electric $\mathbf{E}(\mathbf{r};t)$ and magnetic $\mathbf{B}(\mathbf{r};t)$ fields in S as components of the electromagnetic field-strength[1] tensor $F^{\mu\nu}$ are related to the electric $\mathbf{E}'(\mathbf{r}';t')$ and magnetic $\mathbf{B}'(\mathbf{r}';t')$ fields in S' by [11]

$$F^{\mu\nu} = \Lambda^{\mu}_{\alpha'}\Lambda^{\nu}_{\beta'}F^{\alpha'\beta'}, \tag{2.1}$$

where $\Lambda^{\mu}_{\nu'}$ is the Lorentz transformation matrix between the reference frames S and S', given by [12]

$$\Lambda^{\mu}_{\nu'} = \frac{\partial x^{\mu}}{\partial x^{\nu'}} = \begin{pmatrix} \gamma & 0 & 0 & \gamma\beta \\ 0 & 1 & 0 & 0 \\ 0 & 0 & 1 & 0 \\ \gamma\beta & 0 & 0 & \gamma \end{pmatrix}, \tag{2.2}$$

with $x^{\mu} = (x^0, x^1, x^2, x^3) = (ct, x, y, z)$ and $x^{\nu'} = (x^{0'}, x^{1'}, x^{2'}, x^{3'}) = (ct', x', y', z')$ the position 4-vectors in S and S', respectively; c is the speed of light; $\gamma = 1/\sqrt{1-\beta^2}$ is the Lorentz factor and $\boldsymbol{\beta} = \mathbf{v}/c$ with $\mathbf{v}$ the electron's velocity, therefore $\beta = v/c$. Moreover, Faraday's matrix tensor referred to S' is given explicitly by [12]

$$F^{\mu'\nu'} = \begin{pmatrix} 0 & -E_{x'} & -E_{y'} & -E_{z'} \\ E_{x'} & 0 & -B_{z'} & B_{y'} \\ E_{y'} & B_{z'} & 0 & -B_{x'} \\ E_{z'} & -B_{y'} & B_{x'} & 0 \end{pmatrix}. \tag{2.3}$$

Thus, substituting Eqs. (2.2) and (2.3) into Eq. (2.1), it is straightforward to obtain the electromagnetic field-strength tensor in S system, if the electromagnetic field-strength tensor

---

[1] Also known as Faraday's tensor.

is known in S' system. When the matrix product $\Lambda^{\mu}_{\alpha'}\Lambda^{\nu}_{\beta'}F^{\alpha'\beta'}$ is computed, the electric and magnetic components in S and S' can be identified with the following relations

$$\mathbf{E}_{\perp} = \gamma\left(\mathbf{E}'_{\perp} - \boldsymbol{\beta} \times \mathbf{B}'\right), \tag{2.4a}$$

$$\mathbf{E}_{\parallel} = \mathbf{E}'_{\parallel}, \tag{2.4b}$$

$$\mathbf{B}_{\perp} = \gamma\left(\mathbf{B}'_{\perp} + \boldsymbol{\beta} \times \mathbf{E}'\right), \tag{2.4c}$$

$$\mathbf{B}_{\parallel} = \mathbf{B}'_{\parallel}, \tag{2.4d}$$

where the subindex "$\parallel$" stands for the component of the electric or magnetic fields parallel (longitudinal) to the electron's velocity, while the subindex "$\perp$" stands for the component of the electric or magnetic fields perpendicular (transverse) to the electron's velocity[2]. With this tool in hand is immediate to obtain the electromagnetic fields produced by the electron, traveling with constant velocity $\mathbf{v} = v\hat{\mathbf{e}}_z$, in the frame of reference of the NP. Since, in S' the electromagnetic field produced by the electron will be the same as the one produced by a static charged particle. Thus, in the field point P with coordinates $\mathbf{r}' = x'\hat{\mathbf{e}}_{x'} + y'\hat{\mathbf{e}}_{y'} + z'\hat{\mathbf{e}}_{z'}$, observed from S', the electromagnetic field produced by the electron, in CGS units, is

$$\mathbf{E}'(\mathbf{r}';t') = -\frac{e}{|\mathbf{r}'|^2}\,\hat{\mathbf{e}}_{r'} = -\frac{e}{\left[(x')^2 + (y')^2 + (z')^2\right]^{3/2}}\left[x'\hat{\mathbf{e}}_{x'} + y'\hat{\mathbf{e}}_{y'} + z'\hat{\mathbf{e}}_{z'}\right] \tag{2.5a}$$

and

$$\mathbf{B}'(\mathbf{r}';t') = \mathbf{0}, \tag{2.5b}$$

and according to Eqs. (2.4) the electromagnetic field produced by the electron in P but now observed from S is given by

$$\mathbf{E}_{\perp} = \gamma\mathbf{E}'_{\perp} = \gamma\left(\mathbf{E}_{x'} + \mathbf{E}_{y'}\right), \tag{2.6a}$$

$$\mathbf{E}_{\parallel} = \mathbf{E}_{z'}, \tag{2.6b}$$

$$\mathbf{B}_{\perp} = \gamma\,\boldsymbol{\beta} \times \mathbf{E}', \tag{2.6c}$$

$$\mathbf{B}_{\parallel} = \mathbf{0}, \tag{2.6d}$$

with $\mathbf{E}_{i'} = E_{i'}\,\hat{\mathbf{e}}_{i'}$ and $i' = \{x', y', z'\}$. However, Eqs. (2.6) are not the complete description of the electromagnetic field in P "looked" from S since $\mathbf{E}_{i'}$ is written in terms of the time t' and the position vector $\mathbf{r}'$ associated with an observer in S'. Denoting the time and position vector of P measured in S by t and $\mathbf{r} = x\,\hat{\mathbf{e}}_x + y\,\hat{\mathbf{e}}_y + z\,\hat{\mathbf{e}}_z$, respectively, the two spacetime events (t, P) and (t', P) are related via the Lorentz transformation

$$x^{\mu'} = \Lambda^{\mu'}_{\nu}x^{\nu}, \tag{2.7}$$

which in components reads

$$x' = x - x_0, \tag{2.8a}$$

$$y' = y, \tag{2.8b}$$

$$z' = \gamma(z - vt), \tag{2.8c}$$

---

[2]It must be noted that $\mathbf{E} = \mathbf{E}_{\parallel} + \mathbf{E}_{\perp}$ and $\mathbf{B} = \mathbf{B}_{\parallel} + \mathbf{B}_{\perp}$.

$$ct' = \gamma(ct - \beta z). \tag{2.8d}$$

Hence, substituting Eqs. (2.8) into Eqs. (2.5), in terms of t and $\mathbf{r}$, the electromagnetic field the electron produces in P viewed in its own frame of reference is

$$\mathbf{E}'(\mathbf{r};t) = -\frac{e}{[(x-x_0)^2 + (y)^2 + \gamma^2(z-vt)^2]^{3/2}} \left[(x-x_0)\hat{\mathbf{e}}_x + y\,\hat{\mathbf{e}}_y + \gamma(z-vt)\hat{\mathbf{e}}_z \right] \tag{2.9a}$$

and

$$\mathbf{B}'(\mathbf{r};t) = \mathbf{0}, \tag{2.9b}$$

where $\hat{\mathbf{e}}_{i'} = \hat{\mathbf{e}}_i$ as it is shown in Fig. 2.1. Finally, substituting Eqs. (2.9) into Eqs. (2.6) the electromagnetic field produced by the electron at P, observed from S, results in

$$\mathbf{E}^{ext}(\mathbf{r};t) = -\frac{e\gamma}{|(x,y,\gamma\,z) - (x_0,0,\gamma\,vt)|^3} \left[\mathbf{r} - (x_0,0,vt) \right], \tag{2.10a}$$

$$\mathbf{B}^{ext}(\mathbf{r};t) = -\frac{e\gamma}{|(x,y,\gamma\,z) - \gamma\,(x_0,0,vt)|^3} \boldsymbol{\beta} \times \left[(x,y,\gamma\,z) - (x_0,0,vt) \right]. \tag{2.10b}$$

Defining $R^2 = (x-x_0)^2 + y^2$, Eqs. (2.10) can be written in cartesian components as

$$E_x^{ext}(\mathbf{r};t) = -\frac{e\gamma}{[R^2 + \gamma^2(z-vt)^2]^{3/2}}(x-x_0), \tag{2.11a}$$

$$E_y^{ext}(\mathbf{r};t) = -\frac{e\gamma}{[R^2 + \gamma^2(z-vt)^2]^{3/2}}y, \tag{2.11b}$$

$$E_z^{ext}(\mathbf{r};t) = -\frac{e\gamma}{[R^2 + \gamma^2(z-vt)^2]^{3/2}}(z-vt), \tag{2.11c}$$

for the electric field, and for the magnetic field

$$B_x^{ext}(\mathbf{r};t) = \frac{e\gamma\beta}{[R^2 + \gamma^2(z-vt)^2]^{3/2}}y, \tag{2.12a}$$

$$B_y^{ext}(\mathbf{r};t) = -\frac{e\gamma\beta}{[R^2 + \gamma^2(z-vt)^2]^{3/2}}(x-x_0), \tag{2.12b}$$

$$B_z^{ext}(\mathbf{r};t) = 0. \tag{2.12c}$$

Electromagnetic field in the frequency domain: Fourier Transform

The total electromagnetic field in any region of the space corresponds to the superposition of the electromagnetic field produced by the fast electron ($\mathbf{E}^{ext}, \mathbf{H}^{ext}$) plus the electromagnetic field scattered by the nanoparticle ($\mathbf{E}^{scat}, \mathbf{H}^{scat}$) and, given that the scattered electromagnetic field will be obtained in Section 2.2 as function of frequency, it is essential to figure out the electromagnetic field produced by the electron in ω's space. The usual method to achieve the latter is through a time Fourier Transform[3] of each field, electric and magnetic.

---

[3]The time Fourier Transform will be performed in the nanoparticle's frame of reference. As must be noted, the time Fourier Transform of a function is not a covariant operation. A way to define it as Lorentz invariant is

The time Fourier Transform of a "well-behaved"[4] function $f(t) : \mathbb{R} \to \mathbb{R}$ is defined by [13]

$$f(\omega) = \int_{-\infty}^{\infty} f(t)\, e^{i\omega t}\, dt, \tag{2.13}$$

and its inverse is given by

$$f(t) = \frac{1}{2\pi} \int_{-\infty}^{\infty} f(\omega)\, e^{-i\omega t}\, d\omega. \tag{2.14}$$

Thus, the cartesian components of the time Fourier Transform for the electric field produced by the electron [Eqs. (2.11)], according to Eq. (2.13), are given by

$$E_x^{ext}(\mathbf{r}; \omega) = -e\gamma(x - x_0) \int_{-\infty}^{\infty} \frac{e^{i\omega t}}{[R^2 + \gamma^2(z - vt)^2]^{3/2}}\, dt, \tag{2.15a}$$

$$E_y^{ext}(\mathbf{r}; \omega) = -e\gamma y \int_{-\infty}^{\infty} \frac{e^{i\omega t}}{[R^2 + \gamma^2(z - vt)^2]^{3/2}}\, dt, \tag{2.15b}$$

$$E_z^{ext}(\mathbf{r}; \omega) = -e\gamma \int_{-\infty}^{\infty} \frac{e^{i\omega t}}{[R^2 + \gamma^2(z - vt)^2]^{3/2}}\, (z - vt)\, dt, \tag{2.15c}$$

and for the magnetic field [Eqs. (2.12)] are given by

$$B_x^{ext}(\mathbf{r}; \omega) = e\gamma\beta y \int_{-\infty}^{\infty} \frac{e^{i\omega t}}{[R^2 + \gamma^2(z - vt)^2]^{3/2}}\, dt, \tag{2.16a}$$

$$B_y^{ext}(\mathbf{r}; \omega) = -e\gamma\beta(x - x_0) \int_{-\infty}^{\infty} \frac{e^{i\omega t}}{[R^2 + \gamma^2(z - vt)^2]^{3/2}}\, dt, \tag{2.16b}$$

$$B_z^{ext}(\mathbf{r}; \omega) = 0. \tag{2.16c}$$

Now, using the change of variable $\eta = \gamma(z - vt)/R$, Eqs. (2.15) and (2.16) can be rewritten as follows

$$E_x^{ext}(\mathbf{r}; \omega) = -\frac{e}{R^2\, v}(x - x_0)\, e^{i\omega z/v} F_1\left(\frac{\omega R}{v\gamma}\right), \tag{2.17a}$$

$$E_y^{ext}(\mathbf{r}; \omega) = -\frac{e}{R^2\, v}\, y\, e^{i\omega z/v} F_1\left(\frac{\omega R}{v\gamma}\right), \tag{2.17b}$$

$$E_z^{ext}(\mathbf{r}; \omega) = -\frac{e}{R\, v\gamma}\, e^{i\omega z/v} F_2\left(\frac{\omega R}{v\gamma}\right), \tag{2.17c}$$

and

$$B_x^{ext}(\mathbf{r}; \omega) = \frac{e\,\beta}{R^2\, v}\, y\, e^{i\omega z/v} F_1\left(\frac{\omega R}{v\gamma}\right), \tag{2.18a}$$

---

presented in [14], where the Fourier Transform takes also into account the spatial coordinates as

$$f(k) = \int_{\mathbb{R}^{1,3}} f(x) e^{ik_\mu x^\mu}\, d^4 x,$$

where $\mathbb{R}^{1,3}$ is the Minkowski spacetime, $k^\mu = (\omega/c, \mathbf{k})$ is the wave 4-vector and $d^4 x$ is the Lorentz invariant 4-volume element.

[4]A well-behaved function [15] is the one that is differentiable everywhere any number of times and such that it and all its derivatives are $O(|x|^{-N})$ as $|x| \to \infty$ for all $N \in \mathbb{N}$.

$$B_y^{ext}(\mathbf{r};\omega) = -\frac{e\,\beta}{R^2\,v}(x - x_0)\,e^{i\omega z/v}F_1\left(\frac{\omega R}{v\gamma}\right), \tag{2.18b}$$

$$B_z^{ext}(\mathbf{r};\omega) = 0, \tag{2.18c}$$

where

$$F_1\left(\frac{\omega R}{v\gamma}\right) = \int_{-\infty}^{\infty} e^{-i(\omega R/v\gamma)\eta}\,f_1(\eta)\,d\eta \quad \text{and} \quad F_2\left(\frac{\omega R}{v\gamma}\right) = \int_{-\infty}^{\infty} e^{-i(\omega R/v\gamma)\eta}\,f_2(\eta)\,\eta\,d\eta, \tag{2.19}$$

can be thought as the inverse Fourier Transform of functions $f_1(\eta) = 1/(1+\eta^2)^{3/2}$ and $f_2(\eta) = \eta/(1+\eta^2)^{3/2}$ with respect to the variables $\xi = \omega R/v\gamma$ and η. In addition, functions $f_1(\eta)$ and $f_2(\eta)$ obey the following relations

$$f_1(\eta) = -\frac{1}{\eta}\frac{d}{d\eta}\left[\frac{1}{(1+\eta^2)^{1/2}}\right] \quad \text{and} \quad f_2(\eta) = -\frac{d}{d\eta}\left[\frac{1}{(1+\eta^2)^{1/2}}\right]. \tag{2.20}$$

Hence, Eqs. (2.19) read as

$$
\begin{aligned}
F_1(\xi) &= -\int_{-\infty}^{\infty}\frac{1}{\eta}\frac{d}{d\eta}\left[\frac{1}{(1+\eta^2)^{1/2}}\right]e^{-i\xi\eta}\,d\eta \\
&= i\int\int_{-\infty}^{\infty}\frac{d}{d\eta}\left[\frac{1}{(1+\eta^2)^{1/2}}\right]e^{-i\xi\eta}\,d\eta\,d\xi \\
&= -i\int F_2(\xi)\,d\xi
\end{aligned} \tag{2.21}
$$

and

$$
\begin{aligned}
F_2(\xi) &= -\int_{-\infty}^{\infty}\frac{d}{d\eta}\left[\frac{1}{(1+\eta^2)^{1/2}}\right]e^{-i\xi\eta}\,d\eta \\
&= -\underbrace{\left.\frac{e^{-i\xi\eta}}{(1+\eta^2)^{1/2}}\right|_{\eta=-\infty}^{\eta=\infty}}_{=0} -i\xi\int_{-\infty}^{\infty}\left[\frac{1}{(1+\eta^2)^{1/2}}\right]e^{-i\xi\eta}\,d\eta \\
&= -i\xi\int_{-\infty}^{\infty}\frac{e^{-i\xi\eta}}{(1+\eta^2)^{1/2}}\,d\eta.
\end{aligned} \tag{2.22}
$$

From [16][5], it is known that

$$\int_{-\infty}^{\infty}\frac{e^{\frac{\nu}{\sinh\eta}}}{(1+\eta^2)^{1/2}}\,e^{-i\xi\eta}\,d\eta \overset{|Re(\nu)|<1}{=} \begin{cases} 2e^{-\frac{1}{2}\nu\pi i}\,K_\nu(\xi) & \text{if } \xi > 0, \\ -2e^{\frac{1}{2}\nu\pi i}\,K_\nu(-\xi) & \text{if } \xi < 0. \end{cases}, \tag{2.23}$$

with K_ν the modified Bessel functions of the second kind. Thus, taking $\nu = 0$ in Eq. (2.23) it follows that

$$\int_{-\infty}^{\infty}\frac{e^{-i\xi\eta}}{(1+\eta^2)^{1/2}}\,d\eta = \begin{cases} 2\,K_0(\xi) & \text{if } \xi > 0, \\ 2\,K_0(-\xi) & \text{if } \xi < 0 \end{cases} = 2\,K_0(|\xi|). \tag{2.24}$$

---

[5]It is important to highlight that Eq. (2.23) as written in [16] is mistaken. Since integral in Eq. (2.23) for $\xi > 0$ results in $2e^{-\frac{1}{2}\nu\pi i}\,K_\nu(\xi)$, as can be obtained from [17], Eq. (9.6.21), which states that

$$K_0(\xi) = \int_0^{\infty}\frac{\cos(\xi\eta)}{(1+\eta^2)^{1/2}}\,d\eta = \frac{1}{2}\int_{-\infty}^{\infty}\frac{e^{-i\xi\eta}}{(1+\eta^2)^{1/2}}\,d\eta,$$

where the last equality follows from the even and odd parity of the cosine and sine functions, respectively.

Then, substituting Eq. (2.24) into Eq. (2.22), the function $F_2(\xi)$ yields

$$F_2(\xi) = -i\,2\,\xi K_0(|\xi|),$$

(2.25)

and substituting $F_2(\xi)$ into Eq. (2.21) the function $F_1(\xi)$ results in the following integral

$$F_1(\xi) = -2\int \xi\,K_0(|\xi|)\,d\xi,$$

(2.26)

which can be solved using the relation fulfilled in general by modified Bessel functions K_0 of the second kind [18]

$$\int \xi\,K_0(|\xi|)\,d\xi = -|\xi|\,K_1(|\xi|).$$

(2.27)

So using relation (2.27) into Eq. (2.26), function $F_1(\xi)$ yields

$$F_1(\xi) = -2\int \xi\,K_0(|\xi|)\,d\xi, = 2\,|\xi|\,K_1(|\xi|).$$

(2.28)

Finally, substituting Eqs. (2.25) and (2.28) into Eqs. (2.17) and (2.18), turns out that the electromagnetic field produced by the electron (in the reference frame of the NP) in the frequency domain is given by

$$E_x^{ext}(\mathbf{r};\omega) = -\frac{2\,e}{R\,v^2\gamma}\,|\omega|\,e^{i\omega z/v}K_1\left(\frac{|\omega|R}{v\gamma}\right)(x-x_0),$$

(2.29a)

$$E_y^{ext}(\mathbf{r};\omega) = -\frac{2\,e}{R\,v^2\gamma}\,|\omega|\,e^{i\omega z/v}K_1\left(\frac{|\omega|R}{v\gamma}\right)y,$$

(2.29b)

$$E_z^{ext}(\mathbf{r};\omega) = i\frac{2\,e}{v^2\gamma^2}\,\omega\,e^{i\omega z/v}K_0\left(\frac{|\omega|R}{v\gamma}\right),$$

(2.29c)

for the electric field components, and for the magnetic field components

$$B_x^{ext}(\mathbf{r};\omega) = -\frac{2\,e\,\beta}{R\,v^2\gamma}\,|\omega|\,e^{i\omega z/v}K_1\left(\frac{|\omega|R}{v\gamma}\right)y,$$

(2.30a)

$$B_y^{ext}(\mathbf{r};\omega) = \frac{2\,e\,\beta}{R\,v^2\gamma}\,|\omega|\,e^{i\omega z/v}K_1\left(\frac{|\omega|R}{v\gamma}\right)(x-x_0),$$

(2.30b)

$$B_z^{ext}(\mathbf{r};\omega) = 0.$$

(2.30c)

Both expressions can be summarized in vector notation as

$$\mathbf{E}^{ext}(\mathbf{r};\omega) = -\frac{2e\omega}{v^2\gamma}e^{i\omega\frac{z}{v}}\left\{\left[\frac{\text{sgn}(\omega)}{R}K_1\left(\frac{|\omega|R}{v\gamma}\right)\right][(x-x_0)\hat{\mathbf{e}}_x + y\hat{\mathbf{e}}_y] - \frac{i}{\gamma}K_0\left(\frac{|\omega|R}{v\gamma}\right)\hat{\mathbf{e}}_z\right\},$$

(2.31a)

$$\mathbf{B}^{ext}(\mathbf{r};\omega) = \frac{2e\beta}{Rv^2\gamma}|\omega|e^{i\omega\frac{z}{v}}K_1\left(\frac{|\omega|R}{v\gamma}\right)[y\hat{\mathbf{e}}_x - (x-x_0)\hat{\mathbf{e}}_y],$$

(2.31b)

where sgn stands for the sign function. In Figs. 2.2, we show the modulus for each component (in cartesian coordinates) of the electric and magnetic fields produced by the electron as a function

of frequency. The plots correspond to the external electromagnetic field in the space coordinates $\mathbf{r} = (0, 1, 0)$ nm, considering the electron traveling with velocity 0.5c in the $\hat{\mathbf{z}}$ direction and with an impact parameter of 5 nm. The electric and magnetic fields are expressed in atomic units, whereas the frequency is expressed in eV.
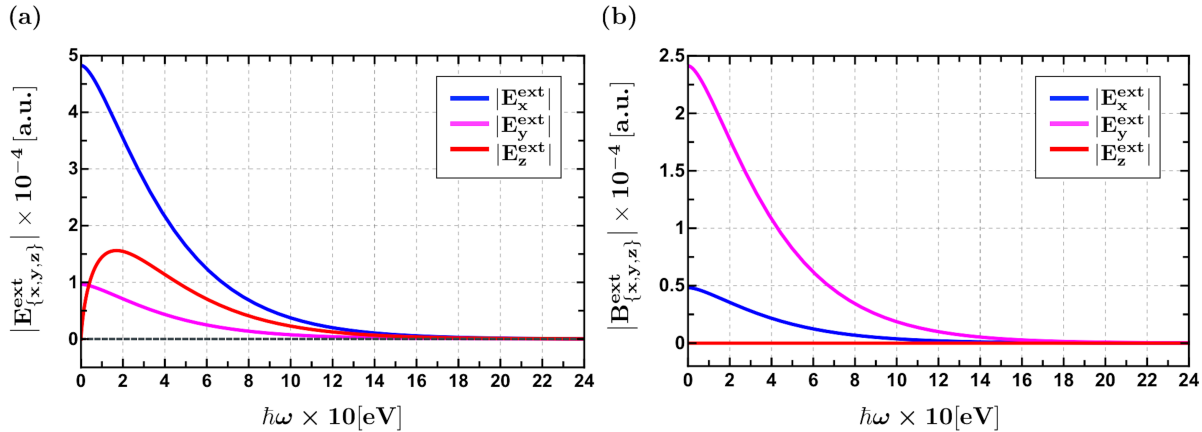
(a)   **(b)**

Figure 2.2. Plots of the magnitude of (a) the electric field and (b) the magnetic field components produced by an electron (traveling with constant velocity 0.5c in the $\hat{\mathbf{z}}$ direction and 5 nm impact parameter) versus frequency. The fields are evaluated in the field point $\mathbf{r} = (0, 1, 0)$ nm.

2.2   Electromagnetic field scattered by the nanoparticle: an extended Mie solution

The NP theoretically modeled as a sphere rather naturally invites to describe the scattered field due to the presence of the electron in a similar way such as Mie theory[6] is addressed. However, the electromagnetic field produced by the electron is not a single plane wave with a defined frequency, but a superposition of infinite plane waves as Fig. 2.2 indicates. This is the reason why an extended Mie solution which takes into account more than one monochromatic plane wave must be considered to calculate the scattered electromagnetic field by the NP in the presence of the electron. Nowadays, Mie solution is understood as the exact solution for the absorption and scattering by a sphere with arbitrary radius and dielectric function ϵ embedded in a linear, isotropic, homogeneous medium illuminated with a plane monochromatic wave. The outline of the solution is as follows: construct vector harmonics $\mathbf{N}$ and $\mathbf{M}$, and a generating function ψ, which satisfy [13]

$$\nabla^2\psi + k^2\psi = 0, \tag{2.32a}$$

$$\mathbf{M} = \nabla \times (\mathbf{r}\psi), \tag{2.32b}$$

$$\mathbf{N} = \frac{\nabla \times \mathbf{M}}{k}; \tag{2.32c}$$

with $k = \omega/c$ the magnitude of the wave vector. Then, seek for solutions of the generating function convenient to the symmetry involved. That is, look for ψ (satisfying Helmholtz equation) in spherical coordinates and construct with Eqs. (2.32a) and (2.32b) the vector harmonics $\mathbf{N}$ and

---

[6]In fact, Mie theory is the solution of Maxwell's equations for an incident plane wave on a sphere. Thus, it should be strictly referred to, as Mie solution.

M[7]. Due to linear independence and completeness of vector harmonics, the incident plane wave, the scattered and the inside of the sphere electromagnetic fields are expanded as a superposition of **N** and **M**, where in addition the time dependence of the fields are assumed to be the same as the incident wave, harmonic. Thus, imposing boundary conditions between the sphere and the surrounding medium the expansion coefficients are determined for the electromagnetic field inside the sphere and the scattered one, which at the same time give rise to a close solution for the Mie problem.

In order to tackle down the extended Mie solution, it shall be considered as a fundamental block of the solution the steps followed to solve Mie problem. For instance, it is convenient to expand the incident electromagnetic field (the one the electron produces), the scattered field and field inside the NP in vector multipoles. According to Helmholtz theorem, any smooth vector field $\mathbf{F}(\mathbf{r})$ can be expanded into two orthogonal projections (longitudinal and transverse) [19]

$$\mathbf{F}(\mathbf{r}) = \nabla\psi_1(\mathbf{r}) + \nabla\times\mathbf{Q}. \tag{2.33}$$

The transverse component $\nabla\times\mathbf{Q}$ can also be separated into two orthogonal projections as[8] [20]

$$\mathbf{F}(\mathbf{r}) = \nabla\psi_1(\mathbf{r}) + \mathbf{L}\psi_2(\mathbf{r}) - i\nabla\times\mathbf{L}\psi_3(\mathbf{r}), \tag{2.34}$$

where $\mathbf{L} = -i\mathbf{r}\times\nabla$ stands for the quantum mechanical orbital-angular momentum operator. Since $\{\nabla, \mathbf{L}, -i\nabla\times\mathbf{L}\}$ constitute a set of three orthogonal operators [20], $\psi_1(\mathbf{r})$, $\psi_2(\mathbf{r})$ and $\psi_3(\mathbf{r})$ can be calculated projecting $\mathbf{F}(\mathbf{r})$ in each direction. In other words

$$\nabla\cdot\mathbf{F}(\mathbf{r}) = \nabla^2\psi_1(\mathbf{r}), \tag{2.35a}$$

$$\mathbf{L}\cdot\mathbf{F}(\mathbf{r}) = \mathbf{L}^2\psi_2(\mathbf{r}), \tag{2.35b}$$

$$-i(\mathbf{L}\times\nabla)\cdot\mathbf{F}(\mathbf{r}) = (\nabla\times\mathbf{L})\cdot(\nabla\times\mathbf{L})\psi_3(\mathbf{r}) = \nabla^2\mathbf{L}^2\psi_3(\mathbf{r}). \tag{2.35c}$$

With this tool in hand, the electric field can be decomposed into three scalar functions as

$$\boxed{\mathbf{E}(\mathbf{r};\omega) = \nabla\psi^L(\mathbf{r};\omega) + \mathbf{L}\psi^M(\mathbf{r};\omega) - \frac{i}{k}\nabla\times\mathbf{L}\psi^E(\mathbf{r};\omega)} \tag{2.36}$$

where L stands for longitudinal, M for magnetic and E for electric. Moreover, according to Eqs. (2.35)

$$\boxed{\nabla^2\psi^L(\mathbf{r};\omega) = \nabla\cdot\mathbf{E}(\mathbf{r};\omega) = 4\pi\rho(\mathbf{r};\omega),} \tag{2.37a}$$

$$\mathbf{L}^2\psi^M(\mathbf{r};\omega) = \mathbf{L}\cdot\mathbf{E}(\mathbf{r};\omega), \tag{2.37b}$$

$$\nabla^2\mathbf{L}^2\psi^E(\mathbf{r};\omega) = -ik(\mathbf{L}\times\nabla)\cdot\mathbf{E}(\mathbf{r};\omega). \tag{2.37c}$$

Thus, Eq. (2.37a) establishes the instant propagation of the longitudinal modes, since Laplace equation does not take into account any retardation effects, and as consequence, leading to

---

[7]Since separation of variables is the method commonly used to solve Helmholtz equation in different coordinates systems, the generating function and the vector harmonics will generally appear as a superposition of solutions of the partial differential equation. Then, **M** and **N** inherit the linear independence and completeness of the set of solutions for ψ.

[8]In the case of Mie solution the three orthogonal projections correspond to $\nabla\psi$, **M** and **N**.

instant propagation in Eq. (2.37c) since outside the charge distribution $\nabla^2 \psi^E = 0$ once $\nabla^2 \psi^L = 0$. Hence, longitudinal modes are explicitly left out imposing $\psi^L = 0$, whereas in vacuum, free of charge and currents, the transverse scalar functions ψ^M and ψ^E obey Helmholtz equation [6]

$$\nabla^2 \psi^{\{E,M\}}(\mathbf{r};\omega) + k^2 \psi^{\{E,M\}}(\mathbf{r};\omega) = 0, \tag{2.38}$$

since in vacuum, the electromagnetic field satisfy Helmholtz equation. So using the fact that ∇^2 and $\mathbf{L}^2$ commutes[9], Eqs. (2.37b) and (2.37c) read

$$\psi^M(\mathbf{r};\omega) = \frac{1}{L^2}\mathbf{L}\cdot\mathbf{E}(\mathbf{r};\omega), \tag{2.39a}$$

$$\psi^E(\mathbf{r};\omega) = \frac{i}{k}\frac{1}{L^2}(\mathbf{L}\times\nabla)\cdot\mathbf{E}(\mathbf{r};\omega). \tag{2.39b}$$

with $L^2 = \ell(\ell+1)$ the eigenvalues of $\mathbf{L}^2$ operator.

On the other hand, substituting Faraday-Henry-Lenz law $\nabla \times \mathbf{E}(\mathbf{r};\omega) = ik\mathbf{H}(\mathbf{r};\omega)$ into Eq. (2.36), the magnetic field results in

$$\mathbf{H} = -\frac{i}{k}\nabla\times\mathbf{L}\psi^M - \frac{1}{k^2}\nabla\times\left[\nabla\times\mathbf{L}\psi^E\right] = -\frac{i}{k}\nabla\times\mathbf{L}\psi^M + \frac{1}{k^2}\nabla^2\mathbf{L}\psi^E. \tag{2.40}$$

Using Eq. (2.38) and the commutation relation between ∇^2 and $\mathbf{L}$, the magnetic field can be rewritten as

$$\mathbf{H}(\mathbf{r};\omega) = -\frac{i}{k}\nabla\times\mathbf{L}\psi^M(\mathbf{r};\omega) - \mathbf{L}\psi^E(\mathbf{r};\omega). \tag{2.41}$$

Equations (2.36), (2.39) and (2.41) gives rise to a recipe for calculating the electromagnetic fields in the absence of charges and currents once the two transverse scalar functions ψ^M and ψ^E are known. This procedure is known as the scalar function method. Now, as it is of interest to expand in vector multipoles the electromagnetic field produced by the swift electron, it is worth noting that the external electromagnetic field has to be made up of spherical waves with no net flux, since a particle with constant velocity gives no radiation. Thus, the scalar functions which describe this external field must have the following form [6]

$$\psi^{M,ext}(\mathbf{r};\omega) = \sum_{\ell=1}^{\infty}\sum_{m=-\ell}^{\ell} i^\ell j_\ell(kr)Y_{\ell m}(\Omega_\mathbf{r})\psi_{\ell,m}^{M,ext}, \tag{2.42}$$

$$\psi^{E,ext}(\mathbf{r};\omega) = \sum_{\ell=1}^{\infty}\sum_{m=-\ell}^{\ell} i^\ell j_\ell(kr)Y_{\ell m}(\Omega_\mathbf{r})\psi_{\ell,m}^{E,ext}, \tag{2.43}$$

where j_ℓ are the spherical Bessel functions, $(r,\Omega_\mathbf{r})$ are the spherical coordinates of $\mathbf{r}$, $Y_{\ell m}$ are the scalar spherical harmonics functions and $\psi_{\ell,m}^{M,ext}$, $\psi_{\ell,m}^{E,ext}$ are expansion coefficients to be determined. Equations (2.42) and (2.43) are only fulfilled within free of charges and currents regions, in particular they will be satisfied in the region between the NP and the electron trajectory. That is, for $a < r < x_0 - a$, as it was discussed in Section 2.3.

---

[9]In [21] it is shown that $[L_i, p_j] = i\epsilon_{ijk}p^k$ in atomic units, where $\mathbf{p} = -i\nabla$ is the linear momentum operator and ϵ_{ijk} is the Levi-Civita symbol. Thus, $[\mathbf{L}^2,\mathbf{p}^2] = 2i\epsilon_{ijk}(L^i p^j p^k + p^j p^k L^i) = 2i\epsilon_{ijk}T^{ijk}$, but tensor T^{ijk} is symmetric in the last two indices therefore $[\mathbf{L}^2,\mathbf{p}^2] = 0$. Analogously, $[L_i,\mathbf{p}^2] = 2i\epsilon_{ijk}p^j p^k = 0$.

On the other side, transverse scalar functions $\psi^{M,ext}(\mathbf{r})$ and $\psi^{E,ext}(\mathbf{r})$ can be obtained from Eq. (A.19) which establishes that the external electric field can be written in atomic units as

$$\mathbf{E}^{ext}(\mathbf{r};\omega) = \left(\nabla - \frac{i\,\omega\mathbf{v}}{c^2}\right) \int_{-\infty}^{\infty} e^{i\omega t}\, G_0(\mathbf{r} - \mathbf{r}_t)\, dt, \tag{2.44}$$

where G_0 is the Green function of Helmholtz equation and $\mathbf{r}_t = (x_0, 0, vt)$ is the electron's position vector. Now, expanding the Green function of Helmholtz equation in multipoles, substituting this expansion into Eq. (2.44) and using Eqs. (2.39), it is found in [6] that

$$\psi_{\ell,m}^{M,ext} = -\frac{4\pi i^{1-\ell}kv}{c^2} \frac{mA_{\ell m}^+}{\ell(\ell+1)} K_m\left(\frac{\omega x_0}{v\gamma}\right), \tag{2.45a}$$

$$\psi_{\ell,m}^{E,ext} = -\frac{2\pi i^{1-\ell}k}{c\gamma} \frac{B_{\ell m}}{\ell(\ell+1)} K_m\left(\frac{\omega x_0}{v\gamma}\right), \tag{2.45b}$$

by a comparison between the multipole expansion of Eq. (2.44) and its analytical solution. Moreover, $A_{\ell,m}^+$ and $B_{\ell,m}$ are coefficients given by

$$A_{\ell,m}^+ = \frac{1}{\beta^{\ell+1}} \sum_{j=m}^{\ell} \frac{(i)^{\ell-j}(2\ell+1)!!\,\alpha_{\ell,m}}{\gamma^j\, 2^j\,(\ell-j)!\left[\frac{j-m}{2}\right]!\left[\frac{j+m}{2}\right]!} I_{j,\ell-j}^{\ell,m}, \tag{2.46a}$$

$$B_{\ell,m} = A_{\ell,m+1}^+\sqrt{(\ell+m+1)(\ell-m)} - A_{\ell,m-1}^+\sqrt{(\ell-m+1)(\ell+m)}, \tag{2.46b}$$

with $(2\ell+1)!! = (2\ell+1)(2\ell-1)(2\ell-3)\cdots 3\cdot 1$ the double factorial[10] of $(2\ell+1)$,

$$\alpha_{\ell,m} = \sqrt{\frac{2\ell+1}{4\pi}\frac{(\ell-m)!}{(\ell+m)!}}, \tag{2.47}$$

and $I_{j,\ell-j}^{\ell,m}$ are numbers satisfying the following recurrence relation

$$(\ell-m)\,I_{i_1,i_2}^{\ell,m} = (2\ell-1)\,I_{i_1,i_2+1}^{\ell-1,m} - (\ell+m-1)\,I_{i_1,i_2}^{\ell-2,m}, \tag{2.48}$$

with initial values $I_{i_1,i_2}^{m-1,m} = 0$, $I_{i_1,i_2}^{m-2,m} = 0$ and

$$I_{i_1,i_2}^{m,m} = \begin{cases} (-1)^m (2m-1)!!\, B\left(\frac{i_1+m+2}{2}, \frac{i_2+1}{2}\right), & \text{if } i_2 \text{ is even} \\ 0, & \text{if } i_2 \text{ is odd}, \end{cases} \tag{2.49}$$

where $B(z,u)$ is the Beta function. Further details of these calculations are shown in Appendix A.

In the same way, scalar functions corresponding to the scattered electromagnetic field by the NP, by means of the scalar method, can be expanded into spherical waves with the restriction that they must be a combination of only outgoing spherical waves [6]. In other words,

$$\psi^{M,scat}(\mathbf{r};\omega) = \sum_{\ell=1}^{\infty} \sum_{m=-\ell}^{\ell} i^\ell h_\ell^{(+)}(kr) Y_{\ell m}(\Omega_{\mathbf{r}}) \psi_{\ell,m}^{M,scat}, \tag{2.50}$$

---

[10]The double factorial of negative arguments can be performed via the recurrence relation $n!! = n\cdot(n-2)!!$

$$\psi^{E,\,scat}(\mathbf{r};\omega) = \sum_{\ell=1}^{\infty} \sum_{m=-\ell}^{\ell} i^{\ell} h_{\ell}^{(+)}(kr) Y_{\ell m}(\Omega_{\mathbf{r}}) \psi_{\ell,m}^{E,\,scat}. \tag{2.51}$$

with $h_{\ell}^{(+)}$ the spherical Hankel functions of the first kind multiplied by the imaginary unit i, as defined in [22]. Thus, applying boundary conditions to the external and the scattered electromagnetic field (for a spherically symmetric medium) it is found that

$$\psi_{\ell,m}^{M,\,scat} = t_{\ell}^{M} \psi_{\ell,m}^{M,\,ext}, \tag{2.52a}$$

$$\psi_{\ell,m}^{E,\,scat} = t_{\ell}^{E} \psi_{\ell,m}^{E,\,ext}, \tag{2.52b}$$

with

$$t_{\ell}^{E} = \frac{\epsilon_i \, j_{\ell}\left(x_i\right) \left[x \, j_{\ell}\left(x\right)\right]' - j_{\ell}\left(x\right)\left[x_i \, j_{\ell}\left(x_i\right)\right]'}{h_{\ell}^{(+)}\left(x\right)\left[x_i \, j_{\ell}\left(x_i\right)\right]' - \epsilon_i \, j_{\ell}\left(x_i\right)\left[x \, h_{\ell}^{(+)}\left(x\right)\right]'}, \tag{2.53a}$$

$$t_{\ell}^{M} = \frac{j_{\ell}\left(x_i\right)\left[x \, j_{\ell}\left(x\right)\right]' - j_{\ell}\left(x\right)\left[x_i \, j_{\ell}\left(x_i\right)\right]'}{h_{\ell}^{(+)}\left(x\right)\left[x_i \, j_{\ell}\left(x_i\right)\right]' - j_{\ell}\left(x_i\right)\left[x \, h_{\ell}^{(+)}\left(x\right)\right]'}, \tag{2.53b}$$

where $x = ka = \omega a \sqrt{\epsilon\mu}$ is the size parameter, $x_i = x\sqrt{\epsilon_i}$ and ϵ, μ stand for the permittivity and permeability, respectively, of the medium where the sphere is embedded. The prime symbol denotes derivative with respect to the argument.

In this manner, Eqs. (2.45) and (2.52)—together with the multipole expansions of $\psi_{\ell,m}^{M,\,ext}$, $\psi_{\ell,m}^{M,\,scat}$ and $\psi_{\ell,m}^{E,\,ext}$, $\psi_{\ell,m}^{E,\,scat}$—describe the external and induced electromagnetic fields in terms of spherical waves, as it was pursued in order to achieve the prescription set up by Mie solution. Therefore, both external and induced fields can be calculated using Eqs. (2.36) and (2.41). In particular, the scattered electromagnetic field in spherical coordinates results in [23]

$$
\begin{aligned}
\mathbf{E}^{scat}\left(\mathbf{r};\omega\right) = \sum_{\ell=1}^{\infty} \sum_{m=-\ell}^{\ell} e^{im\varphi} \Bigg\{ & \hat{\mathbf{e}}_r \, D_{\ell,m}^{E} \, \ell\left(\ell+1\right) P_{\ell}^{m}\left(\cos\theta\right) \frac{h_{\ell}^{(+)}(k_0 r)}{k_0 r} \\
& - \hat{\mathbf{e}}_{\theta} \Bigg[C_{\ell,m}^{M} \frac{m}{\sin\theta} h_{\ell}^{(+)}(k_0 r) P_{\ell}^{m}\left(\cos\theta\right) + D_{\ell,m}^{E} \Bigg(\left(\ell+1\right) \frac{\cos\theta}{\sin\theta} P_{\ell}^{m}\left(\cos\theta\right) \\
& - \frac{\left(\ell-m+1\right)}{\sin\theta} P_{\ell+1}^{m}\left(\cos\theta\right) \Bigg) \Bigg(\left(\ell+1\right) \frac{h_{\ell}^{(+)}(k_0 r)}{k_0 r} - h_{\ell+1}^{(+)}(k_0 r) \Bigg) \Bigg] \\
& + (i)\,\hat{\mathbf{e}}_{\varphi} \Bigg[C_{\ell,m}^{M} h_{\ell}^{(+)}(k_0 r) \Bigg(\left(\ell+1\right) \frac{\cos\theta}{\sin\theta} P_{\ell}^{m}\left(\cos\theta\right) - \frac{\left(\ell-m+1\right)}{\sin\theta} \\
& \times P_{\ell+1}^{m}\left(\cos\theta\right) \Bigg) + D_{\ell,m}^{E} \frac{m}{\sin\theta} P_{\ell}^{m}\left(\cos\theta\right) \Bigg(\left(\ell+1\right) \frac{h_{\ell}^{(+)}\left(k_0 r\right)}{k_0 r} \\
& - h_{\ell+1}^{(+)}\left(k_0 r\right) \Bigg) \Bigg] \Bigg\},
\end{aligned}
\tag{2.54}
$$

and

$$
\begin{aligned}
\mathbf{H}^{scat}(\mathbf{r};\omega) = \sum_{\ell=1}^{\infty} \sum_{m=-\ell}^{\ell} e^{im\varphi} \Bigg\{ & \hat{\mathbf{e}}_r \, C_{\ell,m}^M \, \ell\,(\ell+1)\, P_\ell^m(\cos\theta)\, \frac{h_\ell^{(+)}(k_0 r)}{k_0 r} \\
& + \hat{\mathbf{e}}_\theta \Bigg[D_{\ell,m}^E \, \frac{m}{\sin\theta}\, h_\ell^{(+)}(k_0 r)\, P_\ell^m(\cos\theta) - C_{\ell,m}^M \Bigg((\ell+1)\,\frac{\cos\theta}{\sin\theta}\, P_\ell^m(\cos\theta) \\
& - \frac{(\ell-m+1)}{\sin\theta}\, P_{\ell+1}^m(\cos\theta) \Bigg) \Bigg((\ell+1)\,\frac{h_\ell^{(+)}(k_0 r)}{k_0 r} - h_{\ell+1}^{(+)}(k_0 r) \Bigg) \Bigg] \\
& + (i)\, \hat{\mathbf{e}}_\varphi \Bigg[C_{\ell,m}^M \, \frac{m}{\sin\theta}\, P_\ell^m(\cos\theta) \Bigg((\ell+1)\,\frac{h_\ell^{(+)}(k_0 r)}{k_0 r} - h_{\ell+1}^{(+)}(k_0 r) \Bigg) \\
& - D_{\ell,m}^E \, h_\ell^{(+)}(k_0 r) \Bigg((\ell+1)\,\frac{\cos\theta}{\sin\theta}\, P_\ell^m(\cos\theta) - \frac{(\ell-m+1)}{\sin\theta} \\
& \times P_{\ell+1}^m(\cos\theta) \Bigg) \Bigg] \Bigg\},
\end{aligned}
\tag{2.55}
$$

with

$$
C_{\ell,m}^M = (i)^\ell \sqrt{\frac{2\ell+1}{4\pi}\frac{(\ell-m)!}{(\ell+m)!}}\, t_\ell^M \, \psi_{\ell,m}^{M,\,ext},
\tag{2.56a}
$$

$$
D_{\ell,m}^E = (i)^\ell \sqrt{\frac{2\ell+1}{4\pi}\frac{(\ell-m)!}{(\ell+m)!}}\, t_\ell^E \, \psi_{\ell,m}^{E,\,ext}.
\tag{2.56b}
$$

2.3 Linear momentum transferred from the electron to the nanoparticle

The traveling electron produces electromagnetic field which at the same time induces charges and currents within the NP, as the result of this induction a second electromagnetic field appears along the region of interest. Thus the total electromagnetic field in any region of space corresponds to the superposition[11] of the electromagnetic fields produced by the fast electron ($\mathbf{E}^{ext}, \mathbf{H}^{ext}$) plus the electromagnetic fields scattered by the nanoparticle ($\mathbf{E}^{scat}, \mathbf{H}^{scat}$), i.e.,

$$
\mathbf{E}(\mathbf{r};\omega) = \mathbf{E}^{ext}(\mathbf{r};\omega) + \mathbf{E}^{scat}(\mathbf{r};\omega),
\tag{2.57a}
$$

$$
\mathbf{H}(\mathbf{r};\omega) = \mathbf{H}^{ext}(\mathbf{r};\omega) + \mathbf{H}^{scat}(\mathbf{r};\omega).
\tag{2.57b}
$$

Besides this induction, the external electromagnetic field carries mechanical properties such as linear momentum which will be transferred to the NP. The total linear momentum[12] trans-

---

[11]It is important to emphasize that the superposition principle in electrodynamics is postulated for the time domain fields, that is: $\alpha(\mathbf{r};t) = \alpha^{(1)}(\mathbf{r};t) + \alpha^{(2)}(\mathbf{r};t)$, where again $\alpha = \{\mathbf{E}, \mathbf{B}\}$. However, due to linearity of Fourier Transform, the superposition principle is also valid in the frequency domain: $\alpha(\mathbf{r};\omega) = \alpha^{(1)}(\mathbf{r};\omega) + \alpha^{(2)}(\mathbf{r};\omega)$.

[12]A similar analysis can be performed for the total angular momentum, that is, from the angular momentum conservation law in classical electrodynamics, it can be derived the total angular momentum transferred from the

ferred by the swift electron to the nanoparticle can be obtained from the linear momentum conservation law [24]

$$-\frac{\partial}{\partial t}\mathbf{g}(\mathbf{r};t) + \nabla \cdot \overset{\leftrightarrow}{\mathbf{T}}(\mathbf{r};t) = \rho_{ind}(\mathbf{r};t)\,\mathbf{E}(\mathbf{r};t) + \frac{1}{c}\,\mathbf{J}_{ind}(\mathbf{r};t) \times \mathbf{B}(\mathbf{r};t) = \mathbf{f}(\mathbf{r};t), \qquad (2.58)$$

where $\mathbf{E}(\mathbf{r};t)$ and $\mathbf{B}(\mathbf{r};t)$ are the total electric and magnetic fields (the one the electron produces plus the one scattered by the NP) acting on the induced charge and induced current distributions $\rho_{ind}(\mathbf{r};t)$ and $\mathbf{J}_{ind}(\mathbf{r};t)$, $\mathbf{g}(\mathbf{r};t)$ is the electromagnetic linear momentum density of the total electromagnetic field, $\overset{\leftrightarrow}{\mathbf{T}}(\mathbf{r};t)$ is the Maxwell's stress tensor (that can be identified with the flux of the total electromagnetic linear momentum density) and $\mathbf{f}(\mathbf{r};t)$ is the Lorentz force density which can be understood as the force per unit volume that the total electromagnetic fields executes over the induced charge and current distributions in the NP. Alternatively, $\mathbf{f}(\mathbf{r};t)$ can be though as the time rate change of a linear momentum density associated with Lorentz force. That is,

$$\mathbf{f}(\mathbf{r};t) = \frac{\partial}{\partial t}\,\mathbf{p}(\mathbf{r};t) = \rho_{ind}(\mathbf{r};t)\,\mathbf{E}(\mathbf{r};t) + \frac{1}{c}\,\mathbf{J}_{ind}(\mathbf{r};t) \times \mathbf{B}(\mathbf{r};t), \qquad (2.59)$$

where $\mathbf{p}(\mathbf{r};t)$ is the total mechanical linear momentum density that the collection of induced charges have. In CGS units $\mathbf{g}(\mathbf{r};t)$ and $\overset{\leftrightarrow}{\mathbf{T}}(\mathbf{r};t)$ are given by [24]

$$\mathbf{g}(\mathbf{r};t) = \frac{\mathbf{S}(\mathbf{r};t)}{c^2} = \frac{\mathbf{E}(\mathbf{r};t) \times \mathbf{B}(\mathbf{r};t)}{4\pi c}, \qquad (2.60)$$

$$\overset{\leftrightarrow}{\mathbf{T}}(\mathbf{r};\mathbf{t}) = \frac{1}{4\pi}\left[\mathbf{E}(\mathbf{r};t)\mathbf{E}(\mathbf{r};t) + \mathbf{B}(\mathbf{r};t)\mathbf{B}(\mathbf{r};t) - \frac{\overset{\leftrightarrow}{\mathbf{I}}}{2}\Big(\mathbf{E}(\mathbf{r};t)\cdot\mathbf{E}(\mathbf{r};t) + \mathbf{B}(\mathbf{r};t)\cdot\mathbf{B}(\mathbf{r};t)\Big)\right], \quad (2.61)$$

where $\mathbf{S}(\mathbf{r};t)$ is the Poynting vector and $\overset{\leftrightarrow}{\mathbf{I}}$ is the unit dyadic.

For the calculation of the total linear momentum ($\Delta\mathbf{P}$) transferred by the electron to the NP, it is necessary to consider the linear momentum conservation law in an integral form. Hence, the integration of Eq. (2.58) over a volume V—which is constant in time and encloses the nanoparticle but does not intersect the electron's path[13]—yields

$$\frac{\partial}{\partial t}\int_V \mathbf{p}(\mathbf{r};t)\,d^3r = -\frac{\partial}{\partial t}\int_V \mathbf{g}(\mathbf{r};t)\,d^3r + \oint_S \overset{\leftrightarrow}{\mathbf{T}}(\mathbf{r};t)\cdot\hat{\mathbf{n}}\,da, \qquad (2.62)$$

where S is the boundary of V with surface element $d\mathbf{a} = \hat{\mathbf{n}}\,da$. For numerical purposes, the integration surface S will be always considered as a sphere of radius R larger than the nanoparticle's radius a, but smaller than the electron's impact parameter x_0, as shown in Fig. 1.3(b). Defining

$$\frac{\partial}{\partial t}\int_V \mathbf{p}(\mathbf{r};t)\,d^3r = \frac{\partial}{\partial t}\mathbf{P}(t) \quad \text{and} \quad \frac{\partial}{\partial t}\int_V \mathbf{g}(\mathbf{r};t)\,d^3r = \frac{\partial}{\partial t}\mathbf{G}(t), \qquad (2.63)$$

Eq. (2.62) becomes

---

electron to a nanoparticle.

[13]This restriction imposed on V (not intersecting the electron's path) is due to the fact that the electron carries, besides electromagnetic momentum, mechanical linear momentum $m_e\mathbf{v}$. So it must be taken into account in the total linear mechanical momentum inside V but only when the electron (strictly, the linear momentum $m_e\mathbf{v}$) is inside the integration volume V. Nevertheless, the calculation of $\Delta\mathbf{P}$ does not depend on the choice of integration volume.

$$\frac{d}{dt}\mathbf{P}(t) = -\frac{d}{dt}\mathbf{G}(t) + \oint_S \overset{\leftrightarrow}{\mathbf{T}}(\mathbf{r};t) \cdot \hat{\mathbf{n}}\, da, \tag{2.64}$$

where, according to Eqs. (2.59) and (2.60), $\mathbf{P}(t)$ and $\mathbf{G}(t)$ are the mechanical and electromagnetic linear momentum at time t inside the volume V.

As it is of interest to obtain the total linear momentum transferred from the electron to the NP along the whole trajectory of the electron, Eq. (2.64) must be integrated in time from the beginning of the interaction—between the electron and the NP—until the end of it. Thus, the total momentum transferred can be calculated as

$$\Delta\mathbf{P} = -\Delta\mathbf{G} + \oint_S \int_{-\infty}^{\infty} \overset{\leftrightarrow}{\mathbf{T}}(\mathbf{r};t) \cdot \hat{\mathbf{n}}\, dt\, da, \tag{2.65}$$

with $\Delta\mathbf{P} = \mathbf{P}(\infty) - \mathbf{P}(-\infty)$ and $\Delta\mathbf{G} = \mathbf{G}(\infty) - \mathbf{G}(-\infty)$. Since the nanoparticle is not charged, it is worth noting that at the beginning, when the electron is far from the nanoparticle, the total electromagnetic linear momentum inside V is zero. That is,

$$\mathbf{G}(t = -\infty) = 0, \tag{2.66}$$

because close to the nanoparticle the total electromagnetic fields are zero, given that the electron's electromagnetic field vanish as $1/r^2$ and therefore there will not be induced charges nor currents on the NP. In addition, when the electron has already interacted with the nanoparticle and is far from it, due to dissipation effects, there will not be induced electric and magnetic fields. In other words, when the electron has already interacted with the NP and is far from it, it is expected that all induced charges and currents within the metallic sphere will disappear, and therefore, inside the volume V the total electromagnetic fields will vanish again. Then,

$$\mathbf{G}(t = \infty) = 0. \tag{2.67}$$

Thus, substituting Eqs. (2.66) and (2.67) into Eq. (2.65), the total linear momentum transferred from the electron to the NP is given by

$$\boxed{\Delta\mathbf{P} = \oint_S \int_{-\infty}^{\infty} \overset{\leftrightarrow}{\mathbf{T}}(\mathbf{r};t) \cdot \hat{\mathbf{n}}\, dt\, da = \oint_S \overset{\leftrightarrow}{\mathbf{T}}(\mathbf{r};\omega = 0) \cdot \hat{\mathbf{n}}\, da,} \tag{2.68}$$

since the time Fourier Transform of Maxwell's stress tensor is

$$\overset{\leftrightarrow}{\mathbf{T}}(\mathbf{r};\omega) = \int_{-\infty}^{\infty} \overset{\leftrightarrow}{\mathbf{T}}(\mathbf{r};t)\, e^{i\omega t}\, dt. \tag{2.69}$$

Equation (2.69) establishes a direct method to calculate the total linear momentum transferred from the electron to the NP, where $\overset{\leftrightarrow}{\mathbf{T}}(\mathbf{r};\omega = 0)$ is given explicitly by

$$\overset{\leftrightarrow}{\mathbf{T}}(\mathbf{r};\omega = 0) = \int_{-\infty}^{\infty} \overset{\leftrightarrow}{\mathbf{T}}(\mathbf{r};t)\, dt = \frac{1}{4\pi} \int_{-\infty}^{\infty} \left\{ \mathbf{E}(\mathbf{r};t)\mathbf{E}(\mathbf{r};t) + \mathbf{B}(\mathbf{r};t)\mathbf{B}(\mathbf{r};t) \right. \tag{2.70}$$
$$\left. - \frac{\overset{\leftrightarrow}{\mathbf{I}}}{2}\left[\mathbf{E}(\mathbf{r};t) \cdot \mathbf{E}(\mathbf{r};t) + \mathbf{B}(\mathbf{r};t) \cdot \mathbf{B}(\mathbf{r};t) \right] \right\} dt,$$

and replacing the electric and magnetic fields with their time Fourier Transform, Eq. (2.70) can

be written as

$$\overset{\leftrightarrow}{\mathbf{T}}(\mathbf{r};\omega=0) = \frac{1}{4\pi}\frac{1}{(2\pi)^2}\int_{-\infty}^{\infty}\int_{-\infty}^{\infty}\int_{-\infty}^{\infty}\left\{\mathbf{E}(\mathbf{r};\omega')\mathbf{E}(\mathbf{r};\omega'') + \mathbf{B}(\mathbf{r};\omega')\mathbf{B}(\mathbf{r};\omega'')\right. \tag{2.71}$$
$$\left. - \frac{\overset{\leftrightarrow}{\mathbf{I}}}{2}\left[\mathbf{E}(\mathbf{r};\omega')\cdot\mathbf{E}(\mathbf{r};\omega'') + \mathbf{B}(\mathbf{r};\omega')\cdot\mathbf{B}(\mathbf{r};\omega'')\right]\right\}e^{-it(\omega'+\omega'')}\,d\omega'\,d\omega''\,dt.$$

In this way $\mathbf{E}(\mathbf{r};\omega)$ and $\mathbf{B}(\mathbf{r};\omega)$ are written in the frequency domain and they do not depend anymore on the variable t, thus Eq. (2.71) results in

$$\overset{\leftrightarrow}{\mathbf{T}}(\mathbf{r};\omega=0) = \frac{1}{8\pi^2}\left\{\int_{-\infty}^{\infty}\int_{-\infty}^{\infty}\left\{\mathbf{E}(\mathbf{r};\omega')\mathbf{E}(\mathbf{r};\omega'') + \mathbf{B}(\mathbf{r};\omega')\mathbf{B}(\mathbf{r};\omega'')\right.\right.$$
$$\left. - \frac{\overset{\leftrightarrow}{\mathbf{I}}}{2}\left[\mathbf{E}(\mathbf{r};\omega')\cdot\mathbf{E}(\mathbf{r};\omega'') + \mathbf{B}(\mathbf{r};\omega')\cdot\mathbf{B}(\mathbf{r};\omega'')\right]\right\}d\omega'\,d\omega''\right\} \tag{2.72}$$
$$\times\left\{\frac{1}{2\pi}\int_{-\infty}^{\infty}e^{-it(\omega'+\omega'')}\,dt\right\},$$

where the last term in the right hand side of Eq. (2.72) can be identified with [11]

$$\frac{1}{2\pi}\int_{-\infty}^{\infty}e^{-it(\omega'-\omega)}\,dt = \delta(\omega'-\omega). \tag{2.73}$$

Hence, Eq. (2.72) reads

$$\overset{\leftrightarrow}{\mathbf{T}}(\mathbf{r};\omega=0) = \frac{1}{8\pi^2}\int_{-\infty}^{\infty}\left\{\mathbf{E}(\mathbf{r};\omega')\mathbf{E}(\mathbf{r};-\omega') + \mathbf{B}(\mathbf{r};\omega')\mathbf{B}(\mathbf{r};-\omega')\right. \tag{2.74}$$
$$\left. - \frac{\overset{\leftrightarrow}{\mathbf{I}}}{2}\left[\mathbf{E}(\mathbf{r};\omega')\cdot\mathbf{E}(\mathbf{r};-\omega') + \mathbf{B}(\mathbf{r};\omega')\cdot\mathbf{B}(\mathbf{r};-\omega')\right]\right\}d\omega'.$$

Moreover, the electric and magnetic fields in the time domain are real functions, therefore

$$\mathbf{E}^*(\mathbf{r};t) = \mathbf{E}(\mathbf{r};t) \quad\text{and}\quad \mathbf{B}^*(\mathbf{r};t) = \mathbf{B}(\mathbf{r};t), \tag{2.75}$$

with $(*)$ denoting complex conjugation. In the frequency domain this restriction, Eqs. (2.75), implies that

$$\mathbf{E}^*(\mathbf{r};\omega) = \int_{-\infty}^{\infty}\mathbf{E}^*(\mathbf{r};t)\,e^{-i\omega t}\,dt = \int_{-\infty}^{\infty}\mathbf{E}(\mathbf{r};t)\,e^{i(-\omega t)}\,dt = \mathbf{E}(\mathbf{r};-\omega), \tag{2.76a}$$
$$\mathbf{B}^*(\mathbf{r};\omega) = \int_{-\infty}^{\infty}\mathbf{B}^*(\mathbf{r};t)\,e^{-i\omega t}\,dt = \int_{-\infty}^{\infty}\mathbf{B}(\mathbf{r};t)\,e^{i(-\omega t)}\,dt = \mathbf{B}(\mathbf{r};-\omega). \tag{2.76b}$$

Thus, substituting Eqs. (2.76) into Eq. (2.74)

$$\overset{\leftrightarrow}{\mathbf{T}}(\mathbf{r};\omega=0) = \frac{1}{8\pi^2}\int_{-\infty}^{\infty}\left[\mathbf{E}(\mathbf{r};\omega')\mathbf{E}^*(\mathbf{r};\omega') - \frac{\overset{\leftrightarrow}{\mathbf{I}}}{2}\mathbf{E}(\mathbf{r};\omega')\cdot\mathbf{E}^*(\mathbf{r};\omega') + \mathbf{B}(\mathbf{r};\omega')\mathbf{B}^*(\mathbf{r};\omega')\right. \tag{2.77}$$
$$\left. - \frac{\overset{\leftrightarrow}{\mathbf{I}}}{2}\mathbf{B}(\mathbf{r};\omega')\cdot\mathbf{B}^*(\mathbf{r};\omega')\right]d\omega' = \overset{\leftrightarrow}{\mathbf{T}}_{\mathbf{E}}(\mathbf{r};\omega=0) + \overset{\leftrightarrow}{\mathbf{T}}_{\mathbf{B}}(\mathbf{r};\omega=0),$$

where

$$\overset{\leftrightarrow}{\mathbf{T}}_{\mathbf{E}}(\mathbf{r};\omega=0) = \frac{1}{8\pi^2} \int_{-\infty}^{\infty} \left[\mathbf{E}(\mathbf{r};\omega')\mathbf{E}^*(\mathbf{r};\omega') - \frac{\overset{\leftrightarrow}{\mathbf{I}}}{2}\mathbf{E}(\mathbf{r};\omega') \cdot \mathbf{E}^*(\mathbf{r};\omega') \right] d\omega' \quad \text{and} \qquad (2.78\text{a})$$

$$\overset{\leftrightarrow}{\mathbf{T}}_{\mathbf{B}}(\mathbf{r};\omega=0) = \frac{1}{8\pi^2} \int_{-\infty}^{\infty} \left[\mathbf{B}(\mathbf{r};\omega')\mathbf{B}^*(\mathbf{r};\omega') - \frac{\overset{\leftrightarrow}{\mathbf{I}}}{2}\mathbf{B}(\mathbf{r};\omega') \cdot \mathbf{B}^*(\mathbf{r};\omega') \right] d\omega', \qquad (2.78\text{b})$$

are the electric and magnetic contributions to $\overset{\leftrightarrow}{\mathbf{T}}(\mathbf{r};\omega=0)$, respectively. Furthermore, Eqs. (2.78) can be simplified using the parity property of the integrands. Let α denote the electric (**E**) or magnetic (**B**) contribution to $\overset{\leftrightarrow}{\mathbf{T}}(\mathbf{r};\omega=0)$, then Eqs. (2.78) can be written in components as

$$T_{ij}^{(\alpha)}(\mathbf{r};\omega=0) = \frac{1}{8\pi^2} \int_{-\infty}^{\infty} \left[\alpha_i(\mathbf{r};\omega')\alpha_j^*(\mathbf{r};\omega') - \frac{\delta_{ij}}{2}|\alpha(\mathbf{r};\omega')|^2 \right] d\omega'. \qquad (2.79)$$

Separating the integral over the intervals $(-\infty,0)$ and $(0,\infty)$, Eq. (2.79) reads

$$T_{ij}^{(\alpha)}(\mathbf{r};\omega=0) = \frac{1}{8\pi^2} \int_{-\infty}^{0} \left[\alpha_i(\mathbf{r};\omega')\alpha_j^*(\mathbf{r};\omega') - \frac{\delta_{ij}}{2}|\alpha(\mathbf{r};\omega')|^2 \right] d\omega' \qquad (2.80)$$
$$+ \frac{1}{8\pi^2} \int_{0}^{\infty} \left[\alpha_i(\mathbf{r};\omega')\alpha_j^*(\mathbf{r};\omega') - \frac{\delta_{ij}}{2}|\alpha(\mathbf{r};\omega')|^2 \right] d\omega',$$

and replacing $\omega' \to -\omega'$ in the first integral of the right hand side in Eq. (2.80)

$$T_{ij}^{(\alpha)}(\mathbf{r};\omega=0) = \frac{1}{8\pi^2} \int_{0}^{\infty} \left[\alpha_i(\mathbf{r};-\omega')\alpha_j^*(\mathbf{r};-\omega') - \frac{\delta_{ij}}{2}|\alpha(\mathbf{r};-\omega')|^2 \right] d\omega' \qquad (2.81)$$
$$+ \frac{1}{8\pi^2} \int_{0}^{\infty} \left[\alpha_i(\mathbf{r};\omega')\alpha_j^*(\mathbf{r};\omega') - \frac{\delta_{ij}}{2}|\alpha(\mathbf{r};\omega')|^2 \right] d\omega'.$$

Taking account of the reality nature of the electromagnetic fields into Eq. (2.81), it follows that

$$T_{ij}^{(\alpha)}(\mathbf{r};\omega=0) = \frac{1}{8\pi^2} \int_{0}^{\infty} \left[\alpha_i^*(\mathbf{r};\omega')\alpha_j(\mathbf{r};\omega') - \frac{\delta_{ij}}{2}|\alpha(\mathbf{r};\omega')|^2 \right] d\omega'$$
$$+ \frac{1}{8\pi^2} \int_{0}^{\infty} \left[\alpha_i(\mathbf{r};\omega')\alpha_j^*(\mathbf{r};\omega') - \frac{\delta_{ij}}{2}|\alpha(\mathbf{r};\omega')|^2 \right] d\omega' \qquad (2.82)$$
$$= \frac{1}{8\pi^2} \int_{0}^{\infty} \left[\left(\alpha_i(\mathbf{r};\omega')\alpha_j^*(\mathbf{r};\omega') + \alpha_i^*(\mathbf{r};\omega')\alpha_j(\mathbf{r};\omega') \right) - 2\frac{\delta_{ij}}{2}|\alpha(\mathbf{r};\omega')|^2 \right] d\omega'$$
$$= \frac{1}{4\pi^2} \int_{0}^{\infty} \text{Re}\left[\alpha_i(\mathbf{r};\omega')\alpha_j^*(\mathbf{r};\omega') - \frac{\delta_{ij}}{2}|\alpha(\mathbf{r};\omega')|^2 \right] d\omega',$$

where Re denotes the real part of a complex number.

In consequence, by substituting Eq. (2.82) into Eq. (2.68), the components of the total linear momentum transferred by the electron to the nanoparticle are given by

$$\Delta P_i = \oint_S T_{ij}(\mathbf{r};\omega=0)\,n^j\,da = \sum_{\alpha=\{\mathbf{E},\mathbf{B}\}} \oint_S T_{ij}^{(\alpha)}(\mathbf{r};\omega=0)\,n^j\,da, \qquad (2.83)$$

then

$$\Delta P_i = \sum_{\alpha=\{\mathbf{E},\mathbf{B}\}} \oint_S \frac{1}{4\pi^2} \int_0^\infty \mathrm{Re}\left[\alpha_i(\mathbf{r};\omega')\alpha_j^*(\mathbf{r};\omega') - \frac{\delta_{ij}}{2}|\alpha(\mathbf{r};\omega')|^2\right] d\omega'\, n^j\, da, \tag{2.84}$$

$$= \frac{1}{4\pi^2} \int_0^\infty \oint_S \mathrm{Re}\left[\sum_{\alpha=\{\mathbf{E},\mathbf{B}\}} \alpha_i(\mathbf{r};\omega')\alpha_j^*(\mathbf{r};\omega') - \frac{\delta_{ij}}{2}|\alpha(\mathbf{r};\omega')|^2\right] n^j\, da\, d\omega',$$

where Einstein's summation convention have been used for repeated indices. In a more compact expression

$$\boxed{\Delta P_i = \int_0^\infty \mathcal{P}_i\left(\omega\right)\, d\omega,} \tag{2.85}$$

with

$$\boxed{\begin{aligned}\mathcal{P}_i\left(\omega\right) = \frac{1}{4\pi^2} \oint_S \mathrm{Re}\Big[&E_i(\mathbf{r};\omega)E_j^*(\mathbf{r};\omega) + B_i(\mathbf{r};\omega)B_j^*(\mathbf{r};\omega) \\ &- \frac{\delta_{ij}}{2}\Big(\mathbf{E}(\mathbf{r};\omega)\cdot\mathbf{E}^*(\mathbf{r};\omega) + \mathbf{B}(\mathbf{r};\omega)\cdot\mathbf{B}^*(\mathbf{r};\omega)\Big)\Big] n^j\, da,\end{aligned}} \tag{2.86}$$

which can be understood as the spectral contribution to the total linear momentum, that is, the differential linear momentum transferred per unit frequency.

LINEAR MOMENTUM TRANSFER WITHIN THE DIPOLE APPROXIMATION

Regarding the interaction between the swift electron and the spherical NP, we are interested in calculating the total electromagnetic field in any region of space, which is given by the sum of both the external and the induced fields, as it was obtained in Chapter 2. Therefore, the total linear momentum is computed numerically by: i) calculating the total electromagnetic field on each point of the discretized spherical integration surface (a sphere enclosing the NP), ii) then obtaining the spectral contribution to the total momentum transferred from the electron to the NP for several frequencies, and iii) finally integrating the spectral contribution to the momentum transferred in order to fulfill Eqs. (2.85) and (2.86). Steps i) and ii) may exceed computing capacities [25] if either the number of multipoles in the scattered field is large or the NP's radius is larger than few nanometers. This motivates the search of analytical solutions of the spectral contribution to the total linear momentum transfer, and the study of the contribution given by each multipole to the total momentum transferred. In this Chapter, the first step of this process is presented by examining only the $\ell = 1$ term in the scattered field, named as the *dipole approximation*. The Maxwell stress tensor and its surface integral are treated in the following two Sections, with the intention of understanding characteristic behaviors of the linear momentum transfer.

3.1 Scattered field produced by the nanoparticle

The aim of this Chapter is to elucidate explicit expressions for the scattered electric and magnetic fields, the surface integral of Maxwell stress tensor and the spectral contribution to the linear momentum transferred from the swift electron to the NP taking only into account the dipole contribution, i. e., $\ell = 1$. In this Section, we perform the calculations related to explicit expressions for the induced fields with $\ell = 1$, by splitting the electric and magnetic fields in spherical coordinates. It is worth noting that the scattered electromagnetic field, Eqs. (2.54) and (2.55), depend on the functions $\psi_{\ell,m}^{E,ext}, \psi_{\ell,m}^{M,ext}$ and P_ℓ^m, yet to be calculated. Therefore, the task of figuring out explicit expressions for the scattered electromagnetic field with $\ell = 1$ is equivalent to computing $\psi_{1,m}^{E,ext}, \psi_{1,m}^{M,ext}, P_1^m$ and P_2^m with $m = -1, 0, 1$. Given that

$$A_{\ell,-m}^+ = (-1)^m A_{\ell,m}^+, \tag{3.1}$$

which can be derived from the property

$$M^+_{\ell,-m}(x_0, 0, 0) = (-1)^m M^+_{\ell,m}(x_0, 0, 0),$$ (3.2)

as shown in Appendix A, the calculations concerning to the extended Mie solution can be restricted only to $m \geq 0$. In this way, substituting $\ell = 1$ into Eqs. (2.45) and using Eq. (2.46b), the scalar functions for the dipole approximation are given by

$$\psi^{E,ext}_{1,-1} = -\psi^{E,ext}_{1,1} = -\sqrt{2} \, \frac{\pi k_0}{c \, \gamma} \, A^+_{1,0} \, K_1\left(\frac{\omega x_0}{v \gamma}\right),$$ (3.3a)

$$\psi^{E,ext}_{1,0} = -2\sqrt{2} \, \frac{\pi k_0}{c \, \gamma} \, A^+_{1,1} \, K_0\left(\frac{\omega x_0}{v \gamma}\right),$$ (3.3b)

$$\psi^{M,ext}_{1,-1} = \psi^{M,ext}_{1,1} = -\frac{2\pi k_0 \, v}{c^2} \, A^+_{1,1} \, K_1\left(\frac{\omega x_0}{v \gamma}\right),$$ (3.3c)

$$\psi^{M,ext}_{1,0} = 0,$$ (3.3d)

where the following relation for the modified Bessel functions (K_ν) [17]

$$K_{-\nu}(z) = K_\nu(z),$$ (3.4)

was used, and the numbers $A^+_{1,0}$, $A^+_{1,1}$ can be calculated using Eq. (2.46a) as

$$A^+_{1,0} = \frac{1}{\beta^2} \sum_{j=0}^{1} \frac{3 \, (i)^{1-j} \, \alpha_{1,0}}{\gamma^j \, 2^j \, (1-j)! \left[\frac{j}{2}\right]! \left[\frac{j}{2}\right]!} I^{1,0}_{j,1-j} = 3 \frac{\alpha_{1,0}}{\beta^2} \left(i \, I^{1,0}_{0,1} + \frac{I^{1,0}_{1,0}}{2\gamma \left[\frac{1}{2}\right]! \left[\frac{1}{2}\right]!} \right),$$ (3.5a)

$$A^+_{1,1} = \frac{1}{\beta^2} \sum_{j=1}^{1} \frac{3 \, (i)^{1-j} \, \alpha_{1,1}}{\gamma^j \, 2^j \, (1-j)! \left[\frac{j-1}{2}\right]! \left[\frac{j+1}{2}\right]!} I^{1,1}_{j,1-j} = 3 \frac{\alpha_{1,1}}{\beta^2} \frac{I^{1,1}_{1,0}}{2\gamma}.$$ (3.5b)

An explicit expression for the coefficients $\alpha_{1,0}$ and $\alpha_{1,1}$ is obtained in accordance to Eq. (2.47). So, it is straightforward to obtain

$$\alpha_{1,0} = \sqrt{3/4\pi} \quad \text{and} \quad \alpha_{1,1} = \sqrt{3/8\pi}.$$ (3.6)

The numbers $I^{1,0}_{0,1}, I^{1,0}_{1,0}$ and $I^{1,1}_{1,0}$, in Eqs. (3.5), are calculated using the initial values set by Eq. (2.48) as

$$I^{1,0}_{0,1} = I^{0,0}_{0,2} = (-1)!! \, B\left(1, \frac{3}{2}\right) = B\left(1, \frac{3}{2}\right) = 2/3,$$ (3.7a)

$$I^{1,0}_{1,0} = I^{0,0}_{1,1} = 0,$$ (3.7b)

$$I^{1,1}_{1,0} = -(1!!) \, B\left(2, \frac{1}{2}\right) = -B\left(2, \frac{1}{2}\right) = -4/3.$$ (3.7c)

Hence, substituting $\alpha_{1,0}, \alpha_{1,1}, I^{1,0}_{0,1}, I^{1,0}_{1,0}, I^{1,1}_{1,0}$ into $A^+_{1,0}$ and $A^+_{1,1}$

$$A^+_{1,0} = \sqrt{\frac{3}{\pi}} \frac{i}{\beta^2} \quad \text{and} \quad A^+_{1,1} = -\sqrt{\frac{3}{2\pi}} \frac{1}{\gamma \beta^2}.$$ (3.8)

Finally, substituting coefficients given by Eq. (3.8) into the Eqs. (3.3), the functions $\psi_{1,m}^{E,ext}$ and $\psi_{1,m}^{M,ext}$ results in

$$\psi_{1,1}^{E,ext} = -\psi_{1,-1}^{E,ext} = i\sqrt{6\pi}\,\frac{k_0}{c\gamma\beta^2}\,K_1\left(\frac{\omega x_0}{v\gamma}\right), \qquad \psi_{1,0}^{E,ext} = \sqrt{3\pi}\,\frac{2k_0}{c\gamma^2\beta^2}\,K_0\left(\frac{\omega x_0}{v\gamma}\right), \tag{3.9a}$$

$$\psi_{1,1}^{M,ext} = \psi_{1,-1}^{M,ext} = \sqrt{6\pi}\,\frac{k_0 v}{c^2\gamma\beta^2}\,K_1\left(\frac{\omega x_0}{v\gamma}\right), \qquad \text{and} \quad \psi_{1,0}^{M,ext} = 0. \tag{3.9b}$$

In order to obtain an explicit expression for the scattered electromagnetic field in the dipole approximation ($\ell = 1$), besides the functions $\psi_{1,m}^{E,ext}$ and $\psi_{1,m}^{M,ext}$, the analytic expressions for the Legendre functions P_1^m and P_2^m are also required. For negative values of m in the Legendre functions, the following relation [11] was considered

$$P_\ell^{-m}(x) = (-1)^m\,\frac{(\ell-m)!}{(\ell+m)!}\,P_\ell^m(x). \tag{3.10}$$

With this tool in hand and substituting Eqs. (3.9) into Eqs. (2.54) and (2.55), the spherical components of the scattered electric field for $\ell = 1$ are given by

$$E_{r,\ell=1}^{scat} = 6\,t_1^E\,\frac{h_1^{(+)}(k_0 r)}{k_0 r}\,\frac{k_0}{c\gamma\beta^2}\left[\sin\theta\,\cos\varphi\,K_1\left(\frac{\omega x_0}{v\gamma}\right) + \frac{i}{\gamma}\cos\theta\,K_0\left(\frac{\omega x_0}{v\gamma}\right)\right], \tag{3.11a}$$

$$E_{\theta,\ell=1}^{scat} = \frac{3k_0}{c\gamma\beta^2}\left\{i\,t_1^M\,h_1^{(+)}(k_0 r)\,\beta\,K_1\left(\frac{\omega x_0}{v\gamma}\right)\cos\varphi + t_1^E\left[2\,\frac{h_1^{(+)}(k_0 r)}{k_0 r} - h_2^{(+)}(k_0 r)\right]\right. \tag{3.11b}$$

$$\left.\times\left[K_1\left(\frac{\omega x_0}{v\gamma}\right)\cos\theta\,\cos\varphi - \frac{i}{\gamma}K_0\left(\frac{\omega x_0}{v\gamma}\right)\sin\theta\right]\right\},$$

$$E_{\varphi,\ell=1}^{scat} = -\frac{3k_0}{c\gamma\beta^2}\sin\varphi\,K_1\left(\frac{\omega x_0}{\gamma v}\right)\left\{t_1^E\left[2\,\frac{h_1^{(+)}(k_0 r)}{k_0 r} - h_2^{(+)}(k_0 r)\right] + i\,t_1^M\,h_1^{(+)}(k_0 r)\right. \tag{3.11c}$$

$$\left.\beta\cos\theta\right\},$$

and for the scattered magnetic field are given by

$$H_{r,\ell=1}^{scat} = 6\,t_1^M\,\frac{h_1^{(+)}(k_0 r)}{k_0 r}\,\frac{k_0}{c\gamma\beta}\,K_1\left(\frac{\omega x_0}{v\gamma}\right)\sin\theta\,\sin\varphi, \tag{3.12a}$$

$$H_{\theta,\ell=1}^{scat} = \frac{3k_0}{c\gamma\beta^2}\,K_1\left(\frac{\omega x_0}{v\gamma}\right)\sin\varphi\left\{t_1^M\left[2\,\frac{h_1^{(+)}(k_0 r)}{k_0 r} - h_2^{(+)}(k_0 r)\right]\beta\,\cos\theta + i\,t_1^E\right. \tag{3.12b}$$

$$\left.\times\,h_1^{(+)}(k_0 r)\right\},$$

$$H_{\varphi,\ell=1}^{scat} = \frac{3k_0}{c\gamma\beta^2}\left\{t_1^M\left[2\,\frac{h_1^{(+)}(k_0 r)}{k_0 r} - h_2^{(+)}(k_0 r)\right]\beta\,K_1\left(\frac{\omega x_0}{v\gamma}\right)\cos\varphi \right. \tag{3.12c}$$

$$\left.+ t_1^E\,h_1^{(+)}(k_0 r)\left[i\,K_1\left(\frac{\omega x_0}{v\gamma}\right)\cos\theta\,\cos\varphi + \frac{1}{\gamma}K_0\left(\frac{\omega x_0}{v\gamma}\right)\sin\theta\right]\right\},$$

where the explicit expressions of the Legendre functions P_1^1, P_1^0, P_2^0 were used, according to the convention stablished in [11] for the Legendre Rodrigues' formula. It is important to emphasize that Mie coefficients t_1^E and t_1^M are functions of the NP's radius and frequency.

In Fig. 3.1 we show the magnitude of the induced electromagnetic field (in free space $\mathbf{H}=\mathbf{B}$) in the dipole approximation. The plots correspond to the electromagnetic field evaluated at $z = 0$, that is, in the XY plane orthogonal to the electron's trajectory. On top of each 3D graph [Figs. 3.1(a) and 3.1(c)] we show a 2D projection. For a better appreciation, in Figs. 3.1(b) and 3.1(d) we show again the 2D plots in a grayscale. The parameters used for Fig. 3.1 were: a 1 nm radius aluminium NP modeled as a Drude-type material with $\hbar\omega_p = 15.1$ eV and $\hbar\Gamma = 0.15$ eV; an impact parameter of the electron's trajectory of $x_0 = 0.5$ nm and an electron's speed of $0.5c$. We set up a frequency of $\hbar\omega = 8.71$ eV corresponding to the dipolar plasmon mode for the aluminium Drude-like NP. As it was expected, the plots for the magnitude of the induced fields [Fig. 3.1] with $\ell = 1$ correspond to an electric [Fig. 3.1(a)] and magnetic [Fig. 3.1(b)] dipoles, respectively.
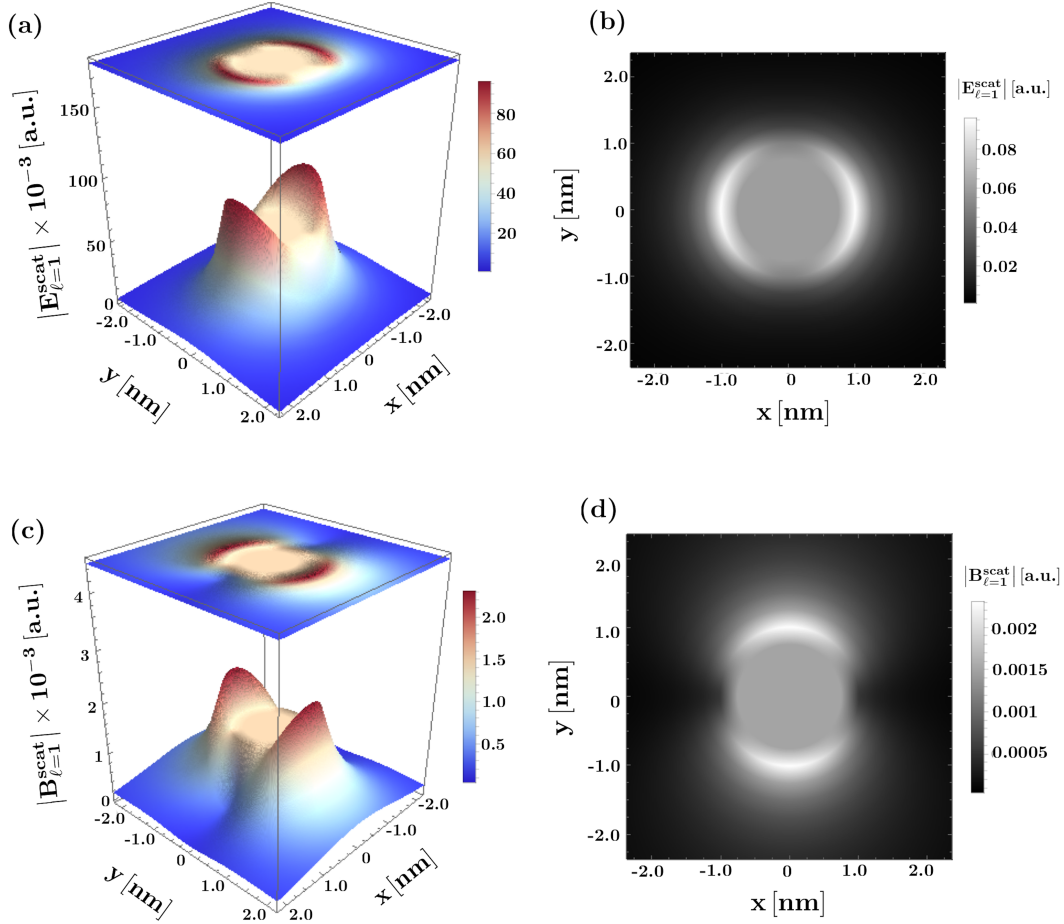

Figure 3.1.   Three dimensional (3D) plots and 2D projections on top, of the magnitude of (a) the electric and (c) the magnetic induced fields in the dipole approximation surrounding a $a = 1$ nm radius NP, modeled as a Dude-type material. Right to each 3D plot, the 2D projection in grayscale for (b) the electric and (d) the magnetic field magnitude are presented. The external electromagnetic field is set up with an impact parameter of $x_0 = 1.5$ nm, an electron's speed of $v = 0.5c$ and a frequency of $\hbar\omega = 8.71$ eV. The electromagnetic field is expressed in atomic units [a.u.].

Since expressions (3.11) and (3.12) represent a closed form for the induced electromagnetic field, it is rather naturally to construct the Maxwell stress tensor for the total electromagnetic field in the dipole approximation, and then write explicitly the integrals involved in the spectral contribution to the total momentum transferred. The next two Sections will be dedicated to construct both the Maxwell stress tensor and its surface integral within the dipole approximation.

3.2 Maxwell stress tensor

Concordant with Maxwell stress tensor definition given by Eq. (2.61), as

$$\overset{\leftrightarrow}{\mathbf{T}} = \frac{1}{4\pi}\left[\mathbf{E}\mathbf{E} + \mathbf{B}\mathbf{B} - \frac{\overset{\leftrightarrow}{\mathbf{I}}}{2}\Big(\mathbf{E}\cdot\mathbf{E} + \mathbf{B}\cdot\mathbf{B}\Big)\right],$$

if the electric $\mathbf{E}$ and magnetic $\mathbf{B}$ fields come from a sum of two different electric and magnetic fields, for instance

$$\mathbf{E} = \mathbf{E}_1 + \mathbf{E}_2 \quad \text{and} \quad \mathbf{B} = \mathbf{B}_1 + \mathbf{B}_2, \tag{3.13}$$

then $\overset{\leftrightarrow}{\mathbf{T}}$ can be separated into four contribution, as

$$\overset{\leftrightarrow}{\mathbf{T}} = \overset{\leftrightarrow}{\mathbf{T}}_1 + \overset{\leftrightarrow}{\mathbf{T}}_2 + \overset{\leftrightarrow}{\mathbf{T}}_{12} + \overset{\leftrightarrow}{\mathbf{T}}_{21}, \tag{3.14}$$

where

$$\overset{\leftrightarrow}{\mathbf{T}}_1 = \frac{1}{4\pi}\left[\mathbf{E}_1\mathbf{E}_1 + \mathbf{B}_1\mathbf{B}_1 - \frac{\overset{\leftrightarrow}{\mathbf{I}}}{2}\Big(\mathbf{E}_1\cdot\mathbf{E}_1 + \mathbf{B}_1\cdot\mathbf{B}_1\Big)\right], \tag{3.15a}$$

$$\overset{\leftrightarrow}{\mathbf{T}}_2 = \frac{1}{4\pi}\left[\mathbf{E}_2\mathbf{E}_2 + \mathbf{B}_2\mathbf{B}_2 - \frac{\overset{\leftrightarrow}{\mathbf{I}}}{2}\Big(\mathbf{E}_2\cdot\mathbf{E}_2 + \mathbf{B}_2\cdot\mathbf{B}_2\Big)\right], \tag{3.15b}$$

$$\overset{\leftrightarrow}{\mathbf{T}}_{12} = \frac{1}{4\pi}\left[\mathbf{E}_1\mathbf{E}_2 + \mathbf{B}_1\mathbf{B}_2 - \frac{\overset{\leftrightarrow}{\mathbf{I}}}{2}\Big(\mathbf{E}_1\cdot\mathbf{E}_2 + \mathbf{B}_1\cdot\mathbf{B}_2\Big)\right], \tag{3.15c}$$

$$\overset{\leftrightarrow}{\mathbf{T}}_{21} = \frac{1}{4\pi}\left[\mathbf{E}_2\mathbf{E}_1 + \mathbf{B}_2\mathbf{B}_1 - \frac{\overset{\leftrightarrow}{\mathbf{I}}}{2}\Big(\mathbf{E}_2\cdot\mathbf{E}_1 + \mathbf{B}_2\cdot\mathbf{B}_1\Big)\right]. \tag{3.15d}$$

Furthermore,

$$\overset{\leftrightarrow}{\mathbf{T}}_{12} = \overset{\leftrightarrow}{\mathbf{T}}_{21}^{\mathsf{T}}, \tag{3.16}$$

with (T) denoting matrix transpose. Therefore, $\overset{\leftrightarrow}{\mathbf{T}}_{(12)} = \overset{\leftrightarrow}{\mathbf{T}}_{12} + \overset{\leftrightarrow}{\mathbf{T}}_{21}$ is a symmetric tensor with mixed terms of both fields and due to the conjugate symmetry property of the scalar product

$$\overset{\leftrightarrow}{\mathbf{T}}_{(\mathbf{12})} = \frac{1}{4\pi}\left[\mathbf{E}_1\mathbf{E}_2 + \mathbf{E}_2\mathbf{E}_1 + \mathbf{B}_1\mathbf{B}_2 + \mathbf{B}_2\mathbf{B}_1 - \overset{\leftrightarrow}{\mathbf{I}}\Big(\mathbf{E_1}\cdot\mathbf{E_2} + \mathbf{B_1}\cdot\mathbf{B_2}\Big)\right]. \tag{3.17}$$

Then Eq. (3.14) can be rewritten by means of $\overset{\leftrightarrow}{\mathbf{T}}_1$, $\overset{\leftrightarrow}{\mathbf{T}}_2$ and $\overset{\leftrightarrow}{\mathbf{T}}_{(12)}$ being entitled, respectively, as the contribution given solely by the label 1 electromagnetic field, plus the contribution given merely by the label 2 electromagnetic field and the coupled contribution between fields 1 and 2.

In particular, concerning to the problem in question, the total electromagnetic field is given

by a combination of the external and the induced fields as

$$\mathbf{E} = \mathbf{E}^{ext} + \mathbf{E}^{scat} \quad \text{and} \quad \mathbf{B} = \mathbf{B}^{ext} + \mathbf{B}^{scat}. \tag{3.18}$$

Thus, the Maxwell stress tensor can be separated in accordance to Eqs. (3.14)-(3.16), as

$$\overset{\leftrightarrow}{\mathbf{T}} = \overset{\leftrightarrow}{\mathbf{T}}^{ext} + \overset{\leftrightarrow}{\mathbf{T}}^{scat} + \overset{\leftrightarrow}{\mathbf{T}}^{(ext,\, scat)}, \tag{3.19}$$

with

$$\overset{\leftrightarrow}{\mathbf{T}}^{ext} = \frac{1}{4\pi}\left[\mathbf{E}^{ext}\mathbf{E}^{ext} + \mathbf{B}^{ext}\mathbf{B}^{ext} - \frac{\overset{\leftrightarrow}{\mathbf{I}}}{2}\left(\mathbf{E}^{ext} \cdot \mathbf{E}^{ext} + \mathbf{B}^{ext} \cdot \mathbf{B}^{ext} \right) \right], \tag{3.20a}$$

$$\overset{\leftrightarrow}{\mathbf{T}}^{scat} = \frac{1}{4\pi}\left[\mathbf{E}^{scat}\mathbf{E}^{scat} + \mathbf{B}^{scat}\mathbf{B}^{scat} - \frac{\overset{\leftrightarrow}{\mathbf{I}}}{2}\left(\mathbf{E}^{scat} \cdot \mathbf{E}^{scat} + \mathbf{B}^{scat} \cdot \mathbf{B}^{scat} \right) \right], \tag{3.20b}$$

$$\overset{\leftrightarrow}{\mathbf{T}}^{(ext,\, scat)} = \overset{\leftrightarrow}{\mathbf{T}}^{ext,\, scat} + \overset{\leftrightarrow}{\mathbf{T}}^{scat,\, ext}. \tag{3.20c}$$

Then, using Eq. (2.68) the total linear momentum transferred from the electron to the NP is given by three contributions

$$\Delta\mathbf{P} = \int_{-\infty}^{\infty} \oint_S \overset{\leftrightarrow}{\mathbf{T}}(\mathbf{r};t) \cdot \hat{\mathbf{n}}\, da\, dt = \int_{-\infty}^{\infty} \oint_S \left[\overset{\leftrightarrow}{\mathbf{T}}^{ext}(\mathbf{r};t) + \overset{\leftrightarrow}{\mathbf{T}}^{scat}(\mathbf{r};t) + \overset{\leftrightarrow}{\mathbf{T}}^{(ext,\, scat)}(\mathbf{r};t) \right] \cdot \hat{\mathbf{n}}\, da\, dt$$

$$= \int_{-\infty}^{\infty} \oint_S \left[\overset{\leftrightarrow}{\mathbf{T}}^{scat}(\mathbf{r};t) + \overset{\leftrightarrow}{\mathbf{T}}^{(ext,\, scat)}(\mathbf{r};t) \right] \cdot \hat{\mathbf{n}}\, da\, dt, \tag{3.21}$$

where the last equality follows from the fact that the Maxwell stress tensor flux (over a closed surface not intersecting the electron's path and integrated in time) of the electromagnetic field produced by the electron is zero, as it is demonstrated in Appendix B.

Finally, recalling that [Eq. (2.84)]

$$\Delta\mathbf{P} = \oint_S \overset{\leftrightarrow}{\mathbf{T}}(\mathbf{r};\omega = 0) \cdot \hat{\mathbf{n}}\, da.$$

$$= \int_0^{\infty} \frac{1}{4\pi^2} \oint_S \mathrm{Re}\left[\sum_{\boldsymbol{\alpha}=\{\mathbf{E},\mathbf{B}\}} \boldsymbol{\alpha}(\mathbf{r};\omega)\boldsymbol{\alpha}^*(\mathbf{r};\omega) - \frac{\overset{\leftrightarrow}{\mathbf{I}}}{2}|\boldsymbol{\alpha}(\mathbf{r};\omega)|^2 \right] \cdot \hat{\mathbf{n}}\, da\, d\omega$$

$$= \int_0^{\infty} \boldsymbol{\mathcal{P}}\left(\omega'\right)\, d\omega'.$$

Equation (3.21) may be rewritten as

$$\boxed{\Delta\mathbf{P} = \int_0^{\infty} \left[\boldsymbol{\mathcal{P}}_{\mathbf{E}}^{scat}(\omega) + \boldsymbol{\mathcal{P}}_{\mathbf{B}}^{scat}(\omega) + \boldsymbol{\mathcal{P}}_{\mathbf{E}}^{(ext,\, scat)}(\omega) + \boldsymbol{\mathcal{P}}_{\mathbf{B}}^{(ext,\, scat)}(\omega) \right] d\omega,} \tag{3.22}$$

with each term of the spectral contribution $\boldsymbol{\mathcal{P}}$ given by,

$$\boldsymbol{\mathcal{P}}_{\mathbf{E}}^{scat}(\omega) = \frac{1}{4\pi^2} \oint_S \mathrm{Re}\left\{ \mathbf{E}^{scat}(\mathbf{r};\omega)[\mathbf{E}^{scat}(\mathbf{r};\omega)]^* - \frac{\overset{\leftrightarrow}{\mathbf{I}}}{2}|\mathbf{E}^{scat}(\mathbf{r};\omega)|^2 \right\} \cdot \hat{\mathbf{n}}\, da, \tag{3.23a}$$

$$\boldsymbol{\mathcal{P}}_{\mathbf{B}}^{scat}\left(\omega\right) = \frac{1}{4\pi^2} \oint_S \mathrm{Re}\left\{\mathbf{B}^{scat}(\mathbf{r};\omega)[\mathbf{B}^{scat}(\mathbf{r};\omega)]^* - \frac{\overleftrightarrow{\mathbf{I}}}{2}|\mathbf{B}^{scat}(\mathbf{r};\omega)|^2\right\} \cdot \hat{\mathbf{n}}\,da, \qquad (3.23b)$$

$$\boldsymbol{\mathcal{P}}_{\mathbf{E}}^{(ext,\,scat)}\left(\omega\right) = \frac{1}{4\pi^2} \oint_S \mathrm{Re}\left\{\mathbf{E}^{ext}(\mathbf{r};\omega)[\mathbf{E}^{scat}(\mathbf{r};\omega)]^* + \mathbf{E}^{scat}(\mathbf{r};\omega)[\mathbf{E}^{ext}(\mathbf{r};\omega)]^* \right. \qquad (3.23c)$$

$$\left. -\ \overleftrightarrow{\mathbf{I}}\,\mathbf{E}^{ext}(\mathbf{r};\omega)\cdot[\mathbf{E}^{scat}(\mathbf{r};\omega)]^*\right\} \cdot \hat{\mathbf{n}}\,da,$$

$$\boldsymbol{\mathcal{P}}_{\mathbf{B}}^{(ext,\,scat)}\left(\omega\right) = \frac{1}{4\pi^2} \oint_S \mathrm{Re}\left\{\mathbf{B}^{ext}(\mathbf{r};\omega)[\mathbf{B}^{scat}(\mathbf{r};\omega)]^* + \mathbf{B}^{scat}(\mathbf{r};\omega)[\mathbf{B}^{ext}(\mathbf{r};\omega)]^* \right. \qquad (3.23d)$$

$$\left. -\ \overleftrightarrow{\mathbf{I}}\,\mathbf{B}^{ext}(\mathbf{r};\omega)\cdot[\mathbf{B}^{scat}(\mathbf{r};\omega)]^*\right\} \cdot \hat{\mathbf{n}}\,da.$$

This general decomposition of the spectral contribution to the total linear momentum transfer, by virtue of the Maxwell stress tensor decomposition, concludes that the linear momentum transferred from the electron to the NP is set up by two main contributions: the electromagnetic field scattered by the nanoparticle and the coupling between the electromagnetic field produced by the electron and the induced one.

3.3   Analytical solutions to the spectral linear momentum

The intention of Section 3.2 is to point out a path in order to address the problem of finding analytical solutions to the closed surface integral of the Maxwell stress tensor in spite of numerical limitations.

Within the dipole approximation, the electric field scattered by the NP can be rewritten in accordance to Eqs. (3.11) as

$$E_{r,\,\ell=1}^{scat} = \mathbb{E}_{r1}\,\sin\theta\cos\varphi + \mathbb{E}_{r2}\,\cos\theta, \qquad (3.24a)$$

$$E_{\theta,\,\ell=1}^{scat} = \mathbb{E}_{\theta1}\,\cos\varphi + \mathbb{E}_{\theta2}\,\cos\theta\cos\varphi + \mathbb{E}_{\theta3}\,\sin\theta, \qquad (3.24b)$$

$$E_{\varphi,\,\ell=1}^{scat} = \mathbb{E}_{\varphi1}\,\sin\varphi + \mathbb{E}_{\varphi2}\,\cos\theta\sin\varphi, \qquad (3.24c)$$

and the scattered magnetic field ($\mathbf{H} = \mathbf{B}$ in free space) in accordance to Eqs. (3.12) as

$$B_{r,\,\ell=1}^{scat} = \mathbb{B}_{r1}\,\sin\theta\sin\varphi, \qquad (3.25a)$$

$$B_{\theta,\,\ell=1}^{scat} = \mathbb{B}_{\theta1}\,\cos\theta\sin\varphi + \mathbb{B}_{\theta2}\,\sin\varphi, \qquad (3.25b)$$

$$B_{\varphi,\,\ell=1}^{scat} = \mathbb{B}_{\varphi1}\,\cos\varphi + \mathbb{B}_{\varphi2}\,\cos\theta\cos\varphi + \mathbb{B}_{\varphi3}\,\sin\theta, \qquad (3.25c)$$

with

$$\mathbb{E}_{r1} = \frac{6k_0}{c\gamma\beta^2}\,t_1^E\,\frac{h_1^{(+)}(k_0 r)}{k_0 r}K_1\left(\frac{\omega x_0}{v\gamma}\right); \quad \mathbb{E}_{r2} = i\frac{6k_0}{c\gamma^2\beta^2}\,t_1^E\,\frac{h_1^{(+)}(k_0 r)}{k_0 r}K_0\left(\frac{\omega x_0}{v\gamma}\right);$$

$$\mathbb{E}_{\theta1} = i\frac{3\,k_0}{c\gamma\beta}\,t_1^M\,h_1^{(+)}(k_0 r)\,K_1\left(\frac{\omega x_0}{v\gamma}\right); \quad \mathbb{E}_{\varphi2} = -\,i\frac{3\,k_0}{c\gamma\beta}\,t_1^M\,h_1^{(+)}(k_0 r)\,K_1\left(\frac{\omega x_0}{\gamma v}\right);$$

$$\mathbb{E}_{\theta2} = \frac{3\,k_0}{c\gamma\beta^2}\,t_1^E\left[2\,\frac{h_1^{(+)}(k_0 r)}{k_0 r} - h_2^{(+)}(k_0 r)\right]K_1\left(\frac{\omega x_0}{v\gamma}\right); \qquad (3.26)$$

$$\mathbb{E}_{\theta3} = -\,i\frac{3\,k_0}{c\gamma^2\beta^2}\,t_1^E\left[2\,\frac{h_1^{(+)}(k_0 r)}{k_0 r} - h_2^{(+)}(k_0 r)\right]K_0\left(\frac{\omega x_0}{v\gamma}\right);$$

$$\mathbb{E}_{\varphi 1} = -\frac{3\,k_0}{c\gamma\beta^2} t_1^E \left[2\,\frac{h_1^{(+)}(k_0 r)}{k_0 r} - h_2^{(+)}(k_0 r) \right] K_1 \left(\frac{\omega x_0}{\gamma v} \right)$$

and

$$\mathbb{B}_{r1} = \frac{6k_0}{c\gamma\beta} t_1^M \frac{h_1^{(+)}(k_0 r)}{k_0 r} K_1 \left(\frac{\omega x_0}{v\gamma} \right); \quad \mathbb{B}_{\theta 2} = i\frac{3k_0}{c\gamma\beta^2} t_1^E h_1^{(+)}(k_0 r) K_1 \left(\frac{\omega x_0}{v\gamma} \right);$$

$$\mathbb{B}_{\theta 1} = \frac{3k_0}{c\gamma\beta} t_1^M \left[2\,\frac{h_1^{(+)}(k_0 r)}{k_0 r} - h_2^{(+)}(k_0 r) \right] K_1 \left(\frac{\omega x_0}{v\gamma} \right);$$

$$\mathbb{B}_{\varphi 1} = \frac{3k_0}{c\gamma\beta} t_1^M \left[2\,\frac{h_1^{(+)}(k_0 r)}{k_0 r} - h_2^{(+)}(k_0 r) \right] K_1 \left(\frac{\omega x_0}{v\gamma} \right); \tag{3.27}$$

$$\mathbb{B}_{\varphi 2} = i\frac{3k_0}{c\gamma\beta^2} t_1^E h_1^{(+)}(k_0 r) K_1 \left(\frac{\omega x_0}{v\gamma} \right); \quad \mathbb{B}_{\varphi 3} = \frac{1}{\gamma} t_1^E h_1^{(+)}(k_0 r) K_0 \left(\frac{\omega x_0}{v\gamma} \right),$$

functions which only depend on the frequency (ω), the electron's velocity (v), the NP's radius (a) and the magnitude of the position vector (r) where the total electromagnetic field will be evaluated[1]. It is worth noting that these functions do not depend on the angular variables (θ, φ). Thus, substituting Eqs. (3.24) and (3.25) into Eqs. (3.23a) and Eqs. (3.23b), the electric and magnetic spectral contributions of the scattered field, in the dipole approximation, are given in spherical components by

$$\mathcal{P}_{\mathbf{E},\,r}^{scat}(\omega) = \frac{r^2}{12\pi} \operatorname{Re}[2\,\mathbb{E}_{r1}\mathbb{E}_{r1}^* + 2\,\mathbb{E}_{r2}\mathbb{E}_{r2}^* - 3\,\mathbb{E}_{\theta 1}\mathbb{E}_{\theta 1}^* - \mathbb{E}_{\theta 2}\mathbb{E}_{\theta 2}^* - 4\,\mathbb{E}_{\theta 3}\mathbb{E}_{\theta 3}^* \tag{3.28a}$$
$$- \mathbb{E}_{\varphi 1}\mathbb{E}_{\varphi 1}^* - \mathbb{E}_{\varphi 2}\mathbb{E}_{\varphi 2}^*],$$

$$\mathcal{P}_{\mathbf{E},\,\theta}^{scat}(\omega) = \frac{r^2}{8} \operatorname{Re}[\mathbb{E}_{\theta 1}\,\mathbb{E}_{r1}^*], \tag{3.28b}$$

$$\mathcal{P}_{\mathbf{E},\,\varphi}^{scat}(\omega) = 0, \tag{3.28c}$$

and

$$\mathcal{P}_{\mathbf{B},\,r}^{scat}(\omega) = \frac{r^2}{12\pi} \operatorname{Re}[2\,\mathbb{B}_{r1}\mathbb{B}_{r1}^* - \mathbb{B}_{\theta 1}\mathbb{B}_{\theta 1}^* - 3\,\mathbb{B}_{\theta 2}\mathbb{B}_{\theta 2}^* - 3\,\mathbb{B}_{\varphi 1}\mathbb{B}_{\varphi 1}^* - \mathbb{B}_{\varphi 2}\mathbb{B}_{\varphi 2}^* - 4\,\mathbb{B}_{\varphi 3}\mathbb{B}_{\varphi 3}^*], \tag{3.29a}$$

$$\mathcal{P}_{\mathbf{B},\,\theta}^{scat}(\omega) = \frac{r^2}{8} \operatorname{Re}[\mathbb{B}_{\theta 2}\,\mathbb{B}_{r1}^*], \tag{3.29b}$$

$$\mathcal{P}_{\mathbf{B},\,\varphi}^{scat}(\omega) = 0. \tag{3.29c}$$

In a similar way, according to Eqs. (2.29) and (2.30), the electromagnetic field produced by the electron can be rewritten as

$$E_x^{ext}(\mathbf{r};\omega) = -\xi(\omega)\frac{e^{i\omega z}}{R} K_1 \left(\frac{\omega R}{v\gamma} \right) (x - x_0), \tag{3.30a}$$

$$E_y^{ext}(\mathbf{r};\omega) = -\xi(\omega)\frac{e^{i\omega z}}{R} K_1 \left(\frac{\omega R}{v\gamma} \right) y, \tag{3.30b}$$

---

[1]In the calculation of the total linear momentum transferred, r corresponds to the integration surface radius.

$$E_z^{ext}(\mathbf{r};\omega) = i\frac{\xi(\omega)}{\gamma}\frac{e^{i\omega z}}{R}K_0\left(\frac{\omega R}{v\gamma}\right), \tag{3.30c}$$

and

$$B_x^{ext}(\mathbf{r};\omega) = -\beta\xi(\omega)\frac{e^{i\omega z}}{R}K_1\left(\frac{\omega R}{v\gamma}\right)y, \tag{3.31a}$$

$$B_y^{ext}(\mathbf{r};\omega) = \beta\xi(\omega)\frac{e^{i\omega z}}{R}K_1\left(\frac{\omega R}{v\gamma}\right)(x-x_0), \tag{3.31b}$$

$$B_z^{ext}(\mathbf{r};\omega) = 0, \tag{3.31c}$$

where $R = \sqrt{(x-x_0)^2 + y^2}$, $\xi(\omega) = 2e\omega/v^2\gamma$ and $|\omega| = \omega$ since the integration of the spectral contribution to the total linear momentum transferred [Eq. (3.22)] is performed for positive frequencies. Then, writing the external electromagnetic field in spherical coordinates and substituting these expressions into Eqs. (3.23c) and (3.23d), the coupling—between the external electromagnetic field and the electromagnetic field scattered by the NP—spectral contribution is given in spherical components by

$$\mathcal{P}_{\mathbf{E},r}^{(ext,\,scat)}(\omega) = \frac{r^2}{4\pi^2}\xi(\omega)\int_0^{2\pi}\int_0^{\pi}\text{Re}\big[\mathbb{T}_r^E\big]\sin\theta\,d\theta\,d\varphi, \tag{3.32a}$$

$$\mathcal{P}_{\mathbf{E},\theta}^{(ext,\,scat)}(\omega) = \frac{r^2}{4\pi^2}\xi(\omega)\int_0^{2\pi}\int_0^{\pi}\text{Re}\big[\mathbb{T}_\theta^E\big]\sin\theta\,d\theta\,d\varphi, \tag{3.32b}$$

$$\mathcal{P}_{\mathbf{E},\varphi}^{(ext,\,scat)}(\omega) = \frac{r^2}{4\pi^2}\xi(\omega)\int_0^{2\pi}\int_0^{\pi}\text{Re}\big[\mathbb{T}_\varphi^E\big]\sin\theta\,d\theta\,d\varphi, \tag{3.32c}$$

with

$$\begin{aligned}
\mathbb{T}_r^E = \frac{1}{\gamma R}\Bigg\{&e^{-iz\omega/v}\bigg[-i\,K_0\left(\frac{\omega R}{v\gamma}\right)\cos\theta + \gamma K_1\left(\frac{\omega R}{v\gamma}\right)\Big((x_0-x)\sin\theta\cos\varphi\\
&-y\sin\theta\sin\varphi\Big)\bigg]\Big[\mathbb{E}_{r1}\sin\theta\cos\varphi + \mathbb{E}_{r2}\cos\theta\Big] - e^{iz\omega/v}\bigg[-iK_0\left(\frac{\omega R}{v\gamma}\right)\sin\theta\\
&+\gamma K_1\left(\frac{\omega R}{v\gamma}\right)\Big((x_0-x)\cos\theta\cos\varphi - y\cos\theta\sin\varphi\Big)\bigg]\Big[\mathbb{E}_{\theta1}^*\cos\varphi + \mathbb{E}_{\theta2}^*\cos\theta\\
&\times\cos\varphi + \mathbb{E}_{\theta3}^*\sin\theta\Big] + e^{iz\omega/v}\gamma K_1\left(\frac{\omega R}{v\gamma}\right)\bigg[y\sin\varphi\cos\varphi + (x_0-x)\sin^2\varphi\bigg]\\
&\times\bigg[\mathbb{E}_{\varphi1}^* + \mathbb{E}_{\varphi2}^*\cos\theta\bigg]\Bigg\},
\end{aligned} \tag{3.33a}$$

$$\begin{aligned}
\mathbb{T}_\theta^E = \frac{1}{\gamma R}\Bigg\{&e^{-iz\omega/v}\bigg[-i\,K_0\left(\frac{\omega R}{v\gamma}\right)\cos\theta + \gamma K_1\left(\frac{\omega R}{v\gamma}\right)\Big((x_0-x)\sin\theta\cos\varphi\\
&-y\sin\theta\sin\varphi\Big)\bigg]\Big[\mathbb{E}_{\theta1}\cos\varphi + \mathbb{E}_{\theta2}\cos\theta\cos\varphi + \mathbb{E}_{\theta3}\sin\theta\Big] + e^{iz\omega/v}\times\\
&\times\bigg[-i\,K_0\left(\frac{\omega R}{v\gamma}\right)\sin\theta + \gamma K_1\left(\frac{\omega R}{v\gamma}\right)\Big((x_0-x)\cos\theta\cos\varphi - y\cos\theta\sin\varphi\Big)\bigg]
\end{aligned} \tag{3.33b}$$

$$\times \left[\mathbb{E}_{r1}^* \sin\theta \cos\varphi + \mathbb{E}_{r2}^* \cos\theta \right] \Bigg\},$$

$$\mathbb{T}_\varphi^E = \frac{1}{\gamma R} \Bigg\{ e^{-iz\omega/v} \Bigg[-i\, K_0 \left(\frac{\omega R}{v\gamma}\right) \cos\theta \sin\varphi + \gamma K_1 \left(\frac{\omega R}{v\gamma}\right) \Bigg((x_0 - x) \sin\theta \sin\varphi$$

$$\times \cos\varphi + y \sin\theta \sin^2\varphi \Bigg) \Bigg] \left[\mathbb{E}_{\varphi1} + \mathbb{E}_{\varphi2} \cos\theta \right] - \gamma e^{iz\omega/v} K_1 \left(\frac{\omega R}{v\gamma}\right) \Bigg[(x_0 - x) \qquad (3.33\mathrm{c})$$

$$\times \sin\varphi + y \cos\varphi \Bigg] \left[\mathbb{E}_{r1}^* \sin\theta \cos\varphi + \mathbb{E}_{r2}^* \cos\theta \right] \Bigg\},$$

and

$$\mathcal{P}_{\mathbf{B},\,r}^{(ext,\,scat)} (\omega) = \frac{r^2}{4\pi^2}\, \xi(\omega) \int_0^{2\pi} \int_0^{\pi} \mathrm{Re}\left[\mathbb{T}_r^B\right] \sin\theta\, d\theta\, d\varphi, \qquad (3.34\mathrm{a})$$

$$\mathcal{P}_{\mathbf{B},\,\theta}^{(ext,\,scat)} (\omega) = \frac{r^2}{4\pi^2}\, \xi(\omega) \int_0^{2\pi} \int_0^{\pi} \mathrm{Re}\left[\mathbb{T}_\theta^B\right] \sin\theta\, d\theta\, d\varphi, \qquad (3.34\mathrm{b})$$

$$\mathcal{P}_{\mathbf{B},\,\varphi}^{(ext,\,scat)} (\omega) = \frac{r^2}{4\pi^2}\, \xi(\omega) \int_0^{2\pi} \int_0^{\pi} \mathrm{Re}\left[\mathbb{T}_\varphi^B\right] \sin\theta\, d\theta\, d\varphi, \qquad (3.34\mathrm{c})$$

with

$$\mathbb{T}_r^B = \frac{\beta}{R} K_1 \left(\frac{\omega R}{v\gamma}\right) \Bigg\{ e^{-iz\omega/v} \Bigg[-\sin^2\theta \sin\varphi \Bigg(y \cos\varphi + (x_0 - x) \sin\varphi \Bigg) \mathbb{B}_{r1} \Bigg]$$

$$+ e^{iz\omega/v} \cos\theta \sin\varphi \Bigg[y \cos\varphi + (x_0 - x) \sin\varphi \Bigg] \Bigg[\mathbb{B}_{\theta1}^* \cos\theta + \mathbb{B}_{\theta2}^* \Bigg] \qquad (3.35\mathrm{a})$$

$$+ e^{iz\omega/v} \Bigg[(x_0 - x) \cos\varphi - y \sin\varphi \Bigg] \Bigg[\mathbb{B}_{\varphi1}^* \cos\varphi + \mathbb{B}_{\varphi2}^* \cos\theta \cos\varphi$$

$$+ \mathbb{B}_{\varphi3}^* \sin\theta \Bigg] \Bigg\},$$

$$\mathbb{T}_\theta^B = -\frac{\beta}{R} K_1 \left(\frac{\omega R}{v\gamma}\right) \sin\theta \sin\varphi \Bigg[y \cos\varphi + (x_0 - x) \sin\varphi \Bigg] \Bigg[\mathbb{B}_{\theta1}\, e^{-iz\omega/v} \cos\theta \qquad (3.35\mathrm{b})$$

$$+ \mathbb{B}_{\theta2}\, e^{-iz\omega/v} + \mathbb{B}_{r1}^*\, e^{iz\omega/v} \cos\theta \Bigg],$$

$$\mathbb{T}_\varphi^B = \frac{\beta}{R} K_1 \left(\frac{\omega R}{v\gamma}\right) \sin\theta \Bigg\{ -e^{-iz\omega/v} \Bigg[y \cos\varphi + (x_0 - x) \sin\varphi \Bigg] \Bigg[\mathbb{B}_{\varphi1} \cos\varphi$$

$$+ \mathbb{B}_{\varphi2} \cos\theta \cos\varphi + \mathbb{B}_{\varphi3} \sin\theta \Bigg] + \mathbb{B}_{r1}^*\, e^{iz\omega/v} \Bigg[y \sin^2\varphi - (x_0 - x) \sin\varphi \qquad (3.35\mathrm{c})$$

$$\times \cos\varphi \Bigg] \Bigg\},$$

where (x, y, z) are functions of (r, θ, φ) in the usual way cartesian and spherical coordinates are related [19].

In general, we have not yet solved integrals (3.32) and (3.34) analytically. Nonetheless, for

large impact parameters compared with the NP's radius, the following relations are satisfied

$$x_0 \gg a \quad \text{and} \quad x_0 \gg r, \tag{3.36}$$

then

$$(x, y, z) \sim 0 \quad \text{and} \quad R \sim x_0. \tag{3.37}$$

For this particular case, integrals (3.32) and (3.34), together with functions $\mathbb{T}_{\{r,\theta,\varphi\}}^{\{E,B\}}$, have analytical solutions given by

$$\mathcal{P}_{\mathbf{E},r}^{(ext,\,scat)}(\omega; x_0 \gg a) = \frac{r^2}{6\pi} \xi(\omega) \left[\frac{2}{x_0\gamma} K_0\left(\frac{\omega x_0}{v\gamma}\right) \mathrm{Re}\left(i\, 2\, \mathbb{E}_{\theta 3}^* - i\, \mathbb{E}_{r2}\right) + K_1\left(\frac{\omega x_0}{v\gamma}\right) \right. \tag{3.38a}$$

$$\left. \times \mathrm{Re}\left(2\, \mathbb{E}_{r1} - \mathbb{E}_{\theta 2}^* + 3\, \mathbb{E}_{\varphi 1}^*\right) \right],$$

$$\mathcal{P}_{\mathbf{E},\theta}^{(ext,\,scat)}(\omega; x_0 \gg a) = \frac{r^2}{8} \xi(\omega) K_1\left(\frac{\omega x_0}{v\gamma}\right) \mathrm{Re}\left(\mathbb{E}_{\theta 1}\right), \tag{3.38b}$$

$$\mathcal{P}_{\mathbf{E},\varphi}^{(ext,\,scat)}(\omega; x_0 \gg a) = 0, \tag{3.38c}$$

and

$$\mathcal{P}_{\mathbf{B},r}^{(ext,\,scat)}(\omega; x_0 \gg a) = \frac{r^2}{6\pi} \beta\, \xi(\omega) K_1\left(\frac{\omega x_0}{v\gamma}\right) \mathrm{Re}\left(\mathbb{B}_{\theta 1}^* + 3\, \mathbb{B}_{\varphi 1}^* - 2\, \mathbb{B}_{r1}\right), \tag{3.39a}$$

$$\mathcal{P}_{\mathbf{B},\theta}^{(ext,\,scat)}(\omega; x_0 \gg a) = -\frac{r^2}{8} \beta\, \xi(\omega) K_1\left(\frac{\omega x_0}{v\gamma}\right) \mathrm{Re}\left(\mathbb{B}_{\theta 2}\right), \tag{3.39b}$$

$$\mathcal{P}_{\mathbf{B},\varphi}^{(ext,\,scat)}(\omega; x_0 \gg a) = 0. \tag{3.39c}$$

NUMERICAL RESULTS FOR THE MOMENTUM TRANSFER WITHIN THE DIPOLE APPROXIMATION

As a first glance for solving closed surface integral of the Maxwell stress tensor for the total linear momentum transfer, the dipole approximation elucidates the kind of integrals involved within the calculations of the spectral contribution, and even though they may or may not be analytically solved it is relevant to study (at least in a numerical approach) the contribution given by this first multipole to the total linear momentum transferred. Indeed, studying the part played by the multipole $\ell = 1$ in the attraction-repulsion effect—inside the linear momentum transfer mechanism—provides us with information for a better understanding of such phenomenon. In this Chapter we study the numerical results for metallic nanoparticles (aluminium and gold) within the dipole approximation in order to answer the question to whether the first multipole contribution is sufficient to have a repulsion effect or not. The first Section is devoted to study the characteristic behavior of the transverse and longitudinal spectral contributions for both aluminium and gold nanoparticles. In Section 2 we present a comparison between the dipole approximation and a model proposed in [10], where the nanoparticle is considered as a pure point-like dipole. Finally, the last Section is committed to discuss the problematic concerning the attraction-repulsion phenomenon in the dipole approximation by means of general results obtained from the total linear momentum against the electron's velocity.

4.1 Metallic nanoparticles: Aluminium and gold characteristic behavior

Our initial interest in studying metallic[1] nanoparticles arose from the fact that the first STEM experiments in 2008 involved gold (Au) NPs as samples [5]. In these experiments, the Au NPs on a thin carbon substrate displayed an attraction-repulsion effect when pumped with electron beams, as explained in Chapter 1. Moreover, in 1999 the first calculations of the total linear momentum transferred were accomplished using aluminium (Al) [6], and in 2010 theoretical calculations predicted a transition in the transverse component of the total linear momentum transfer from attractive (positive linear momentum) to repulsive (negative linear

---

[1]As matter of fact, novel calculations have been made concerning dielectric materials such as MgO and SiC, showing that the dielectric materials may or may not exhibit an attraction-repulsion transition [26].

momentum) for gold dimer NPs [23]. Motivated with those results, it is of interest to study the contribution given by the dipole approximation to the differential momentum transfer per unit frequency ($\mathcal{P}$) for materials such as Al and Au; and also to obtain the spectral information of the particle response to the broadband probing electron in order to observe the sign of the differential momentum contributed by each frequency. For this reason, a numerical programming code (see Appendix C) was developed for calculating the spectral contribution and the total linear momentum transferred, for both Al and Au materials, within the dipole approximation.

It is also important to note that for a spherical scattering source the resonance of each mode is determined by Mie coefficient denominators, since the electromagnetic field scattered by the sphere was obtained in multipolar contributions, constructed explicitly in Chapter 2. According to Eqs. (2.36), (2.41) and (2.52)

$$\mathbf{E}(\mathbf{r};\omega) = \mathbf{L}\psi^M(\mathbf{r};\omega) - \frac{i}{k}\nabla\times\mathbf{L}\psi^E(\mathbf{r};\omega),$$

$$\mathbf{H}(\mathbf{r};\omega) = -\frac{i}{k}\nabla\times\mathbf{L}\psi^M(\mathbf{r};\omega) - \mathbf{L}\psi^M(\mathbf{r};\omega),$$

$$\psi^{M,\,scat}_{\ell,m} = t^M_\ell \psi^{M,\,ext}_{\ell,m},$$

$$\psi^{E,\,scat}_{\ell,m} = t^E_\ell \psi^{E,\,ext}_{\ell,m},$$

then, the electric and magnetic scattered fields can be rewritten in the general form[2],

$$\mathbf{E}^{scat}(\mathbf{r};\omega) = \sum_{\ell=1}^{\infty}\left(t^M_\ell\mathbf{E}^M_\ell + t^E_\ell\mathbf{E}^E_\ell\right) \quad\text{and}\quad \mathbf{B}^{scat}(\mathbf{r};\omega) = \sum_{\ell=1}^{\infty}\left(t^M_\ell\mathbf{B}^M_\ell + t^E_\ell\mathbf{B}^E_\ell\right). \tag{4.1}$$

In this way, the contribution given by the ℓ multipole to the induced field will dominate against the other multipoles when t^M_ℓ and t^E_ℓ achieved a maximum value, that is, when the denominator of Mie coefficients t^E_ℓ and t^M_ℓ are equal to zero. For instance, this last condition implies on t^E_ℓ

$$t^E_\ell = \frac{\epsilon_i\, j_\ell\,(x_i)\,[x\, j_\ell\,(x)]' - j_\ell\,(x)\,[x_i\, j_\ell\,(x_i)]'}{h^{(+)}_\ell\,(x)\,[x_i\, j_\ell\,(x_i)]' - \epsilon_i\, j_\ell\,(x_i)\,\left[x\, h^{(+)}_\ell\,(x)\right]'},$$

that for a certain frequency (or several frequencies) ω_ℓ,

$$h^{(+)}_\ell\,(x)\,[x_i\, j_\ell\,(x_i)]' - \epsilon_i(\omega_\ell)\, j_\ell\,(x_i)\,\left[x\, h^{(+)}_\ell\,(x)\right]' = 0. \tag{4.2}$$

Thus, expanding Eq. (4.2) in the small particle limit[3] and taking the following expressions at the origin for spherical Bessel and Hankel functions [17]

$$j_\ell(z\to 0) = \frac{z^\ell}{(2\ell+1)!!}, \tag{4.3a}$$

$$h^{(+)}_\ell(z\to 0) = ih^{(1)}_\ell(z\to 0) = \frac{(2\ell-1)!!}{z^{\ell+1}}, \tag{4.3b}$$

---

[2]In Eqs. (4.1) repeated indices do not imply sum over them, they only play the role of dummy labels corresponding to the electric (E) and the magnetic (M) components defined in the scalar decomposition method.

[3]The small particle limit considers the particle radius smaller than the wavelength of the incident electromagnetic field. Thus, $x = ka = 2\pi\frac{a}{\lambda} \ll 1$ and similarly $x_i = x\sqrt{\epsilon_i} \ll 1$.

it is straightforward to find out that

$$\epsilon_i(\omega_\ell) = -\frac{\ell + 1}{\ell}, \tag{4.4}$$

as obtained in a similar way in [27] for the Mie solution in the small particle approximation. Therefore, Eq. (4.4) establishes a way to calculate the eigenfrequencies of the spherical nano-particle embedded in vacuum, once its dielectric function is known. Particularly, for a material modeled as a free electron gas, like metals used to be considered in first approach, the dielectric function is specified according to the Drude's model [11]. Whilst for a more sophisticated electric response, several models are suggested in order to reproduce experimental data like for example a superposition of Lorentz functions [28], as will be shown as follows.

Nanoparticle modeled as a Drude-type aluminium material

The NP modeled as aluminium was characterized by a dielectric function $\epsilon_i(\omega)$ determined in the free electron gas model, also known as Drude model, given by, see [11] and [9],

$$\epsilon_i(\omega) = 1 - \frac{\omega_p^2}{\omega(\omega + i\Gamma)}, \tag{4.5}$$

with $\omega_p = \sqrt{4\pi n e^2/m_e}$ the bulk plasma frequency, n the number of electrons per unit volume, m_e the electron's mass and Γ the phenomenological damping constant.
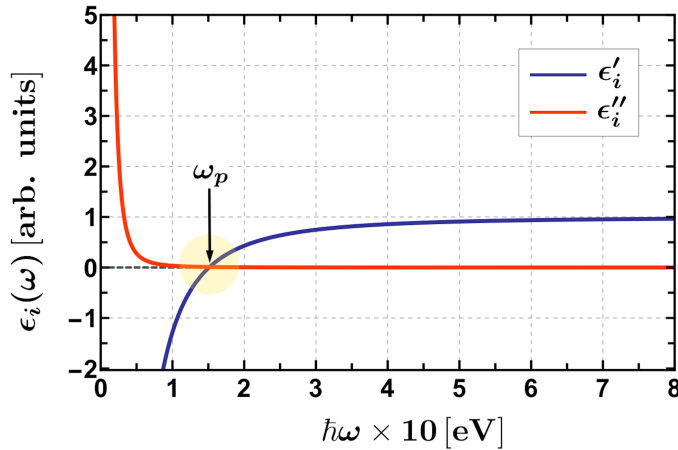

Figure 4.1. Real (blue line) and imaginary (red line) parts of the Al dielectric function modeled as a Drude-type material. The frequency in which the intersection between both lines happens is equal to the bulk plasma frequency, which for aluminium is $\hbar\omega_p = 15.1\,\text{eV}$. The dielectric function is displayed in arbitrary units [arb. units].

The case of aluminium corresponds to plasma frequency $\hbar\omega_p = 15.1\,\text{eV}$ and to electron gas damping $\hbar\Gamma = 0.19\,\text{eV}$ [29]. However, since the peaks of the spectral contribution to the total linear momentum are related to plasmon resonances in metals, the width of each resonance is inversely proportional to the mean lifetime of plasmons, and for a Drude-type model this time corresponds to the inverse of the damping constant [30]. Thus, the electron gas damping for the Al studied was set up as $\hbar\Gamma = \hbar\omega_p/100 = 0.151\,\text{eV}$ in order to clarify the visualization of

each peak in the spectral contribution plots. In Fig. 4.1 Drude's dielectric function is displayed with the parameters set up for the Al. The real (blue curve in Fig. 4.1) and the imaginary (red curve in Fig. 4.1) parts of the dielectric function were plotted according to the decomposition $\epsilon_i(\omega) = \epsilon'_i(\omega) + i\epsilon''_i(\omega)$, since in general, the dielectric function in the frequency domain is a complex function.

Moreover, multipolar resonances can be obtained by substituting Eq. (4.5) into Eq. (4.4). In this way, the resonance frequency of the ℓ-plasmon mode is determined by the following relation

$$\frac{\omega_\ell^2}{\omega_p^2} + i\frac{\Gamma}{\omega_p^2}\omega_\ell = \frac{\ell}{2\ell+1}, \tag{4.6}$$

and separating the eigenfrequency as $\omega_\ell = \omega'_\ell + i\omega''_\ell$, the ℓ-resonance frequency ω_ℓ results in

$$\omega'_\ell = \omega_p\sqrt{\frac{\ell}{2\ell+1} - \left(\frac{\Gamma}{2\omega_p}\right)^2}, \tag{4.7a}$$

$$\omega''_\ell = -\frac{\Gamma}{2}. \tag{4.7b}$$

Hence, in the limit when $\Gamma \to 0$

$$\omega'_\ell \approx \omega_p\sqrt{\frac{\ell}{2\ell+1}}. \tag{4.8}$$

Equation (4.8) indicates that frequency bandwidth for which plasmonics resonances should be expected relies within the interval

$$\omega_l \in [\omega_p/\sqrt{3}, \omega_p/\sqrt{2}], \tag{4.9}$$

with $\omega_d = \omega_p/\sqrt{2}$ the eigenfrequency associated with the dipolar ($\ell = 1$) plasmon mode and $\omega_s = \omega_p/\sqrt{2}$ the eigenfrequency associated with the surface ($\ell \to \infty$) plasmon mode. For the aluminium, since $\Gamma/\omega_p = 1/100 < 1$, it is expected that dipolar plasmon mode should be closed to the resonance frequency

$$\omega_d \approx \frac{\omega_p}{\sqrt{3}} = 8.72\,\text{eV}. \tag{4.10}$$

In Figure 4.2 we show, in SI units, the calculations concerning the longitudinal [component parallel to the electron's velocity, Fig. 4.2(a)] and the transverse [component orthogonal to the electron's velocity, Fig. 4.2(b)] spectral contributions against frequency, for an aluminium nanoparticle and six different electron velocities: 0.15c, 0.2c, 0.3c, 0.4c, 0.5c, 0.99c. In order to compute these spectral contributions the following parameters were considered: the metallic NP was modeled as an aluminium Drude-type material with radius equal to $a = 1\,\text{nm}$ and the electron's impact parameter was set up as $x_0 = 1.5\,\text{nm}$. As shown in Fig. 4.2, the spectral intensity decreases as the electron's velocity is increased, and both the transverse [Fig. 4.2(a)] and longitudinal [Fig. 4.2(b)] spectral contributions are almost the same order of magnitude for each velocity. However, the longitudinal component is always positive indicating that the longitudinal momentum transferred (area under $\mathcal{P}_\parallel$ curve) is always positive. These results are in agreement with previously theoretical calculations obtained, as for example, in [23] and [31].

On the other hand, the transverse spectral contribution exhibits a positive-negative transition suggesting, remarkably, that the total transverse momentum transferred (area under $\mathcal{P}_\perp$ curve) may be positive or negative[4]. In addition, the highest contribution in both graphs are located close to the eigenfrequency $\hbar\omega = 8.72\,\text{eV}$, as predicted by Eq. (4.10).
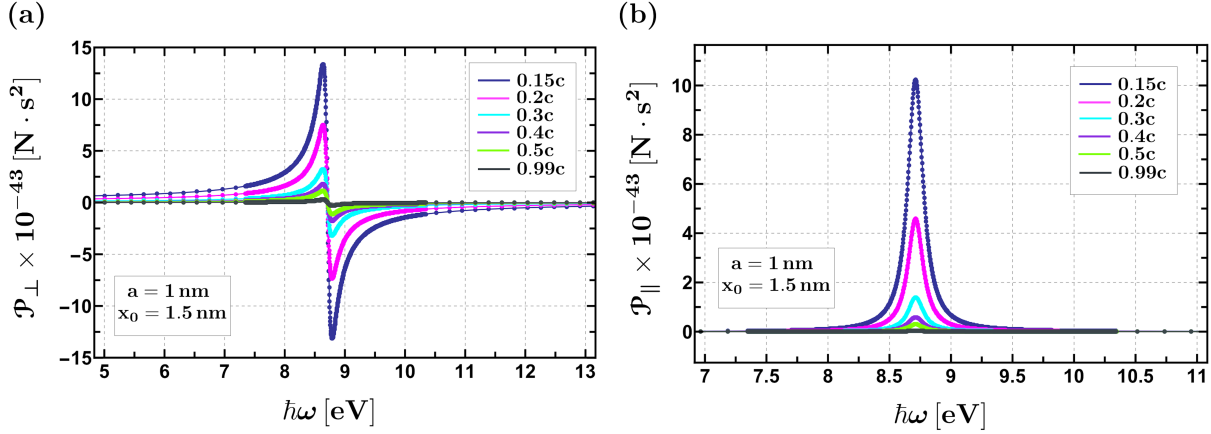
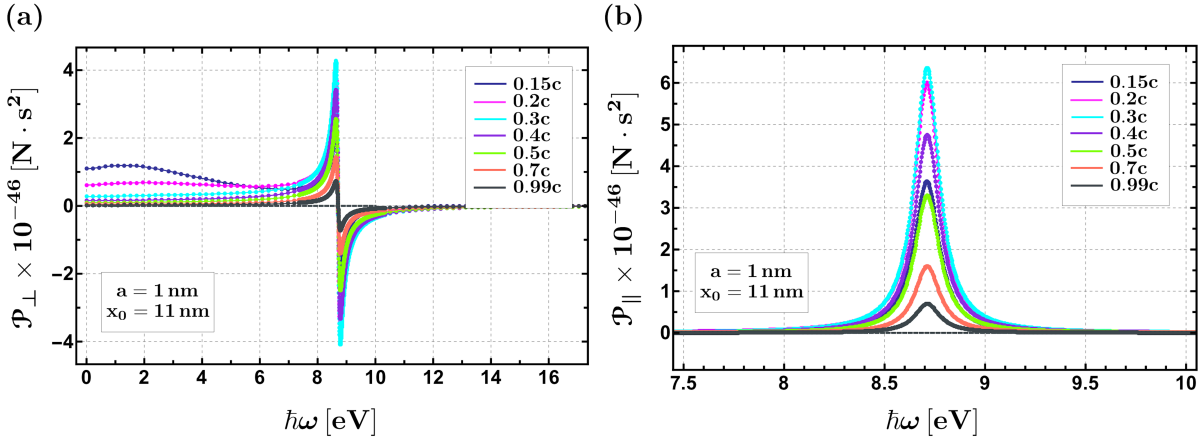**(a)**   **(b)**

Figure 4.2. (a) transverse and (b) longitudinal components of the spectral contribution to the total linear momentum transferred from the fast electron, with different velocities, to an aluminium Drude-type NP of radius $a = 1\,\text{nm}$, with an impact parameter of the electron's trajectory equal to $x_0 = 1.5\,\text{nm}$.

Figure 4.3 shows, the transverse [Fig. 4.3(a)] and the longitudinal [Fig. 4.3(b)], spectral contributions to the total linear momentum transferred for an electron impact parameter equal to $x_0 = 11\,\text{nm}$. The NP's radius was left the same as before, $1\,\text{nm}$.

(a)   **(b)**

Figure 4.3. (a) transverse and (b) longitudinal components of the spectral contribution to the total linear momentum transferred from the fast electron, with different velocities, to an aluminium Drude-type NP of radius $a = 1\,\text{nm}$, with an impact parameter of the electron's trajectory equal to $x_0 = 11\,\text{nm}$.

Important differences arouse between Figs. 4.2 ($x_0 = 1.5\,\text{nm}$) and 4.3 ($x_0 = 11\,\text{nm}$). The first one is that, near the dipole resonance, the spectral contribution profiles in Figs. 4.2 are larger for small velocities (compared with the speed of light) than for ultra-relativistic velocities. While in Figs. 4.3, near the dipole resonance, the profiles of the spectral contribution does not behave in a descendant way, instead, 0.15 and 0.2c velocity curves are below 0.3c, 0.4c, 0.5c, 0.7c and 0.99c

---

[4]Even though the transverse spectral curves [Fig. 4.2(a)] appear to be odd functions, they are not, since the area under each velocity curve is different from zero, as will be shown in Section 4.3.

velocity profiles. The second difference relies in the fact that for lower and higher frequencies than the dipole resonance frequency (8.72 eV), the contribution in Figs. 4.2 is negligible in comparison to the one given close to the dipole resonance. Whilst, for low frequencies, the spectral contribution in Figs. 4.3, for 0.15c and 0.2c velocity curves, is almost half the intensity they present around the resonance frequency.

Nanoparticle modeled as a Lorentz-type gold material

The dielectric function for the NP modeled as gold was taken from [28], obtained from experimental REELS (Reflection Electron Energy Loss Spectroscopy) data and fitted[5] with a superposition of one Drude term (when $\omega_j = 0$) and nine Drude-Lorentz terms [32], given by

$$\epsilon_i(\omega) = 1 + \sum_{j=1}^{10} \frac{A_j}{\omega_j^2 - \omega(\omega + i\Gamma_j)}, \qquad (4.11)$$

where, in addition to free electrons, each bound electron in the material is modeled as a particle bounded to massive nucleus by spring with natural frequency ω_j, and each oscillator strength given by A_j. Also, Γ_j represents—as in Drude model—the phenomenological damping constant simulating dissipative forces, see [32].

Figure 4.4 shows the dielectric function $\epsilon_i = \epsilon_i' + i\epsilon_i''$ (real part in blue and imaginary part in red) for the gold fitted model (Eq. (4.11)) as a function of frequency, using the data reported in [28] (see Table 4.1 for the specific values of A_i, Γ_j and ω_i). For better appreciation, inset in Fig. 4.4 displays the dielectric function between 0 to 40 eV.
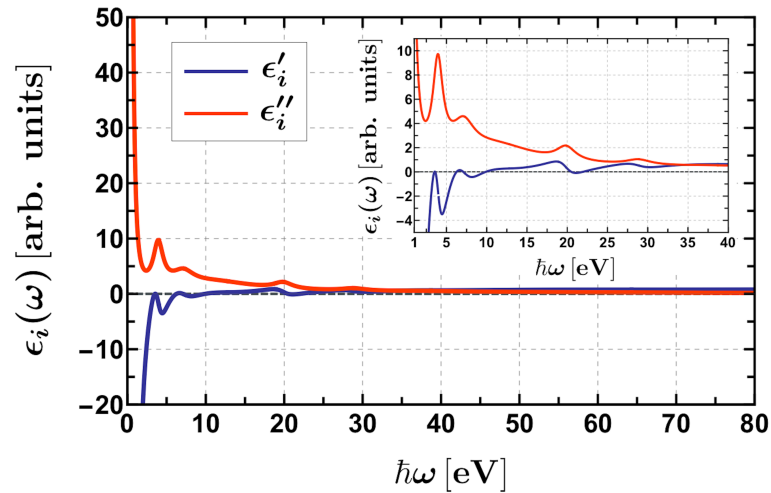

Figure 4.4. Plots of the real (blue line) and imaginary (red line) parts of the Au dielectric function modeled as a superposition of Drude-Lorentz oscillators. The inset shows the structure of the dielectric function within the 0-40 eV range.

According to Eq. (4.4), the resonances of the ℓ-mode in the Drude-Lorentz model shall be

---

[5]Recent studies on analytical models for the dielectric response of gold demonstrated that causality property of fitting functions are essential to obtain physically sound results for the total linear momentum transferred from electrons to NPs.

determined by the relation

$$\frac{2\ell+1}{\ell} + \sum_{j=1}^{10} \frac{A_j}{\omega_j^2 - \omega_\ell(\omega_\ell + i\Gamma)} = 0, \tag{4.12}$$

which in general corresponds to an eighteenth order polynomial in ω_ℓ. In spite of the non-analyticity of Eq. (4.12) we can infer gold electric response behavior by looking at Fig. 4.4. In this, five resonances ($\hbar\omega = 0\,\text{eV}$ is the resonance corresponding to the Drude's model) appeared between 0 to 40 eV and, furthermore, when $\Gamma_i \to 0$ it is expected a resonance frequency around ω_j, as indicated by Eq. (4.12).

Natural frequency ω_j [eV]	Damping Γ_j [eV]	Oscillator strength A_j [eV^2]
0.000	0.027	139.3
1.0	7.9	138.2
5.4	7.2	161.8
9.5	0.5	8.6
13.7	7.5	92.5
18.3	1.9	6.5
25.5	3.6	2.3
36.8	4.9	108.4
45.1	7.6	180.6
70.4	70.0	411.2

Table 4.1. Table of the parameters ω_j, Γ_j and A_j taken from [28] to fit experimental gold data through Eq. (4.11).

In Figure 4.5 we show the transverse and the longitudinal components of the spectral contribution to the total linear momentum transferred from the electron to a gold nanoparticle. The NP's radius was set up equal to 1 nm, the electron's impact parameter equal to 1.5 nm and different electron velocities, which relies from 0.1c up to 0.99c, were taken. In agreement to aluminium results, the most intense contributions of $\mathcal{P}$ emerged close to the resonance frequencies, as can be observed from a comparison between the dielectric response (Fig. 4.4) and the spectral contributions (Fig. 4.5). Moreover, slower velocity profiles (0.15c, 0.2c, 0.3c) dominate over fast velocity curves (0.4c, 0.5c and 0.99c) in the same way obtained for an aluminium NP. Therefore, we can conclude that as the velocity is increased the spectral contribution decreases when the electron has an impact parameter equal to 1.5 nm.

As it is of our interest to study the behavior of the spectral contribution (and the total linear momentum transferred) for different impact parameters, we calculated the spectral contribution when the electron is $x_0 = 11$ nm separated from the nanoparticle. In Fig. 4.6 we present the results concerning the spectral contribution for a 1 nm gold NP and an electron impact parameter equal to 11 nm. In both Figs. 4.6(a) and 4.6(b), the magnitude of the spectral profiles decreases four orders of magnitude in comparison to the profiles obtained with an impact parameter equal to 1.5 nm [Figs. 4.5(a) and 4.5(b)]. Also, Fig. 4.6 shows that the spectral contribution, for $x_0 = 11$ nm, is higher for frequencies between 0 to 10 eV and for frequencies higher than 10 eV, the spectral contribution is negligible.
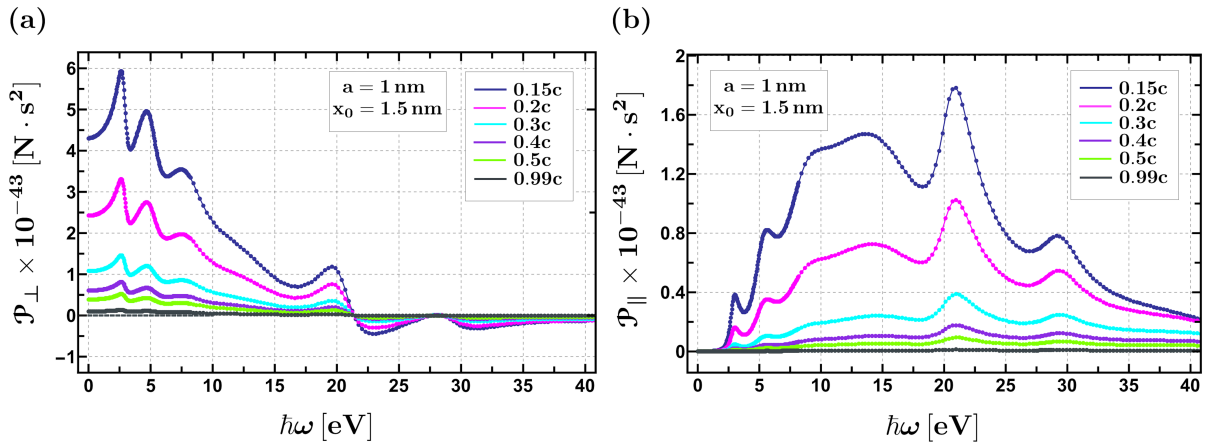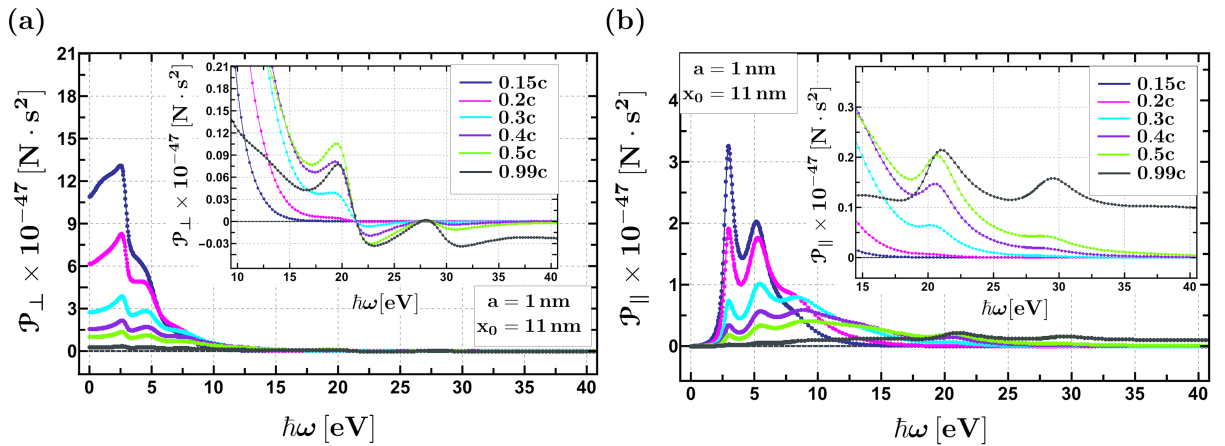
(a)

(b)

Figure 4.5. (a) transverse and (b) longitudinal components of the spectral contribution to the total linear momentum transferred from the fast electron, with different velocities, to a gold NP of radius $a = 1\,\text{nm}$, with an impact parameter equal to $x_0 = 1.5\,\text{nm}$.

It is worth noting that for both impact parameters ($x_0 = 1.5\,\text{nm}$. and $x_0 = 11\,\text{nm}$.) the transverse component of the spectral contribution [Figs. 4.5(a) and 4.6(a)] exhibits a positive-negative transition for frequencies higher than $\hbar\omega = 15\,\text{eV}$, while the longitudinal components [Figs. 4.5(b) and 4.6(b)] are always positive.

(a)

(b)

Figure 4.6. (a) transverse and (b) longitudinal components of the spectral contribution to the total linear momentum transferred from the fast electron, with different velocities, to a gold NP of radius $a = 1\,\text{nm}$, with an impact parameter equal to $x_0 = 11\,\text{nm}$.

4.2 Comparison: pure dipole and dipole approximation

Chapter 3 is devoted to obtain analytical solutions of the spectral contribution to the total linear momentum transferred from the swift electron to the nanoparticle. In Section 3.3, surface integrals concerning the first multipole—the dipole approximation—of the scattered electromagnetic field are studied. Nevertheless, for our research group, the study of the first multipole in the scattered electromagnetic field has also been an important key to understand and compare an approximation proposed in [10] where the NP is modeled as a bare point-like dipole (named in this thesis as *pure dipole approximation*). This dipole has dipole moment given in SI units by

[10]

$$\mathbf{p}(\omega) = \epsilon_0 \alpha(\omega)\mathbf{E}^{ext}(\mathbf{r} = 0; \omega), \tag{4.13}$$

where ϵ_0 stands for the permittivity of free space; $\alpha(\omega)$ stands for the NP polarizability given by

$$\alpha(\omega) = 4\pi a^3 \frac{\epsilon_i(\omega) - \epsilon_0}{\epsilon_i(\omega) + 2\epsilon_0}, \tag{4.14}$$

and $\mathbf{E}^{ext}(\mathbf{r} = 0; \omega)$ stands for the electromagnetic field produced by the swift electron, in the frequency domain, evaluated at the center of the sphere. Thus, a time Fourier Transform can be performed to the dipole moment $\mathbf{p}(\omega)$ [Eq. (4.13)] in order to have a description of the dipole response as a function of time. Then, using Lorentz force

$$\mathbf{F}(t) = (\mathbf{p}(t) \cdot \nabla)\mathbf{E}^{ext}(\mathbf{r} = 0; t) + \frac{d\mathbf{p}(t)}{dt} \times \mathbf{B}^{ext}(\mathbf{r} = 0; t), \tag{4.15}$$

with $\mathbf{B}^{ext}(\mathbf{r} = 0; \omega)$ the external magnetic field, in the time domain, evaluated at the center of the NP, the total momentum transferred from the electron to the NP can be calculated as

$$\boxed{\Delta\mathbf{P} = \int_{-\infty}^{\infty} \mathbf{F}(t)\, dt.} \tag{4.16}$$

In this way, Eq. (4.15) establishes a recipe to study the interaction between the electron and the nanoparticle (at least in a first approach) in the time domain. Moreover, a comparison between the pure dipole and the $\ell = 1$ approximations can be achieved by means of the total momentum transferred, determined by Eqs. (2.86) and (4.15) in each case.

In this Section we present a comparison between the dipole ($\ell = 1$) and the pure dipole approximations. Figures 4.7(a) and 4.7(b) display, respectively, the transverse and the longitudinal components of the total momentum transferred from the electron to the NP as a function of the electron's velocity. The parameters considered for the numerical calculations were: a NP modeled as a Al Drude-type material, with a radius equal to 1 nm, and two different electron impact parameters, $x_0 = 1.5$ nm and $x_0 = 11$ nm.

The total linear momentum transferred from the electron to the NP, for $\ell = 1$ approximation was calculated by integrating in frequency the results obtained in Section 4.1 for the nanoparticle modeled as a Al Drude-type material. That is, by computing the area under the curves of Figs. 4.2 (for 1.5 nm impact parameter) and 4.3 (for 11 nm impact parameter). On the other hand, the total linear momentum transferred for the pure dipole approximation was calculated by Jesús Castrejón, following the steps in accordance to fulfill Eq. (4.16) [10].

While the calculations of the longitudinal component [Fig. 4.7(b)] for the $\ell = 1$ approximation coincides with the calculations of the longitudinal component for the pure dipole approximation (for both impact parameters considered, $x_0 = 1.5$ nm and $x_0 = 11$ nm). The calculations remarkably differ for the transverse components [Fig. 4.7(a)], particularly at high electron velocities, as can be shown in the inset of Fig. 4.7. We believe that these differences are due to the fact that close to the NP (that is, small impact parameters compared with the NP's radius) the pure dipole approximation is no longer valid, because it was developed in the dipolar limit which takes into account that the electron is far from the NP (large impact parameters compared with the NP's radius). Whilst the dipole approximation does not exhibit any restriction in the

closeness and the remoteness of the electron from the nanoparticle, indeed, it only represents the first multipole of the total scattered electromagnetic field without any further assumptions. However, numerical calculations (Figs. 4.8) for larger than 1.5 an 11 nm impact parameters show that the $\ell = 1$ approximation recovers the calculations performed with the pure dipole approximation.
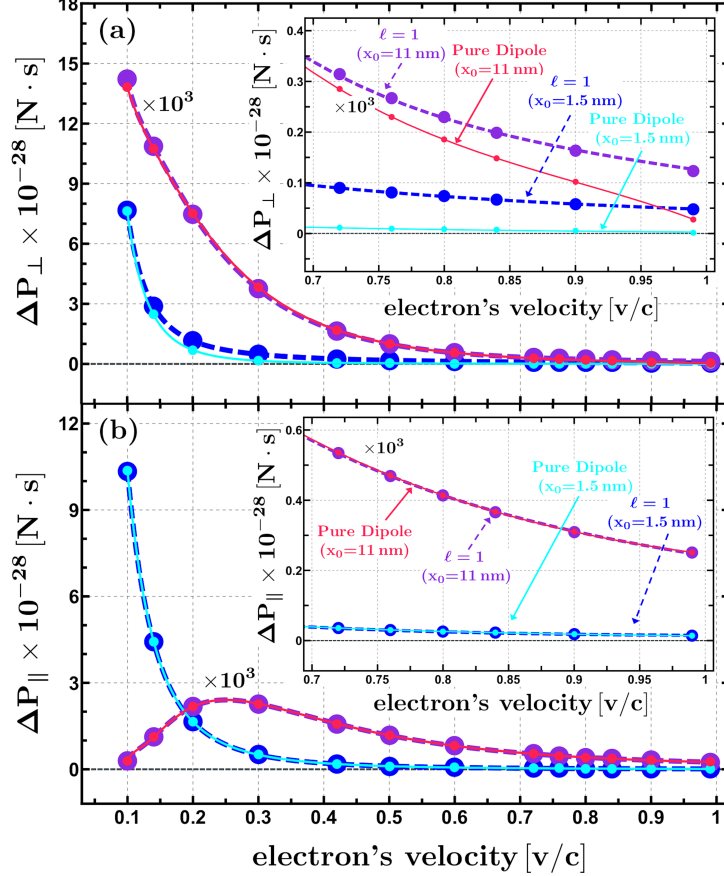

Figure 4.7. Comparison between the dipole and the pure dipole approximations to the total linear momentum transferred from the electron to the NP along (a) the transverse and (b) longitudinal directions as a function of the electron's velocity. The NP was modeled as an aluminium Drude-type material with radius $a = 1$ nm and two different electron impact parameters: $x_0 = 1.5$ nm and $x_0 = 11$ nm (scaled by a factor of 10^3 for a better appreciation). Dashed lines correspond to the dipole approximation while solid lines correspond to the pure dipole approximation.

In Fig. 4.8(b) the transverse component of the total linear momentum transferred is compared for both approaches the dipole and the pure dipole approximations, for a NP's radius of 1 nm and an electron impact parameter of 20 nm. As can be appreciated in Fig. 4.8(b), the pure dipole approximation curve (solid blue curve) coincides with the $\ell = 1$ approximation curve (dashed magenta curve) for almost all velocities, except in the ultra-relativistic regime, that is, for high velocities. This behavior can be explained by the dependance of the external electromagnetic field in the impact parameter, which is given through the modified Bessel functions as [Eq. (2.31)]

$$\mathbf{E}^{ext}(\mathbf{r};\omega) = -\frac{2e\omega}{v^2\gamma}e^{i\omega\frac{z}{v}}\left\{\left[\frac{\mathrm{sgn}(\omega)}{R}K_1\left(\frac{|\omega|R}{v\gamma}\right)\right][(x-x_0)\hat{\mathbf{e}}_x + y\hat{\mathbf{e}}_y] - \frac{i}{\gamma}K_0\left(\frac{|\omega|R}{v\gamma}\right)\hat{\mathbf{e}}_z\right\},$$

$$\mathbf{B}^{ext}(\mathbf{r};\omega) = \frac{2e\beta}{Rv^2\gamma}|\omega|e^{i\omega\frac{z}{v}}K_1\left(\frac{|\omega|R}{v\gamma}\right)[y\hat{\mathbf{e}}_x - (x-x_0)\hat{\mathbf{e}}_y],$$

with $R^2 = (x-x_0)^2 + y^2$. Thus, if the impact parameter is larger than the NP's radius, and as consequence larger than the radius of the integration surface where the Maxwell stress tensor is calculated[6], $R \sim x_0$ and only low frequencies (large wavelengths compared with the NP's radius) will contribute, as it is shown in Fig. 4.9. Therefore, if the impact parameter x_0 increases, the more similar is the small particle limit—and so the pure dipole approximation—to the dipole approximation.

Again, the $\ell = 1$ and the pure dipole approximations show a similar tendency for the longitudinal component of the total linear momentum transferred, see Fig. 4.7(b). Nonetheless, it should be noticed that the longitudinal component of the total momentum transferred exhibits a change in its behavior as a function of the impact parameter. For $x_0 = 1.5$ nm there is no maximum value in the momentum transferred, while for $x_0 = 11$ nm there is a maximum close to the velocity 0.25c, as shown in Fig. (b). This anomalous behavior in the linear momentum transferred may be fully understood once we have the analytical solution to the problem.
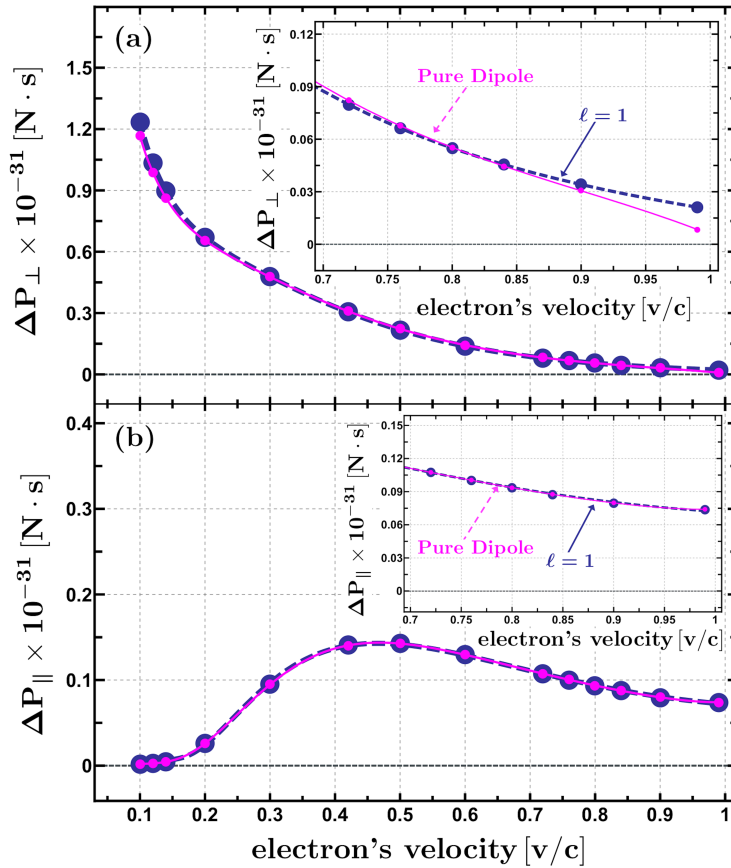

Figure 4.8. Comparison between the dipole and the pure dipole approximations of the total linear momentum transferred from the electron to the NP along (a) the transverse and (b) longitudinal direction as function of the electron's velocity. The NP was modeled as an aluminium Drude-type material with radius $a = 1$ nm and an electron impact parameter of $x_0 = 20$ nm. Dashed lines correspond to the dipole approximation while solid lines correspond to the pure dipole approximation.

---

[6]For numerical purposes the integration radius is considered to be close (half nanometer away) to the NP.

The importance of understanding the equivalence between both approximations lies in the fact that the pure dipole approximation exhibits a prescription for studying the total linear momentum transferred from the electron to the NP in the time domain. Whereas, in the dipole approximation, a time Fourier Transform and the electromagnetic linear momentum must be calculated in order to obtain a description of the problem in the time domain, which may cause numerical noise.

4.3 Linear momentum as function of electron's velocity

One of the most interesting mechanisms inside the total momentum transferred from the electron to the NP is the attraction-repulsion transition exhibited by the transverse component of the total linear momentum transferred, for certain combinations of electron velocities and impact parameters. So a deep understanding in the momentum transferred mechanism should answer the question to whether the attraction-repulsion effect can be obtained in all kind of materials or if it is only restricted to a particular dielectric responses. For this reason, it makes sense to ask how many multipoles in the scattered field should be considered in order to achieve such transition and in this way if the first multipole, that is the dipole contribution, exhibits such behavior, given that the dipole and the pure dipole approximations are not quite the same[7]. An alternative proof for the latter assertion is given by the following argument.
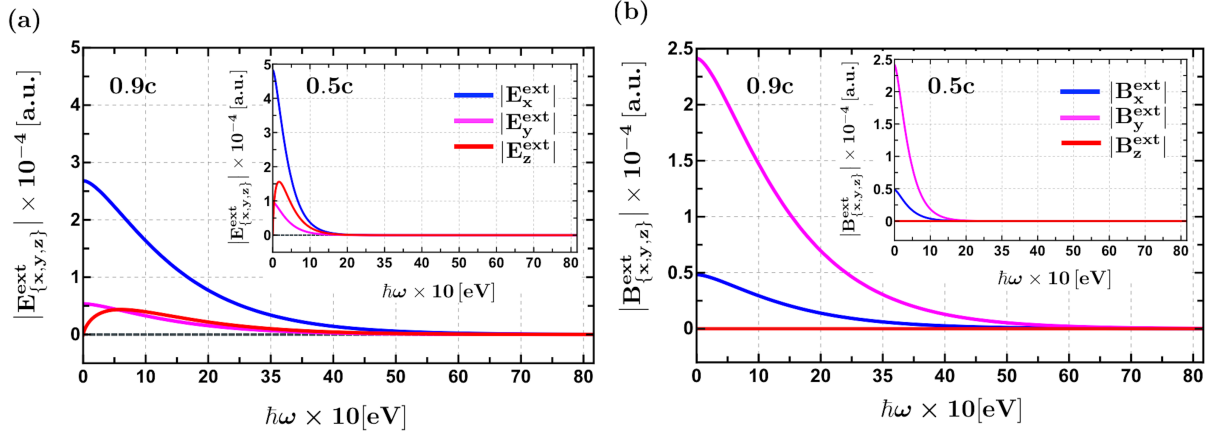

Figure 4.9. Plots of the magnitude of (a) the electric field and (b) the magnetic field components produced by the electron, traveling with constant velocity in $\hat{\mathbf{z}}$ direction and $5\,\mathrm{nm}$ impact parameter, versus frequency. The fields are evaluated in the field point $\mathbf{r} = (0, 1, 0)\,\mathrm{nm}$ for an electron velocity of 0.9c, while insets show both (a) the electric and (b) the magnetic field magnitudes for an electron traveling with constant velocity of 0.5c.

Scattering coefficients t_ℓ^E and t_ℓ^M, given by Eqs. (2.53), can be expanded according to [13] as

$$t_1^E = A_1 x^3 + A_2 x^5 + A_3 x^6 + O(x^7), \tag{4.17a}$$
$$t_1^M = B_1 x^5 + O(x^7), \tag{4.17b}$$

where $x = k_0 a$ is the size parameter and

---

[7]One of the main conclusions set in [10] is that the pure dipole approximation describes only attractive interactions.

$$A_1 = \frac{2}{3}\frac{\epsilon_i - 1}{\epsilon_i + 2}, \quad A_2 = \frac{2}{5}\frac{(\epsilon_i - 2)(\epsilon_i - 1)}{(\epsilon_i + 2)^2}, \quad A_3 = \frac{4}{9}\left(\frac{\epsilon_i - 1}{\epsilon_i + 2}\right)^2 \quad \text{and} \quad B_1 = \frac{1}{45}(\epsilon_i - 1).$$

It can be demonstrated [13] that in the small particle limit $t_1^E \sim A_1 x^3$ and $t_1^M \sim 0$. In Figs. 4.10 we show two different calculations of the total linear momentum transferred from the electron to the NP. The first calculation is related to the linear momentum transferred—black dashed curves in Figs. 4.10—when Mie coefficient t_1^E was considered as defined by Eq. (2.53), while the second calculation is related to the total linear momentum transferred—green solid curves in Figs. 4.10—assuming that Mie coefficient $t_1^E \sim A_1 x^3$ and t_1^M was equal to zero. Both calculations were performed for an Al Drude-type NP of $1\,\text{nm}$ radius and an electron's impact parameter of $1.5\,\text{nm}$. Figures 4.10(a) and 4.10(b) show the results concerning the transverse and the longitudinal components, respectively, of the total linear momentum transferred. In the insets of Figs. 4.10 we display the difference ($\delta\mathbf{P}$) between the calculation performed with the complete expression for t_1^E and when it was approximated by it's first term in the expansion (4.17).
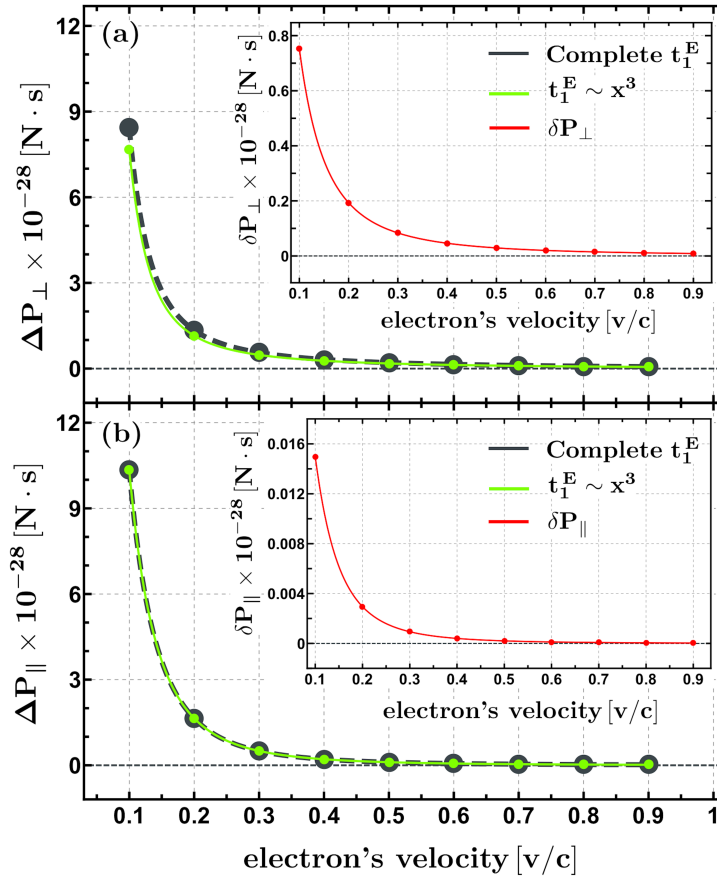

Figure 4.10. Comparison plots of the total linear momentum transferred against electron's velocity between calculations made for an Al Drude-type NP considering the complete scattering coefficient t_1^E (dashed grey curve) and approximating it as $t_1^E \sim A_1 x^3$ (green solid curve). The parameters used were: NP's radius of $1\,\text{nm}$ and impact parameter of $1.5\,\text{nm}$.

The differences, for instance, in the transverse component [inset in Fig. 4.10(a)] establishes that indeed the dipole approximation is not the same as the small particle limit. Moreover, insets in Figs. 4.10 exhibit that both approaches will be the same for ultra-relativistic velocities,

since increasing the velocity is almost the same as increasing the range in frequency for the external electromagnetic field (see Figs. 4.9). Thus, the dipolar resonance frequency (ω_d, equal to 8.72 eV for the Aluminium considered) will be present in both calculations and, as shown in Figs. 4.2 and 4.3, the highest spectral contributions take place close ω_d. This is the reason why in the ultra-relativistic limit, for Al Drude-type material, there is no difference between calculating the linear momentum transferred considering $t_1^E \sim A_1 x^3$ or t_1^E. We expect that this similarity will disappear by changing the material (dielectric function).

On the other hand, in this last Section we present the results concerning the total linear momentum transferred against the electron's velocity and a comparison with previous calculations obtained in [25], for both Al and Au, where up to 15 multipoles in the scattered field were considered for computing the total linear momentum transferred.

Once again, the momentum transferred within the dipole approximation was obtained by calculating the area under the curves of Fig. 4.2 for the Al NP, and of Fig. 4.5 for the Au NP. Whilst the results of the total linear momentum transferred with $\ell = 15$ multipoles were accomplished using the Boundary Element Method (BEM) [33]-[35] to calculate the electromagnetic field scattered by the NP. In these calculations, 15 multipoles were considered for working out the scattered electromagnetic field, then the data given out by BEM numerical program was managed in a *Mathematica notebook* in order to compute the surface and frequency integrals involved in the determination of the total linear momentum transferred.
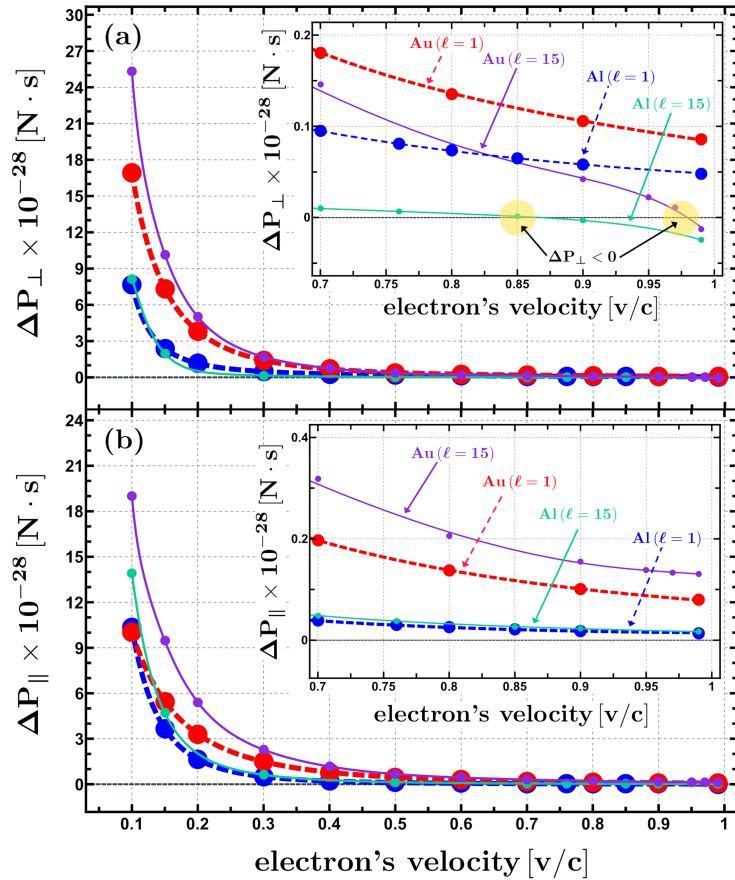

Figure 4.11. Comparison between $\ell = 1$ and $\ell = 15$ computations of the total linear momentum transfer along (a) the transverse and (b) the longitudinal direction as function of the electron's velocity for both Al and Au NPs of radius $a = 1$ nm and impact parameter of $x_0 = 1.5$ nm.

Both $\ell = 1$ and $\ell = 15$ calculations were performed with a nanoparticle of 1 nm radius and an electron's impact parameter of 1.5 nm. Figure 4.11(a) shows that the transverse components for $\ell = 1$, for aluminium (blue dashed curve) and gold (red dashed curve) nanoparticles, are positive (meaning attractive interaction between the electron and the NP) for all velocities. While the transverse components of the total momentum transferred exhibit a transition from positive to negative (meaning attractive interaction between the electron and the NP) when they are calculated considering $\ell = 15$ multipoles in the scattered field. These transitions take place close to the velocity 0.85c for Al (green solid curve) and to the velocity 0.97c for Au (purple solid curve). Both changes are highlighted in Fig. 4.11(a) with a yellow spot.

The longitudinal component of the total linear momentum transferred remains positive for all velocities [Fig. 4.11(b)] and both metals: aluminium and gold. This last result is in agreement with the results obtained in Figs. 4.2(b), 4.3(b), 4.5(b) and 4.6(b), where the longitudinal components of the spectral contribution displayed a positive behavior for all frequencies. This can be understood as a consequence of the electron transferring linear momentum to the nanoparticle.

It is worth noting that the calculations within the dipole approximation, of the total linear momentum transferred, are the same order of magnitude as the calculations performed with $\ell = 15$ multipoles, and both have almost the same behavior except in the ultra-relativistic limit. Moreover, the computation of the total linear momentum transferred with $\ell = 1$ gives an accurate description of the momentum transferred from the electron to the NP when large impact parameters (compared with the NP's radius) are considered, and it gives an insight of the general behavior of the total momentum transferred as a function of the electron's velocity. Even though the calculations of the total linear momentum transferred would have been done with more than $\ell = 15$ multipoles in the scattered field, we believe that for sub-relativistic velocities none positive-negative transition would have appeared. Thus, the dipole approximation reproduces the slow velocities behavior of the total momentum transferred, and we expect that attractive-repulsive transitions for this regime must be looked up when the dipole contribution is negligible.

Further calculations on separating the electric and magnetic contributions of the total linear momentum transferred will allow us to answer the question to which component of the electromagnetic field is attributed the positive-negative transition in the transverse component of the total linear momentum transfer. Nevertheless, these calculations are out of the scope of this thesis. Moreover, based upon models where the NP is considered as an electric quadrupole, we believe that adding the second multipole ($\ell = 2$), of the scattered electromagnetic field, into the calculations of the total linear momentum transferred, will recover the attractive-repulsive transition. Some other important questions are left for future works, for instance, we have not yet develop a theoretical description of the moving electron, so we do not know what happens to the electron when transferring linear momentum to the NP, which may be interesting for EELS experiments. Besides these assignments, attention must be paid to the analytical solutions of the total linear momentum transferred which will ultimately explain the mechanism behind the attractive-repulsive transition. Although, in this thesis we present the first steps to the analytical approach, there is a lot of work to do regarding the integrals that appear when the scattered electromagnetic field is considered beyond the dipole approximation.

CONCLUSIONS AND OUTLOOKS

Conclusions

In this work we have discussed important aspects concerning the total linear momentum transferred from a swift electron to a small metallic nanoparticle within the dipole approximation. From the theoretical analysis and the numerical calculations we can conclude that:

- The computation of the total momentum transferred both analytical and numerical is a hard task to address. In particular, if the NP's radius or the number of multipoles in the scattered field are increased, several numerical problems arises. For this reason, it is important to study the contribution given by each multipole of the scattered electromagnetic field to the total linear momentum transfer.

- In this direction, the first multipole $\ell = 1$ in the scattered field is the beginning of our two main goals: analytical solutions to the total momentum transferred and the description of the interaction between the swift electron and the NP in the time domain. General behaviors of the momentum transferred as a function of the electron's velocity can be reproduced within the dipole approximation, although it does not reproduce the positive-negative transition in the transverse component of the total linear momentum transferred.

- The comparison between the dipole approximation and the pure dipole approximation point's out an alternative path to study the interaction between the swift electron an the NP in the time domain. Since our construction of this interaction is in the frequency domain.

Outlooks

There are several topics left out in this thesis and which will allow a deeper understanding of the interaction between the electromagnetic field produced by the electron and the metallic nanoparticle. This research work shall be continued in:

- Analyzing the contribution given by higher multipoles to the scattered field. I believe, based on models where the nanoparticle is considered as an electric quadrupole, that the next multipole $\ell = 2$ in the scattered field will exhibit the attractive-repulsive transition, expected for the transverse momentum transfer versus the electron's velocity plots.

- Separating the linear momentum transferred in electric and magnetic contributions, to proof wether our hypothesis for the attractive-repulsive transition is correct or not.

- Studying the momentum transferred modeling the nanoparticle as a dielectric material.

- Developing calculations of the momentum transfer as a function of the electron's impact parameter.

- Developing theoretical expression which may help to explain what happens to the electron and it's trajectory when interacting with the nanoparticle.

- Studying the total angular momentum transferred from the electron to the nanoparticle, since the external field carries angular momentum. Thus, an analysis of the total angular velocity of the nanoparticle versus the electron's velocity (or impact parameter) can be obtained.

- Studying the classical and semi-classical theories related to the quantification of the temperature the nanoparticle reaches.

SUPPLEMENTARY CALCULATIONS ON THE EXTENDED MIE SOLUTION

The present Appendix is devoted to show in detail the calculations used in the development of the extended Mie solution.

Maxwell equations in CGS units are given by [24]

$$\nabla \cdot \mathbf{E}\left(\mathbf{r};t\right) = 4\pi\rho_{tot}\left(\mathbf{r};t\right), \qquad\qquad \nabla \times \mathbf{E}\left(\mathbf{r};t\right) = -\tfrac{1}{c}\tfrac{\partial}{\partial t}\mathbf{B}\left(\mathbf{r};t\right),$$

$$\nabla \cdot \mathbf{B}\left(\mathbf{r};t\right) = 0, \qquad\qquad \nabla \times \mathbf{B}\left(\mathbf{r};t\right) = \tfrac{4\pi}{c}\mathbf{J}_{tot}\left(\mathbf{r};t\right) + \tfrac{1}{c}\tfrac{\partial}{\partial t}\mathbf{E}\left(\mathbf{r};t\right). \tag{A.1}$$

Due to magnetic Gauss law and Faraday-Henry-Lenz law, it is known that the electric and magnetic fields can be rewritten in terms of scalar $\phi(\mathbf{r};t)$ and vector $\mathbf{A}(\mathbf{r};t)$ potentials [11] as

$$\mathbf{E}\left(\mathbf{r};t\right) = -\nabla\phi\left(\mathbf{r};t\right) - \frac{1}{c}\frac{\partial\mathbf{A}\left(\mathbf{r};t\right)}{\partial t}, \tag{A.2a}$$

$$\mathbf{B}\left(\mathbf{r};t\right) = \nabla \times \mathbf{A}\left(\mathbf{r};t\right). \tag{A.2b}$$

In the Lorentz gauge

$$\nabla \cdot \mathbf{A}(\mathbf{r};t) + \frac{1}{c}\frac{\partial}{\partial t}\phi(\mathbf{r};t) = 0, \tag{A.3}$$

the potential $\phi(\mathbf{r};t)$ and $\mathbf{A}(\mathbf{r};t)$ satisfy the inhomogeneous wave equation, that is,

$$\nabla^2\phi(\mathbf{r};t) - \frac{1}{c^2}\frac{\partial^2\phi(\mathbf{r};t)}{\partial t^2} = -4\pi\rho_{tot}(\mathbf{r};t), \tag{A.4a}$$

$$\nabla^2\mathbf{A}(\mathbf{r};t) - \frac{1}{c^2}\frac{\partial^2\mathbf{A}(\mathbf{r};t)}{\partial t^2} = -\frac{4\pi}{c}\mathbf{J}_{tot}\left(\mathbf{r},t\right). \tag{A.4b}$$

On the other hand, the space and time Fourier Transform of an arbitrary well-behaved vector function $\mathbf{F}(\mathbf{r};t)$ is given by [13]

$$\mathbf{F}(\mathbf{k};\omega) = \int_{-\infty}^{\infty}\int_{-\infty}^{\infty}\mathbf{F}(\mathbf{r};t)\,e^{-i(\mathbf{k}\cdot\mathbf{r}-\omega t)}\,d^3\mathbf{r}\,dt, \tag{A.5}$$

and its inverse is given by

$$\mathbf{F}(\mathbf{r};t) = \frac{1}{(2\pi)^4}\int_{-\infty}^{\infty}\int_{-\infty}^{\infty}\mathbf{F}(\mathbf{k};\omega)\,e^{i(\mathbf{k}\cdot\mathbf{r}-\omega t)}\,d^3\mathbf{r}\,dt. \tag{A.6}$$

Calculating the time and space Fourier Transform to wave Eqs. (A.4), they read as

$$-k^2\phi(\mathbf{k};\omega) + \frac{\omega^2}{c^2}\phi(\mathbf{k};\omega) = -4\pi\rho_{tot}(\mathbf{k};\omega),\tag{A.7a}$$

$$-k^2\mathbf{A}(\mathbf{k};\omega) + \frac{\omega^2}{c^2}\mathbf{A}(\mathbf{k};\omega) = -\frac{4\pi}{c}\mathbf{J}_{tot}(\mathbf{k},\omega),\tag{A.7b}$$

and, since $\mathbf{J}_{tot}(\mathbf{r};t) = \rho_{tot}(\mathbf{r};t)\mathbf{v}$, the scalar and vector potentials in the frequency and reciprocal space are given by

$$\phi(\mathbf{k};\omega) = \frac{4\pi}{k^2 - \omega^2/c^2}\,\rho_{tot}(\mathbf{k};\omega),\tag{A.8a}$$

$$\mathbf{A}(\mathbf{k};\omega) = \frac{4\pi\mathbf{v}/c}{k^2 - \omega^2/c^2}\,\rho_{tot}(\mathbf{k};\omega) = \frac{\mathbf{v}}{c}\,\phi(\mathbf{k};\omega).\tag{A.8b}$$

Furthermore, calculating the space and time Fourier Transform to Eq. (A.2a), the electric field in the frequency and reciprocal space results in

$$\mathbf{E}(\mathbf{k};\omega) = -i\,\mathbf{k}\phi(\mathbf{k};\omega) + i\,\frac{\omega}{c}\mathbf{A}(\mathbf{k};\omega).\tag{A.9}$$

Substituting Eqs. (A.8b) into (A.9) the electric field as function of the scalar potential ϕ in the frequency and reciprocal space, is

$$\boxed{\mathbf{E}(\mathbf{k};\omega) = \left(-i\mathbf{k} + \frac{i\,\omega\mathbf{v}}{c^2}\right)\phi(\mathbf{k};\omega).}\tag{A.10}$$

Now, as it is of interest to obtain the electric field in the real space and in the frequency domain, an inverse space Fourier Transform must be taken into Eq. (A.10), therefore

$$\begin{aligned}
\mathbf{E}(\mathbf{r};\omega) &= \frac{1}{(2\pi)^3}\int_{-\infty}^{\infty}\mathbf{E}(\mathbf{k};\omega)e^{i\mathbf{k}\cdot\mathbf{r}}\,d^3\mathbf{k}\\
&= \frac{1}{(2\pi)^3}\left[-\int_{-\infty}^{\infty}i\,\mathbf{k}\phi(\mathbf{k};\omega)e^{i\mathbf{k}\cdot\mathbf{r}}\,d^3\mathbf{k} + \frac{i\,\omega\mathbf{v}}{c^2}\int_{-\infty}^{\infty}\phi(\mathbf{k},\omega)e^{i\mathbf{k}\cdot\mathbf{r}}\,d^3\mathbf{k}\right]\\
&= \left(-\nabla + \frac{i\,\omega\mathbf{v}}{c^2}\right)\frac{1}{(2\pi)^3}\int_{-\infty}^{\infty}\phi(\mathbf{k};\omega)e^{i\mathbf{k}\cdot\mathbf{r}}\,d^3\mathbf{k} = \left(-\nabla + \frac{i\,\omega\mathbf{v}}{c^2}\right)\phi(\mathbf{r};\omega),
\end{aligned}\tag{A.11}$$

where the last equality follows from the definition of the inverse space Fourier Transform of $\phi(\mathbf{r};\omega)$. In conclusion,

$$\boxed{\mathbf{E}(\mathbf{r};\omega) = \left(-\nabla + \frac{i\,\omega\mathbf{v}}{c^2}\right)\phi(\mathbf{r};\omega).}\tag{A.12}$$

In a similar way, taking the space and time Fourier Transform to Eq. (A.2b), the magnetic field in the frequency and reciprocal space yields

$$\mathbf{B}(\mathbf{k};\omega) = i\mathbf{k}\times\mathbf{A}(\mathbf{k};\omega) = i\mathbf{k}\times\frac{\mathbf{v}}{c}\phi(\mathbf{k};\omega),\tag{A.13}$$

where the last equality follows form Eq. (A.8b). Thus,

$$\mathbf{B}(\mathbf{r};\omega) = \frac{1}{(2\pi)^3} \int_{-\infty}^{\infty} \mathbf{B}(\mathbf{k};\omega)e^{i\mathbf{k}\cdot\mathbf{r}}\, d^3\mathbf{k} = \nabla\phi(\mathbf{r};\omega) \times \frac{\mathbf{v}}{c}. \tag{A.14}$$

Let us consider the case of a traveling electron with constant velocity $\mathbf{v} = v\hat{\mathbf{e}}_z$ and impact parameter x_0 with respect the origin. The charge density that describes such scenario is

$$\rho_{tot}(\mathbf{r};t) = -e\delta(\mathbf{r} - \mathbf{r}_t), \tag{A.15}$$

with e the electron's charge and $\mathbf{r}_t = (x_0, 0, vt)$ the electron's position vector. Calculating the time Fourier Transform to Eq. (A.4a) and substituting the electron's charge density, it is obtained that the scalar potential $\phi(\mathbf{r};\omega)$ in the frequency domain for a moving electron with constant velocity, satisfies the inhomogeneous Helmholtz equation, given by

$$\nabla^2\phi(\mathbf{r};\omega) + k^2\phi(\mathbf{r};\omega) = -4\pi e \int_{-\infty}^{\infty} e^{i\omega t}\delta(\mathbf{r} - \mathbf{r}_t)\, dt, \tag{A.16}$$

leading to the solution [36]

$$\begin{aligned}
\phi(\mathbf{r};\omega) &= -e \int_{V'} G_0(\mathbf{r} - \mathbf{r}') \int_{-\infty}^{\infty} e^{i\omega t}\delta(\mathbf{r}' - \mathbf{r}_t)\, dt\, d^3\mathbf{r}' \\
&= -e \int_{-\infty}^{\infty} e^{i\omega t} \int_{V'} G_0(\mathbf{r} - \mathbf{r}')\, \delta(\mathbf{r}' - \mathbf{r}_t)\, d^3\mathbf{r}'\, dt \\
&= -e \int_{-\infty}^{\infty} e^{i\omega t}\, G_0(\mathbf{r} - \mathbf{r}_t)\, dt,
\end{aligned} \tag{A.17}$$

where

$$G_0(\mathbf{r} - \mathbf{r}_t) = \frac{e^{ik|\mathbf{r}-\mathbf{r}_t|}}{|\mathbf{r} - \mathbf{r}_t|}, \tag{A.18}$$

is the Green function of Helmholtz equation and V' stands for an integration over all prime space. Substituting Eq. (A.17) into Eq. (A.12), this gives for the electric field produced by the electron

$$\mathbf{E}^{ext}(\mathbf{r};\omega) = e\left(\nabla - \frac{i\,k\mathbf{v}}{c}\right) \int_{-\infty}^{\infty} e^{i\omega t}\, G_0(\mathbf{r} - \mathbf{r}_t)\, dt. \tag{A.19}$$

Indeed, Eq. (A.19) gives an alternative way, to the one presented in Section 2.1, for calculating the electric field produced by the traveling electron, since the time Fourier Transform of the Green function of Helmholtz equation can be performed analytically as [6]

$$\int_{-\infty}^{\infty} e^{i\omega t}\, G_0(\mathbf{r} - \mathbf{r}_t)\, dt = \int_{-\infty}^{\infty} e^{i\omega t}\, \frac{e^{ik|\mathbf{r}-\mathbf{r}_t|}}{|\mathbf{r} - \mathbf{r}_t|}\, dt = \frac{2}{v}K_0\left(\frac{\omega}{v\gamma}\sqrt{(x - x_0)^2 + y^2}\right) e^{i\omega z/v}, \tag{A.20}$$

hence, substituting Eq. (A.20) into Eq. (A.19), the electric field produced by the electron in atomic units is

$$\mathbf{E}^{ext}(\mathbf{r};\omega) = \frac{2}{v}\left(\nabla - \frac{i\,k\mathbf{v}}{c}\right) K_0\left(\frac{\omega R}{\gamma v}\right) e^{i\omega z/v}, \tag{A.21}$$

On the other side, expanding Helmholtz Green's function in terms of multipoles [6]

$$G_0(\mathbf{r} - \mathbf{r}_t) = 4\pi k \sum_{\ell=1}^{\infty} \sum_{m=-\ell}^{\ell} i^\ell j_\ell(kr) h_\ell^{(+)}(kr_t) Y_{\ell m}(\Omega_{\mathbf{r}}) Y_{\ell m}^*(\Omega_{\mathbf{r}_t}), \tag{A.22}$$

which is only valid for $r < r_t$ and where $h_\ell^{(+)}$ are the spherical Hankel functions of the first kind multiplied by the imaginary unit i, as defined in [22]. Hence, substituting expansion (A.22) into Eq. (A.20),

$$4\pi k \sum_{\ell=1}^{\infty} \sum_{m=-\ell}^{\ell} j_\ell(kr) Y_{\ell m}(\Omega_{\mathbf{r}}) M_{\ell,m}^+(x_0,0,0) = \frac{2}{v} K_0\left(\frac{\omega R}{\gamma v}\right) e^{i\omega z/v}, \tag{A.23}$$

with[1]

$$M_{\ell,m}^+(x_0,0,0) = \frac{\phi_{\ell,m}}{4\pi k} = \int_{-\infty}^{\infty} e^{i\omega t} h_\ell^{(+)}(kr_t) Y_{\ell m}^*(\Omega_{\mathbf{r}_t})\, dt. \tag{A.24}$$

By solving analytically Eq. (A.24), as shown in [6], it is found out that

$$\phi_{\ell,m} = 4\pi k \frac{A_{\ell,m}^+}{\omega} K_m\left(\frac{\omega x_0}{v\gamma}\right), \tag{A.25}$$

where

$$A_{\ell,m}^+ = \frac{1}{\beta^{\ell+1}} \sum_{j=m}^{\ell} \frac{(i)^{\ell-j}(2\ell+1)!!\, \alpha_{\ell,m}}{\gamma^j\, 2^j\, (\ell-j)!\, \left[\frac{j-m}{2}\right]!\, \left[\frac{j+m}{2}\right]!} I_{j,\ell-j}^{\ell,m}, \tag{A.26}$$

with

$$\alpha_{\ell,m} = \sqrt{\frac{2\ell+1}{4\pi} \frac{(\ell-m)!}{(\ell+m)!}}, \tag{A.27}$$

and $I_{j,\ell-j}^{\ell,m}$ are numbers satisfying the following recurrence relation

$$(\ell-m) I_{i_1,i_2}^{\ell,m} = (2\ell-1) I_{i_1,i_2+1}^{\ell-1,m} - (\ell+m-1) I_{i_1,i_2}^{\ell-2,m}, \tag{A.28}$$

whose initial values are given by $I_{i_1,i_2}^{m-1,m} = 0$, $I_{i_1,i_2}^{m-2,m} = 0$ and

$$I_{i_1,i_2}^{m,m} = \begin{cases} (-1)^m (2m-1)!!\, B\left(\frac{i_1+m+2}{2}, \frac{i_2+1}{2}\right), & \text{if } i_2 \text{ is even} \\ 0, & \text{if } i_2 \text{ is odd,} \end{cases} \tag{A.29}$$

where $B(z,u)$ is the Beta function defined as [17].

---

[1] It must be noted that

$$M_{\ell,-m}^+(x_0,0,0) = \int_{-\infty}^{\infty} e^{i\omega t} h_\ell^{(+)}(kr_t) Y_{\ell,-m}^*(\Omega_{\mathbf{r}_t})\, dt = (-1)^m M_{\ell,m}^+(x_0,0,0),$$

since $Y_{\ell m}^*(\theta,\varphi) = (-1)^m Y_{\ell,-m}(\theta,\varphi)$ according to [22]. Thus, it is enough to consider $m \geq 0$, and as a consequence

$$A_{\ell,-m}^+ = (-1)^m A_{\ell,m}^+.$$

FLUX OF THE MAXWELL STRESS TENSOR FOR THE BARE SWIFT ELECTRON

For numerical purposes the integration surface S related to the computation of the total linear momentum transfer is considered as a sphere of radius R greater than the nanoparticle's radius a, but less than the electron's impact parameter x_0. For this reason, and as pointed out by Stokes theorem [37], it is expected that the time and the surface integral of the external (produced by the electron) Maxwell stress tensor is zero, that is,

$$\int_{-\infty}^{\infty} \oint_S \overset{\leftrightarrow}{\mathbf{T}}{}^{ext} \cdot \hat{\mathbf{n}} \, da \, dt = 0. \tag{B.1}$$

In this Appendix such claim will be demonstrated using a covariant formalism, but let's first consider the static scenario where the electron and the NP are in rest.

Let us consider the electron centered at the origin and an empty volume V with surface boundary S separated by a distance $\mathbf{r}_0 = z_0 \hat{\mathbf{e}}_z$ from the electron, see Fig. B.1(a). As it is well known, the Maxwell stress tensor produced by a charge particle in rest, at a point $\mathbf{r}_0 + \mathbf{R}$ in the sphere, is

$$\overset{\leftrightarrow}{\mathbf{T}}{}^{ext}(\mathbf{r}_0 + \mathbf{R}) = \frac{e^2}{4\pi} \left[\frac{(\mathbf{r}_0 + \mathbf{R})(\mathbf{r}_0 + \mathbf{R})}{|\mathbf{r}_0 + \mathbf{R}|^3} - \frac{\overset{\leftrightarrow}{\mathbf{I}}}{2} \frac{1}{|\mathbf{r}_0 + \mathbf{R}|^4} \right], \tag{B.2}$$

and, since the sphere has surface element $d\mathbf{a} = \hat{\mathbf{e}}_R \, da$, the flux of the external Maxwell stress tensor around the empty sphere is given by

$$\mathbf{\Phi}^{ext} = \oint_{S(\mathbf{r}_0)} \overset{\leftrightarrow}{\mathbf{T}}{}^{ext}(\mathbf{r}_0 + \mathbf{R}) \cdot \hat{\mathbf{e}}_R \, da = \frac{e^2}{4\pi} \oint_{S(\mathbf{r_0})} \left[\frac{(\mathbf{r}_0 + \mathbf{R})(\mathbf{r}_0 + \mathbf{R}) \cdot \hat{\mathbf{e}}_R}{|\mathbf{r}_0 + \mathbf{R}|^6} - \frac{1}{2} \frac{\overset{\leftrightarrow}{\mathbf{I}} \cdot \hat{\mathbf{e}}_R}{|\mathbf{r}_0 + \mathbf{R}|^4} \right] da, \tag{B.3}$$

with $|\mathbf{R}| = R$ and $S(\mathbf{r}_0)$ stands for the integration sphere located at $\mathbf{r}_0$. Thus, using spherical coordinates to parameterize the sphere, Eq. (B.3) is written as

$$\mathbf{\Phi}^{ext} = \frac{e^2}{8\pi} \int_0^{2\pi} \int_0^{\pi} \frac{2z_0(z_0 \cos\theta + R)\hat{\mathbf{e}}_z + (R^2 - z_0^2)\hat{\mathbf{e}}_R}{(z_0^2 + R^2 + 2z_0 R \cos\theta)^3} R^2 \sin\theta \, d\theta \, d\varphi, \tag{B.4}$$

where the unit dyadic was written in the form $\overset{\leftrightarrow}{\mathbf{I}} = \hat{\mathbf{e}}_R \hat{\mathbf{e}}_R + \hat{\mathbf{e}}_\theta \hat{\mathbf{e}}_\theta + \hat{\mathbf{e}}_\varphi \hat{\mathbf{e}}_\varphi$. Therefore, the cartesian

components for the flux of the external Maxwell stress tensor results in[1]

$$\boldsymbol{\Phi}^{ext} \cdot \hat{\mathbf{e}}_x = \frac{e^2}{4\pi} \int_0^{2\pi} \int_0^{\pi} \frac{R^2(R^2 - z_0^2)}{2(z_0^2 + R^2 + 2z_0 R\cos\theta)^3} \, \hat{\mathbf{e}}_R \cdot \hat{\mathbf{e}}_x \sin\theta \, d\theta \, d\varphi \tag{B.5}$$
$$= \frac{e^2 R^2(R^2 - z_0^2)}{8\pi} \underbrace{\int_0^{2\pi} \cos\varphi \, d\varphi}_{=0} \int_0^{\pi} \frac{\sin^2\theta}{(z_0^2 + R^2 + 2z_0 R\cos\theta)^3} \, d\theta = 0,$$

$$\boldsymbol{\Phi}^{ext} \cdot \hat{\mathbf{e}}_y = \frac{e^2}{4\pi} \int_0^{2\pi} \int_0^{\pi} \frac{R^2(R^2 - z_0^2)}{2(z_0^2 + R^2 + 2z_0 R\cos\theta)^3} \, \hat{\mathbf{e}}_R \cdot \hat{\mathbf{e}}_y \sin\theta \, d\theta \, d\varphi \tag{B.6}$$
$$= \frac{e^2 R^2(R^2 - z_0^2)}{8\pi} \underbrace{\int_0^{2\pi} \sin\varphi \, d\varphi}_{=0} \int_0^{\pi} \frac{\sin^2\theta}{(z_0^2 + R^2 + 2z_0 R\cos\theta)^3} \, d\theta = 0,$$

$$\boldsymbol{\Phi}^{ext} \cdot \hat{\mathbf{e}}_z = \frac{e^2}{4\pi} \int_0^{2\pi} \int_0^{\pi} \frac{2z_0(z_0\cos\theta + R) + (R^2 - z_0^2)\hat{\mathbf{e}}_R \cdot \hat{\mathbf{e}}_z}{(z_0^2 + R^2 + 2z_0 R\cos\theta)^3} \, R^2 \sin\theta \, d\theta \, d\varphi$$
$$= \frac{e^2}{4} \int_0^{\pi} \frac{2z_0 R + (z_0^2 + R^2)\cos\theta}{(z_0^2 + R^2 + 2z_0 R\cos\theta)^3} \, \sin\theta \, d\theta \tag{B.7}$$
$$= \frac{e^2}{4} \left\{ \frac{1}{(z_0 - R)^4} - \frac{1}{(z_0 + R)^4} + \left[\frac{z_0^2 + R^2}{(2z_0 R)^2} \right] \left[\frac{z_0^2 + R^2 - 4z_0 R}{(z_0 - R)^4} \right. \right.$$
$$\left. \left. - \frac{z_0^2 + R^2 + 4z_0 R}{(z_0 + R)^4} \right] \right\} = 0.$$

In this way, the surface integral of the external Maxwell stress tensor over an empty volume with boundary S enclosing or not the electron, is zero. As it should be expected in accordance to the linear momentum conservation law [Eq. (2.58)], given that in the one hand there are not charges and currents densities inside the volume which may feel Lorentz force, and on the other hand a particle can not be self accelerated. Now, if a charge particle Q is added to the center of the integration surface, by means of the Maxwell stress tensor decomposition shown in section 3.2, the flux of the stress tensor over the spherical surface, due to both charged particles, is calculated as

$$\boldsymbol{\Phi} = \oint_{S(\mathbf{r}_0)} \overset{\leftrightarrow}{\mathbf{T}} \cdot \mathbf{n} \, da = \oint_{S(\mathbf{r}_0)} \left[\overset{\leftrightarrow}{\mathbf{T}}^{ext}(\mathbf{r}_0 + \mathbf{R}) + \overset{\leftrightarrow}{\mathbf{T}}^{in}(\mathbf{R}) + \overset{\leftrightarrow}{\mathbf{T}}^{(ext,in)}(\mathbf{r}_0 + \mathbf{R}, \mathbf{R}) \right] \cdot \hat{\mathbf{n}} \, da, \tag{B.8}$$

with the superindex (in) refers to the particle inside the sphere. However, the first term in Eq. (B.8) represents the same as Eq. (B.3): Maxwell stress tensor flux of the external—to the surface—charged particle, so it is equal to zero. The second term in Eq. (B.8) corresponds to Eq. (B.8) setting $\mathbf{r}_0 = \mathbf{0}$, which also leads to zero. Thus, the total flux of the Maxwell stress tensor over the sphere is only determined by the coupling term of both fields, in other words

$$\boldsymbol{\Phi} = \oint_{S(\mathbf{r}_0)} \overset{\leftrightarrow}{\mathbf{T}} \cdot \mathbf{n} \, da = \oint_{S(\mathbf{r}_0)} \overset{\leftrightarrow}{\mathbf{T}}^{(ext,in)}(\mathbf{r}_0 + \mathbf{R}, \mathbf{R}) \cdot \hat{\mathbf{n}} \, da. \tag{B.9}$$

---

[1] The flux of Maxwell stress tensor over a surface enclosing the electron is equal to zero. This statement follows straightforward by setting up $z_0 = 0$ in Eq. (B.4).

In fact, by performing the integral (B.9) and taking the limit when $R \to 0$, Coulomb's force law is recovered, as anticipated for the force exerted by one charged particle onto another.

Using the results for Eq. (B.9), concerning an electron outside S and a charge Q inside S, and recalling that the nanoparticle can be thought as a composite of $N-1$ particles system with density (see [38])

$$\rho(\mathbf{r}) = \sum_{i=1}^{N-1} Q_i \delta(\mathbf{r} - (\mathbf{r}_0 + \mathbf{R}_i)), \tag{B.10}$$

where Q_i is the charge of particle labeled i and $\mathbf{R}_i$ defined in Fig. B.1(b). The flux of Maxwell stress tensor over the surface enclosing the nanoparticle for the complete system (electron plus charge distribution) is given by the following expression

$$\mathbf{\Phi} = \oint_{S(\mathbf{r}_0)} \left[\overset{\leftrightarrow}{\mathbf{T}}^{ext}(\mathbf{r}_0 + \mathbf{R}) + \sum_{k=1}^{N-1} \overset{\leftrightarrow}{\mathbf{T}}_k^{in}(\mathbf{R} - \mathbf{R}_k) + \frac{1}{2} \sum_{\substack{j=1 \\ j \neq k}}^{N} \sum_{k=1}^{N} \overset{\leftrightarrow}{\mathbf{T}}^{(k,j)}(\mathbf{R} - \mathbf{R}_k, \mathbf{R} - \mathbf{R}_j) \right] \cdot \hat{\mathbf{n}} \, da, \tag{B.11}$$

where the last double sum takes into account the electron outside the integration sphere, that is why the limits are extended to N particles. Again, the first and the second integrals in Eq. (B.11) stand for the contributions given by Eq. (B.8), so they are equal to zero. Consequently, the flux of the Maxwell stress tensor is governed by the coupling term as

$$\boxed{\mathbf{\Phi} = \frac{1}{2} \sum_{\substack{j=1 \\ j \neq k}}^{N} \sum_{k=1}^{N} \oint_{S(\mathbf{r}_0)} \overset{\leftrightarrow}{\mathbf{T}}^{(k,j)}(\mathbf{R} - \mathbf{R}_k, \mathbf{R} - \mathbf{R}_j) \cdot \hat{\mathbf{n}} \, da.} \tag{B.12}$$

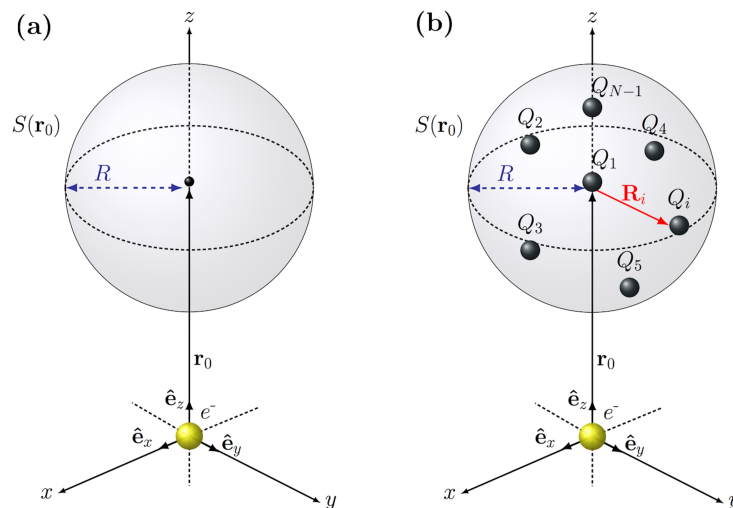Which proof, at least in the static case, statement (B.1).

Figure B.1. Schematic representation of (a) the electron (yellow spot) outside the closed surface S (grey sphere) and (b) the $N-1$ charged particles Q_i, which compose the nanoparticle, and the external—to the integration surface—electron showing the elements involved in Eq. (B.12): the integration surface $S(\mathbf{r}_0)$ and the position vectors $\mathbf{R}_i$ of each particle with respect to S.

The demonstration given above left out a missing link: from the nanoparticle's frame of

reference the electron is moving with velocity **v**. Hence, an integration in space-time should be done in order to ensure that external Maxwell stress tensor is equal to zero. Due to the difficulties integrating the Maxwell stress tensor produced by the moving electron over a spherical surface, this task will be addressed in the covariant formulation of classical electrodynamics, where the covariant quantity which encompasses the conservation of energy and momentum is the symmetrical electromagnetic energy-momentum tensor $\Theta^{\mu\nu}$ defined as [39]

$$\Theta^{\mu\nu} = \frac{1}{4\pi}\left(\eta^{\mu\beta}F_{\beta\alpha}F^{\alpha\nu} + \frac{1}{4}\eta^{\mu\nu}F_{\alpha\beta}F^{\alpha\beta}\right), \tag{B.13}$$

which is divergenceless—in the absence of charge and current densities—and traceless. Moreover, $F^{\mu\nu}$ stands for the Faraday's tensor and $\eta^{\mu\nu}$ stands for the Minkowski metric tensor whose elements are defined by the matrix

$$\eta^{\mu\nu} = \begin{pmatrix} -1 & 0 & 0 & 0 \\ 0 & 1 & 0 & 0 \\ 0 & 0 & 1 & 0 \\ 0 & 0 & 0 & 1 \end{pmatrix}. \tag{B.14}$$

Let us denote the nanoparticle's frame of reference by S and the electron's frame of reference by S', as it is shown in Fig. 2.1. The covariant momentum 4-vector of the electromagnetic field is defined in S as [39]

$$P^{\mu} = \frac{1}{c}\int_{\sigma}\Theta^{\mu\nu}\,d\sigma_{\nu}, \tag{B.15}$$

where σ represents a spacelike surface (three dimensional surface at time t) and $d\sigma^{\mu}$ the surface element on such plane given by

$$d\sigma^{\mu} = n^{\mu}d\sigma, \tag{B.16}$$

with n^{μ} the unit normal 4-vector in the direction of the 4-velocity of S relative to S', and $d\sigma$ an invariant surface element which can be determined by an observer in S, where $n^{\mu} = (1,0,0,0)$.

Thus in the frame of reference with normal $n^{\mu} = (1,0,0,0)$, the derivative of momentum 4-vector with respect the proper time is

$$\frac{dP^{\mu}}{d\tau} = \frac{1}{c}\int_{\sigma}\frac{d\Theta^{\mu\nu}}{d\tau}\,d\sigma_{\nu}, \tag{B.17}$$

and recalling that $n_{\alpha} = -c\frac{\partial\tau}{\partial x^{\alpha}} = (1,0,0,0)$, the change of momentum 4-vector with respect the proper time is

$$\boxed{\frac{dP^{\mu}}{d\tau} = -\int_{\sigma}\frac{d\Theta^{\mu\nu}}{d\tau}\frac{\partial\tau}{\partial x^{\nu}}\,d\sigma = -\int_{\sigma}\frac{\partial\Theta^{\mu\nu}}{\partial x^{\nu}}\,d\sigma.} \tag{B.18}$$

However, in free space the symmetrical electromagnetic energy-momentum tensor is divergenceless, so Eq. (B.18) results in

$$\boxed{\frac{dP^{\mu}}{d\tau} = -\int_{\sigma}\frac{\partial\Theta^{\mu\nu}}{\partial x^{\nu}}\,d\sigma = 0,} \tag{B.19}$$

from which is followed straightforward (since P^{μ} is a covariant quantity) that the integral co-

variant form of the conservation laws[2] for the total electromagnetic field energy and momentum, in a space-time region free of charge and current densities, is given by

$$\boxed{P^\mu = \text{constant.}} \tag{B.20}$$

Expanding Eq. (B.19) in components, it is obtained for the spatial coordinates[3] in S that

$$\frac{d\mathbf{P}}{d\tau} = \int_\sigma \frac{\partial \mathbf{g}}{\partial t}\, d\sigma - \int_\sigma \nabla \cdot \overset{\leftrightarrow}{\mathbf{T}}{}^{ext}\, d\sigma = 0. \tag{B.21}$$

Therefore integrating Eqs. (B.21) and using the fact that $\mathbf{g}$ is equal to zero far away the integration sphere,

$$\int_{-\infty}^{\infty} \int_\sigma \nabla \cdot \overset{\leftrightarrow}{\mathbf{T}}{}^{ext}\, d\sigma\, d\tau = \text{constant.} \tag{B.22}$$

Nonetheless, the constant can be set up to zero since far away the surface σ there is no electromagnetic momentum inside σ. Consequently, Eq. (B.22) proof's assertion (B.1) for any spacelike surface σ, in particular for a sphere.

---

[2]In reference [39] a careful analysis is presented in relation to the covariant formalism and the non relativistic treatment of the energy and momentum conservation laws for the electromagnetic field. In addition, it is demonstrated that tensor P^μ contains all the information about the energy and momentum of the electromagnetic field in a region of space-time, regardless the frame of reference where P^μ is computed.

[3]The time coordinates results in Poynting's theorem in the reference frame S.

PROGRAM CODE FOR CALCULATING THE TOTAL LINEAR MOMENTUM TRANSFERRED

In the following Appendix the Python program code for calculating the total linear momentum transferred from the electron to the NP, within the dipole approximation, is presented. The program is written in atomic units, whereas the results are written in SI units.

The program works as follows:

1. The total electromagnetic field and the Maxwell stress tensor, in the dipole approximation, are calculated for a spherical grid in accordance to the Legendre-Gauss Quadrature, as it is shown in [40]. It is also worth to mention that Mie coefficients, Eqs. (2.53), are recast in terms of the Riccati-Bessel functions

$$\psi_\ell(x) = x j_\ell(x), \tag{C.1a}$$

$$\xi_\ell(x) = x h_\ell^{(+)}(x), \tag{C.1b}$$

   as

$$t_\ell^E = \frac{\sqrt{\epsilon_i}\,\psi_\ell\left(x_i\right)\psi_\ell^{'}\left(x\right) - \psi_\ell\left(x\right)\psi_\ell^{'}\left(x_i\right)}{\xi_\ell\left(x\right)\psi_\ell^{'}\left(x_i\right) - \sqrt{\epsilon_i}\,\psi_\ell\left(x_i\right)\xi_\ell^{'}\left(x\right)}, \tag{C.2a}$$

$$t_\ell^M = \frac{\psi_\ell\left(x_i\right)\psi_\ell^{'}\left(x\right) - \sqrt{\epsilon_i}\,\psi_\ell\left(x\right)\psi_\ell^{'}\left(x_i\right)}{\sqrt{\epsilon_i}\,\xi_\ell\left(x\right)\psi_\ell^{'}\left(x_i\right) - \psi_\ell\left(x_i\right)\xi_\ell^{'}\left(x\right)}, \tag{C.2b}$$

   since they are more suited for numerical calculations than Eqs. (2.53) [13].

2. Then, the surface integral of Maxwell stress tensor is computed via a Legendre-Gauss Quadrature.

3. Moreover, steps 1 and 2 are repeated for a given partition in frequency.

4. Finally, the frequency (ω) and the cartesian components of the spectral contribution ($\mathcal{P}_i$) are written in a ".dat" file.

Note: The frequency integral in Eq. (2.85) is performed later in a Mathematica notebook via a Newton-Cotes formula, see for example [17] and [41].

Program Code

```python
#———————Libraries
import math
import cmath
import scipy.special as sp
import numpy as np
#——————————————#
# General Definitions #
#——————————————#
#———————Global variables
global c
global omegap
global damping
c=137.035999139
omegap=0.555
damping=0.00555
#———————Units Conversion
global Lnmat
global Eatcgs
global Batcgs
global Oatcgs
global DinNew
Lnmat=1/0.052917721067
Eatcgs=4.149004710E−10
Batcgs=4.149004710E−10
Oatcgs=4.13414E16
DinNew=1E−5
#———————Function Distance
def distance(x,y,b):
    f=math.sqrt((x−b)**(2)+(y)**(2))
    return f;
#———————Function Gamma
def gamma(v):
    f=1/(math.sqrt(1−(v/c)**2))
    return f;
#———————————————#
# Mie Coefficients #
#———————————————#
#———————Function Drude Model
def Drude(omega):
    f=1−(omegap)**2/((omega)**2+1j*omega*damping)
    return f;
#———————Function Spherical Bessel
def jnu(n,x):
    j20=sp.sph_jn(2,x)
    j2=j20[0][2]
    j1=j20[0][1]
    j0=j20[0][0]
    if n==0:
        return j0;
    if n==1:
        return j1;
    if n==2:
        return j2;
#———————Function Spherical Bessel
```

```python
def ynu(n,x):
    y20=sp.sph_yn(2,x)
    y2=y20[0][2]
    y1=y20[0][1]
    y0=y20[0][0]
    if n==0:
        return y0;                                                    60
    if n==1:
        return y1;
    if n==2:
        return y2;
#--------Function Spherical Hankel
def hplus(n,x):
    j2=jnu(2,x)
    y2=ynu(2,x)
    j1=jnu(1,x)
    y1=ynu(1,x)                                                       70
    j0=jnu(0,x)
    y0=ynu(0,x)
    h2=j2+1j*y2
    h1=j1+1j*y1
    h0=j0+1j*y0
    hplus2=1j*h2
    hplus1=1j*h1
    hplus0=1j*h0
    if n==0:
        return hplus0;                                               80
    if n==1:
        return hplus1;
    if n==2:
        return hplus2;
#--------Fuction Psi and dPsi
def Psi(component,x):
    Psi1=x*jnu(1,x)
    Psi0=x*jnu(0,x)
    dPsi1=Psi0-Psi1/x
    if component=="normal":                                          90
        return Psi1;
    elif component=="derivative":
        return dPsi1;
#--------Fuction Xi and dXi
def Xi(component,x):
    Xi1=x*hplus(1,x)
    Xi0=x*hplus(0,x)
    dXi1=Xi0-Xi1/x
    if component=="normal":
        return Xi1;                                                  100
    elif component=="derivative":
        return dXi1;
#--------Function Mie coefficients
def t1(component,omega,a):
    normal="normal"
    derivative="derivative"
    k0=omega/c
    xx0=k0*a
```

```python
    xxi=xx0*cmath.sqrt(Drude(omega))
    if component=="e":
        te1aux=cmath.sqrt(Drude(omega))*Psi(normal,xxi)*Psi(derivative,xx0)-
        Psi(normal,xx0)*Psi(derivative,xxi)
        te1aux2=Xi(normal,xx0)*Psi(derivative,xxi)-cmath.sqrt(Drude(omega))*
        Psi(normal,xxi)*Xi(derivative,xx0)
        te1=te1aux/te1aux2
        return te1;
    elif component=="m":
        tm1aux=Psi(normal,xxi)*Psi(derivative,xx0)-cmath.sqrt(Drude(omega))*
        Psi(normal,xx0)*Psi(derivative,xxi)
        tm1aux2=cmath.sqrt(Drude(omega))*Xi(normal,xx0)*Psi(derivative,xxi)-
        Psi(normal,xxi)*Xi(derivative,xx0)
        tm1=tm1aux/tm1aux2
        return tm1;
#------------------------------------#
# Electron's Electromagnetic Field #
#------------------------------------#
#-------Electron's Electric Field in Cartesian Coordinates
def Eelectron(component,x,y,z,omega,v,b):
    if component=='xx':
        f=-2*(omega/(v**2*(gamma(v))*distance(x,y,b)))*
        (cmath.exp(1j*(omega*z)/v))*(sp.k1((omega*distance(x,y,b))/
        (v*gamma(v))))*(x-b)
        return f;
    elif component=='yy':
        f=-2*(omega/(v**2*(gamma(v))*distance(x,y,b)))*
        (cmath.exp(1j*(omega*z)/v))*(sp.k1((omega*distance(x,y,b))/
        (v*gamma(v))))*y
        return f;
    elif component=='zz':
        f=2*1j*(omega/(v**2*(gamma(v))**2))*(cmath.exp(1j*(omega*z)/v))*
        (sp.k0((omega*distance(x,y,b))/(v*gamma(v))))
        return f;
#-------Electrons's Magnetic Field in Cartesian Coordinates
def Belectron(component,x,y,z,omega,v,b):
    if component=='xx':
        f=2*(omega/(v*gamma(v)*c*distance(x,y,b)))*(cmath.exp(1j*
        (omega*z)/v))*(sp.k1((omega*distance(x,y,b))/(v*gamma(v))))*y
        return f;
    elif component=='yy':
        f=-2*(omega/(v*gamma(v)*c*distance(x,y,b)))*
        (cmath.exp(1j*(omega*z)/v))*(sp.k1((omega*distance(x,y,b))/
        (v*gamma(v))))*(x-b)
        return f;
    elif component=='zz':
        f=0
        return f;
#------------------------------------#
# Scattered Electromagnetic Field #
#------------------------------------#
#-------Scattered Electric Field in Spherical Coordinates
def Enpsph(component,r,theta,phi,omega,v,a,b):
    e='e'
    m='m'
```

```python
    k0=omega/c
    if component=='rr':
        f=6*t1(e,omega,a)*(hplus(1,k0*r)/(k0*r))*
        (k0/(c*gamma(v)*(v/c)**2))*(math.sin(theta)*math.cos(phi)*
        sp.k1((omega*b)/(v*gamma(v)))+(1j/gamma(v))*math.cos(theta)*
        sp.k0((omega*b)/(v*gamma(v))))
        return f;                                                                          170
    elif component=='tt':
        f=3*(k0/(c*gamma(v)*(v/c)**2))*(1j*t1(m,omega,a)*hplus(1,k0*r)*(v/c)*
        sp.k1((omega*b)/(v*gamma(v)))*math.cos(phi)+t1(e,omega,a)*
        (2*hplus(1,k0*r)/(k0*r)-hplus(2,k0*r))*(sp.k1((omega*b)/(v*gamma(v)))*
        math.cos(theta)*math.cos(phi)-(1j/gamma(v))*
        sp.k0((omega*b)/(v*gamma(v)))*math.sin(theta)))
        return f;
    elif component=='pp':
        f=-3*(k0/(c*gamma(v)*(v/c)**2))*math.sin(phi)*
        sp.k1((omega*b)/(v*gamma(v)))*(t1(e,omega,a)*(2*hplus(1,k0*r)/(k0*r)-      180
        hplus(2,k0*r))+1j*t1(m,omega,a)*hplus(1,k0*r)*(v/c)*math.cos(theta))
        return f;
#-------Scattered Electric Field in Cartesian Coordinates
def Enpcart(component,r,theta,phi,omega,v,a,b):
    rr='rr'
    tt='tt'
    pp='pp'
    if component=='xx':
        f1=Enpsph(rr,r,theta,phi,omega,v,a,b)*(math.sin(theta))*(math.cos(phi))
        f2=Enpsph(tt,r,theta,phi,omega,v,a,b)*(math.cos(theta))*(math.cos(phi))    190
        f3=Enpsph(pp,r,theta,phi,omega,v,a,b)*(math.sin(phi))
        f=f1+f2-f3
        return f;
    elif component=='yy':
        f1=Enpsph(rr,r,theta,phi,omega,v,a,b)*(math.sin(theta))*(math.sin(phi))
        f2=Enpsph(tt,r,theta,phi,omega,v,a,b)*(math.cos(theta))*(math.sin(phi))
        f3=Enpsph(pp,r,theta,phi,omega,v,a,b)*(math.cos(phi))
        f=f1+f2+f3
        return f;
    elif component=='zz':                                                              200
        f1=Enpsph(rr,r,theta,phi,omega,v,a,b)*(math.cos(theta))
        f2=Enpsph(tt,r,theta,phi,omega,v,a,b)*(math.sin(theta))
        f=f1-f2
        return f;
#-------Scattered Magnetic Field in Spherical Coordinates
def Bnpsph(component,r,theta,phi,omega,v,a,b):
    e='e'
    m='m'
    k0=omega/c
    if component=='rr':                                                                210
        f=6*t1(m,omega,a)*(hplus(1,k0*r)/(k0*r))*(k0/(c*gamma(v)*(v/c)))*
        sp.k1((omega*b)/(v*gamma(v)))*math.sin(theta)*math.sin(phi)
        return f;
    elif component=='tt':
        f=3*(k0/(c*gamma(v)*(v/c)**2))*sp.k1((omega*b)/(v*gamma(v)))*
        math.sin(phi)*(t1(m,omega,a)*(2*hplus(1,k0*r)/(k0*r)-hplus(2,k0*r))*
        (v/c)*math.cos(theta)+1j*t1(e,omega,a)*hplus(1,k0*r))
        return f;
```

```python
        elif component=='pp':
        f=3*(k0/(c*gamma(v)*(v/c)**2))*(t1(m,omega,a)*(2*hplus(1,k0*r)/(k0*r)
            -hplus(2,k0*r))*(v/c)*sp.k1((omega*b)/(v*gamma(v)))*math.cos(phi)+
            t1(e,omega,a)*hplus(1,k0*r)*(1j*sp.k1((omega*b)/(v*gamma(v)))*
            math.cos(theta)*math.cos(phi)+(1/gamma(v))*
            sp.k0((omega*b)/(v*gamma(v)))*math.sin(theta)))
            return f;
#————Scattered Magnetic Field in Cartesian Coordinates
def Bnpcart(component,r,theta,phi,omega,v,a,b):
    rr='rr'
    tt='tt'
    pp='pp'
    if component=='xx':
        f1=Bnpsph(rr,r,theta,phi,omega,v,a,b)*(math.sin(theta))*(math.cos(phi))
        f2=Bnpsph(tt,r,theta,phi,omega,v,a,b)*math.cos(theta)*(math.cos(phi))
        f3=Bnpsph(pp,r,theta,phi,omega,v,a,b)*math.sin(phi)
        f=f1+f2-f3
        return f;
    elif component=='yy':
        f1=Bnpsph(rr,r,theta,phi,omega,v,a,b)*(math.sin(theta))*(math.sin(phi))
        f2=Bnpsph(tt,r,theta,phi,omega,v,a,b)*(math.cos(theta))*(math.sin(phi))
        f3=Bnpsph(pp,r,theta,phi,omega,v,a,b)*(math.cos(phi))
        f=f1+f2+f3
        return f;
    elif component=='zz':
        f1=Bnpsph(rr,r,theta,phi,omega,v,a,b)*(math.cos(theta))
        f2=Bnpsph(tt,r,theta,phi,omega,v,a,b)*(math.sin(theta))
        f=f1-f2
        return f;
#————————————————————————#
# Total Electromagnetic Field #
#————————————————————————#
#————Total Electric Field in cartesian coordinates
def Etot(component,r,theta,phi,omega,v,a,b):
    x=r*(math.cos(phi))*(math.sin(theta))
    y=r*(math.sin(phi))*(math.sin(theta))
    z=r*(math.cos(theta))
    if component=='xx':
        Etotx1=Eelectron(component,x,y,z,omega,v,b)
        Etotx2=Enpcart(component,r,theta,phi,omega,v,a,b)
        Etotx=Etotx1+Etotx2
        return Etotx;
    elif component=='yy':
        Etoty1=Eelectron(component,x,y,z,omega,v,b)
        Etoty2=Enpcart(component,r,theta,phi,omega,v,a,b)
        Etoty= Etoty1 + Etoty2
        return Etoty;
    elif component=='zz':
        Etotz1=Eelectron(component,x,y,z,omega,v,b)
        Etotz2=Enpcart(component,r,theta,phi,omega,v,a,b)
        Etotz=Etotz1+Etotz2
        return Etotz;
#————Total Magnetic Field in cartesian coordinates
def Btot(component,r,theta,phi,omega,v,a,b):
    x=r*(math.cos(phi))*(math.sin(theta))
```

```
        y=r*(math.sin(phi))*(math.sin(theta))
        z=r*(math.cos(theta))
        if component=='xx':
            Btotx1=Belectron(component,x,y,z,omega,v,b)
            Btotx2=Bnpcart(component,r,theta,phi,omega,v,a,b)
            Btotx=Btotx1 + Btotx2
            return Btotx;                                                        280
        elif component=='yy':
            Btoty1=Belectron(component,x,y,z,omega,v,b)
            Btoty2=Bnpcart(component,r,theta,phi,omega,v,a,b)
            Btoty= Btoty1 + Btoty2
            return Btoty;
        elif component=='zz':
            Btotz1=Belectron(component,x,y,z,omega,v,b)
            Btotz2=Bnpcart(component,r,theta,phi,omega,v,a,b)
            Btotz=Btotz1 + Btotz2
            return Btotz;                                                        290
#————————————————#
# Maxwell  Stress  Tensor #
#————————————————#
def Mij(i,j,Ax,Ay,Az):
    if (i==1 and j==1):
        f1=(0.5)*((Ax)*(np.conjugate(Ax)))
        f2=(0.5)*(Ay*(np.conjugate(Ay)))
        f3=(0.5)*(Az*(np.conjugate(Az)))
        f=f1-f2-f3
        return f;                                                               300
    elif (i==1 and j==2):
        f=Ax*(np.conjugate(Ay))
        return f;
    elif (i==1 and j==3):
        f=Ax*(np.conjugate(Az))
        return f;
    elif (i==2 and j==1):
        f=Ay*(np.conjugate(Ax))
        return f;
    elif (i==2 and j==2):                                                       310
        f1=(0.5)*(Ax*(np.conjugate(Ax)))
        f2=(0.5)*(Ay*(np.conjugate(Ay)))
        f3=(0.5)*(Az*(np.conjugate(Az)))
        f=f2-f1-f3
        return f;
    elif (i==2 and j==3):
        f=Ay*(np.conjugate(Az))
        return f;
    elif (i==3 and j==1):
        f=Az*(np.conjugate(Ax))                                                 320
        return f;
    elif (i==3 and j==2):
        f=Az*(np.conjugate(Ay))
        return f;
    elif (i==3 and j==3):
        f1=(0.5)*(Ax*(np.conjugate(Ax)))
        f2=(0.5)*(Ay*(np.conjugate(Ay)))
        f3=(0.5)*(Az*(np.conjugate(Az)))
```

```python
            f=f3-f1-f2
            return f;                                                          330
#---------------------#
# Spherical Grid #
#---------------------#
def sphergrid(n):
    grid=np.zeros((n,2*n,2))
    deg=n
    deg2=2*n
    x,w=np.polynomial.legendre.leggauss(deg)
    x2,w2=np.polynomial.legendre.leggauss(deg2)
    for i in range(len(x)):                                                    340
        theta=math.pi*(x[i]+1.0)/2.0
        for j in range(len(x2)):
            phi= math.pi*(x2[j]+1.0)
            grid[i][j][0]=theta
            grid[i][j][1]=phi
    return grid
#------#
# Main #
#------#
#file2=open('EBtot.dat','w')                                                   350
xx='xx'
yy='yy'
zz='zz'
#--------Integration Variables
intradius=1.05 #nm
beta=0.99
v=beta*c #atomic
a=1. #nm
b=1.5 #nm
file1=open('dP_a=%snm_v=%sc_b=%snm.dat' % (a,beta,b),'w')                       360
#--------Omega Partition
omegai=1E-6
omegai2=0
omegaf=0.8
nomega=100
nomega2=1000
homega=(omegaf-omegai)/nomega
homega2=(omegaf-omegai)/nomega2
omegadipolar=omegap/math.sqrt(3)
#--------Theta and Phi Partitions                                              370
ntheta=20
nphi=2*ntheta
deg=ntheta
deg2=nphi
x,w=np.polynomial.legendre.leggauss(deg)
x2,w2=np.polynomial.legendre.leggauss(deg2)
grid=np.zeros((ntheta,nphi,2))
grid=sphergrid(ntheta)
#--------Initializing
dPEx,dPEx1,dPEx2,dPEx3,dPEx4=0,0,0,0,0                                          380
dPEy,dPEy1,dPEy2,dPEy3,dPEy4=0,0,0,0,0
dPEz,dPEz1,dPEz2,dPEz3,dPEz4=0,0,0,0,0
dPBx,dPBx1,dPBx2,dPBx3,dPBx4=0,0,0,0,0
```

```
dPBy,dPBy1,dPBy2,dPBy3,dPBy4=0,0,0,0,0
dPBz,dPBz1,dPBz2,dPBz3,dPBz4=0,0,0,0,0
omega=omegai
omegaprint,i,iprev,iprev2,l=0,0,0,0,1
#————Surface Integral
while (omega<=omegaf):
    if (omega>=omegadipolar−0.01 and omega<=omegadipolar+0.01):        390
        omega=omegai2+l*homega2
        omegaprint=nomega2
        omegai=omega
        iprev2=iprev
        l=l+1
        i=1
    else:
        omega=omegai+i*homega
        omegaprint=nomega
        omegai2=omega                                                  400
        iprev=i
        i=i+1
    for j in range(0,ntheta):
        if (omegaprint==nomega):
            print("%s/%s _−_%s\n" % (i+iprev2,omegaprint,j))
        elif (omegaprint==nomega2):
            print("%s/%s _−_%s\n" % (l,omegaprint,j))
        for k in range(0,nphi):
            theta=grid[j][k][0]
            phi=grid[j][k][1]                                          410
            #————Total Fields
            Etotx=Etot(xx,intradius*Lnmat,theta,phi,omega,v,a*Lnmat,b*Lnmat)*Eatcgs
            Etoty=Etot(yy,intradius*Lnmat,theta,phi,omega,v,a*Lnmat,b*Lnmat)*Eatcgs
            Etotz=Etot(zz,intradius*Lnmat,theta,phi,omega,v,a*Lnmat,b*Lnmat)*Eatcgs
            Btotx=Btot(xx,intradius*Lnmat,theta,phi,omega,v,a*Lnmat,b*Lnmat)*Batcgs
            Btoty=Btot(yy,intradius*Lnmat,theta,phi,omega,v,a*Lnmat,b*Lnmat)*Batcgs
            Btotz=Btot(zz,intradius*Lnmat,theta,phi,omega,v,a*Lnmat,b*Lnmat)*Batcgs
            #————X Component
            #Electric
            dPEx1=(Mij(1,1,Etotx,Etoty,Etotz))*((math.sin(theta))**2)*  420
            (math.cos(phi))
            dPEx2=(Mij(1,2,Etotx,Etoty,Etotz))*((math.sin(theta))**2)*
            (math.sin(phi))
            dPEx3=(Mij(1,3,Etotx,Etoty,Etotz))*(math.sin(theta))*
            (math.cos(theta))
            dPEx4=dPEx1+dPEx2+dPEx3
            dPEx=(dPEx4.real)*w[j]*w2[k]*((math.pi)**2./2.)+dPEx
            #Magnetic
            dPBx1=(Mij(1,1,Btotx,Btoty,Btotz))*((math.sin(theta))**2)*
            (math.cos(phi))                                            430
            dPBx2=(Mij(1,2,Btotx,Btoty,Btotz))*((math.sin(theta))**2)*
            (math.sin(phi))
            dPBx3=(Mij(1,3,Btotx,Btoty,Btotz))*(math.sin(theta))*
            (math.cos(theta))
            dPBx4=dPBx1+dPBx2+dPBx3
            dPBx=(dPBx4.real)*w[j]*w2[k]*((math.pi)**2./2.)+dPBx
            #————Y Component
            #Electric
```

```
                    dPEy1=(Mij(2,1,Etotx,Etoty,Etotz))*((math.sin(theta))**2)*
                    (math.cos(phi))                                                        440
                    dPEy2=(Mij(2,2,Etotx,Etoty,Etotz))*((math.sin(theta))**2)*
                    (math.sin(phi))
                    dPEy3=(Mij(2,3,Etotx,Etoty,Etotz))*(math.sin(theta))*
                    (math.cos(theta))
                    dPEy4=dPEy1+dPEy2+dPEy3
                    dPEy=(dPEy4.real)*w[j]*w2[k]*((math.pi)**2./2.)+dPEy
                    #Magnetic
                    dPBy1=(Mij(2,1,Btotx,Btoty,Btotz))*((math.sin(theta))**2)*
                    (math.cos(phi))
                    dPBy2=(Mij(2,2,Btotx,Btoty,Btotz))*((math.sin(theta))**2)*  450
                    (math.sin(phi))
                    dPBy3=(Mij(2,3,Btotx,Btoty,Btotz))*(math.sin(theta))*
                    (math.cos(theta))
                    dPBy4=dPBy1+dPBy2+dPBy3
                    dPBy=(dPBy4.real)*w[j]*w2[k]*((math.pi)**2./2.)+dPBy
                    #------Z Component
                    #Electric
                    dPEz1=(Mij(3,1,Etotx,Etoty,Etotz))*((math.sin(theta))**2)*
                    (math.cos(phi))
                    dPEz2=(Mij(3,2,Etotx,Etoty,Etotz))*((math.sin(theta))**2)*  460
                    (math.sin(phi))
                    dPEz3=(Mij(3,3,Etotx,Etoty,Etotz))*(math.sin(theta))*
                    (math.cos(theta))
                    dPEz4=dPEz1+dPEz2+dPEz3
                    dPEz=(dPEz4.real)*w[j]*w2[k]*((math.pi)**2./2.)+dPEz
                    #Magnetic
                    dPBz1=(Mij(3,1,Btotx,Btoty,Btotz))*((math.sin(theta))**2)*
                    (math.cos(phi))
                    dPBz2=(Mij(3,2,Btotx,Btoty,Btotz))*((math.sin(theta))**2)*
                    (math.sin(phi))                                                        470
                    dPBz3=(Mij(3,3,Btotx,Btoty,Btotz))*(math.sin(theta))*
                    (math.cos(theta))
                    dPBz4=dPBz1+dPBz2+dPBz3
                    dPBz=(dPBz4.real)*w[j]*w2[k]*((math.pi)**2./2.)+dPBz
    #------Writing the (omega,dPx,dPy,dPz) in a .dat file in SI
    dPx=(((intradius*1E-7)/(2*math.pi))**2)*(dPEx+dPBx)
    dPy=(((intradius*1E-7)/(2*math.pi))**2)*(dPEy+dPBy)
    dPz=(((intradius*1E-7)/(2*math.pi))**2)*(dPEz+dPBz)
    file1.write("%s %s %s %s\n" % (omega*Oatcgs,dPx*DinNew,dPy*DinNew,dPz*DinNew))
    #------Initializing                                                                    480
    dPEx,dPEx1,dPEx2,dPEx3,dPEx4=0,0,0,0,0
    dPEy,dPEy1,dPEy2,dPEy3,dPEy4=0,0,0,0,0
    dPEz,dPEz1,dPEz2,dPEz3,dPEz4=0,0,0,0,0
    dPBx,dPBx1,dPBx2,dPBx3,dPBx4=0,0,0,0,0
    dPBy,dPBy1,dPBy2,dPBy3,dPBy4=0,0,0,0,0
    dPBz,dPBz1,dPBz2,dPBz3,dPBz4=0,0,0,0,0
    dPx,dPy,dPz=0,0,0
```

[1] S. de Vega and F. J. García de Abajo, "Plasmon generation through Electron Tunneling in Graphene", arXiv:1706.09674v1 (2017).

[2] D. K. Yi, I. Sun, J. H. Ryu, H. Koo, C. W. Park, I. Youn, K. Choi, I. C. Kwon, K. Kim and C. Ahn, "Matrix Metalloproteinase Sensitive Gold Nanorod for Simultaneous Bioimaging nd Photothermal Therapy of Cancer", Bioconjug. Chem., **21** (12), 2173-2177 (2010).

[3] L. Tian, L. Lu, Y. Qiao, S. Ravi, F. Salatan and M. P. Melancon, "Stimuli-Responsive Gold Nanoparticles for Cancer Diagnosis and Therapy", J. Funct. Biomater., **7** (19), 1-31 (2016).

[4] S. T. Jones, R. W. Taylor, R. Esteban, E. K. Abo-Hamed, P. H. H. Bomans, N. A. J. M. Sommerdijk, J. Aizpurua, J. J. Baumberg and O. A. Scherman, "Gold Nanorods with Sub-Nanometer Separation using Cucurbit[n]uril for SERS Applications", Small, **10** (21), 4298-4303 (2014).

[5] P. E. Batson, "Motion of Gold Atoms on Carbon in the Aberration-Corrected STEM", Microsc. Microanal, **14**, 89-97 (2008).

[6] F. J. García de Abajo, "Relativistic energy loss and induced photon emission in the interaction of a dielectric sphere with an external electron beam", Phys. Rev. B, **59** (4), 3095-3107 (1999).

[7] P. E. Batson, A. Reyes-Coronado, R. G. Barrera, A. Rivacoba, P. M. Echenique and J. Aizpurua, "Plasmonic Nanobilliards: Controlling Nanoparticle Movement Using Forces Induced by Swift Electrons", Nano Lett., **11**, 3388-3393 (2011).

[8] P. E. Batson, A. Reyes-Coronado, R. G. Barrera, A. Rivacoba, P. M. Echenique and J. Aizpurua, "Nanoparticle movement: Plasmonic forces and physical constraints", Ultramicroscopy, **123**, 50-58 (2012).

[9] N. W. Ashcroft and N. D. Mermin, *Solid State Physics*, (Harcourt College Publishers, United States, 1976).

[10] J. Castrejón-Figueroa, *Fuerzas de interacción entre un haz de electrones y nanopartículas metálicas*, B. Sc. thesis, Mexico, 2015.

[11] J. D. Jackson, *Classical Electrodynamics*, 2nd ed. (John Wiley & Sons, United States, 1962).

[12] J. D. Jackson, *Classical Electrodynamics*, 3rd ed. (John Wiley & Sons, United States, 1998).

[13] C. F. Bohren and D. R. Huffman, *Absorption and Scattering of Light by Small Particles* (John Wiley & Sons, United States, 1983).

[14] M. E. Peskin and D. V. Schroeder, *An Introduction to Quantum Field Theory*, (Perseus Books, United States, 1995).

[15] M. J. Lighthill , *An introduction to Fourier analysis and generalised functions*, (Cambridge University Press, New York, 1958).

[16] H. Bateman, *Tables of Integral Transforms*, (McGaw Hill Book Company, United States, 1954) Vol. 1.

[17] M. Abramowitz and I. A. Stegun, *Handbook of Mathematical Functions with Formulas, Graphs, and Mathematical Tables*, 10th ed. (National Bureau of Standards Applied Mathematics Series 55, United States, 1972).

[18] The Wolfram Functions Site, http://functions.wolfram.com/PDF/BesselK.pdf

[19] G. Arfken, *Mathematical Methods for Physicists*, 3rd ed. (Academic Press, United Kingdom, 1985).

[20] F. E. Low, *Classical Field Theory: Electromagnetism and Gravitation*, (John Wiley & Sons, Federal Republic of Germany, 1997).

[21] E. Merzbacher, *Quantum Mechanics*, 2nd ed. (John Wiley & Sons, United States, 1970).

[22] A. Messiah, *Quantum mechanics*, Vol. 1 (North-Holland Publishing Company, Netherlands, 1961).

[23] A. Reyes-Coronado, R. G. Barrera, P. E. Batson, P. M. Echenique, A. Rivacoba, J. Aizpurua, "Electromagnetic forces on plasmonic nanoparticles induced by fast electron beams", Phys. Rev. B, **82** (235429), 1-19 (2010).

[24] R. H. Good, Jr. and T. J. Nelson, *Classical Theory of Electric and Magnetic Fields*, 2nd ed. (Academic Press, New York and London, 1971).

[25] A. Santos-Gómez, *Estudio de la transferencia de momento a nanopartículas plasmónicas por electrones rápidos en función de su velocidad*, M. Sc. thesis, Mexico, 2014.

[26] J. A. Castellanos-Reyes, *Transferencia de momento lineal de electrones rápidos a nanopartículas dieléctricas*, M. Sc. thesis, Mexico, 2017.

[27] R. Fuchs and K. L. Kliewer, "Optical Modes of Vibration in an Ionic Crystal Sphere", J. Opt. Soc. Am., **58** (3), 319-330 (1968).

[28] W. S. M. Werner, K. Glantschnig and C. Ambrosch-Draxl, "Optical Constants and Inelastic Electron-Scattering Data for 17 Elemental Metals", J. Phys. Chem. Ref. Data, **38** (4), 1013-1092 (2009).

[29] M. I. Marković and A. D. Rakić, "Determination of optical properties of aluminium including electron reradiation in the Lorentz-Drude model", Opt. Laser Technol, **22** (6), 394-398 (1990).

[30] S. A. Maier, *Plasmonics: Fundamentals and Applications*, (Springer, United States, 2007).

[31] F. J. García de Abajo, "Momentum transfer to small particles by passing electron beams", Phys. Rev. B, **70** (115422), 1-6 (2004).

[32] A. Zangwill, *Modern Electrodynamics*, (Cambridge University Press, United States, 2012).

[33] F. J. García de Abajo and J. Aizpurua, "Numerical simulation of electron energy loss near inhomogeneous dielectrics", Phys. Rev. B, **56** (24), 15873-15884 (1997).

[34] F. J. García de Abajo and A. Howie, "Numerical simulation of electron energy loss near inhomogeneous dielectrics", Phys. Rev. Lett., **80** (23), 5180-5183 (1998).

[35] F. J. García de Abajo and A. Howie, "Retarded field calculation of electron energy loss in inhomogeneous dielectrics", Phys. Rev. B., **65** (115418), 1-17 (2002).

[36] G. Barton, *Elements of Green's Functions and Propagation: Potentials, Diffusion, and Waves*, (Oxford University Press, United States, 1989).

[37] J. M. Lee, *Introduction to Smooth Manifolds*, 2nd ed. (Springer, United States, 2013).

[38] S. R. de Groot and L. G. Suttorp, *Foundations of Electrodynamics*, (North-Holland Publishing Company, Netherlands, 1972).

[39] F. Rohrlich, *Classical Charged Particles*, 3rd ed. (World Scientific, United States, 2007).

[40] P. Abbott, "Tricks of The Trade: Legendre-Gauss Quadrature", Mathematica J., **9**, 689-691 (2005).

[41] A. Quarteroni, R. Sacco and F. Saleri, *Numerical Mathematics*, (Springer, United States, 2000).